Maximally Helicity Violating amplitudes

Andrew Lifson

ID:22635416

Supervised by Assoc. Prof. Peter Skands

School of Physics & Astronomy

A thesis submitted in partial fulfilment for the degree of Bachelor of Science Advanced with Honours

MONASH University

November 13, 2015

Abstract

An important aspect in making quantum chromodynamics (QCD) predictions at the Large Hadron Collider (LHC) is the speed of the Monte Carlo (MC) event generators which are used to calculate them. MC event generators simulate a pure QCD collision at the LHC by first using fixed-order perturbation theory to calculate the hard (i.e. energetic) $2 \to n$ scatter, and then adding radiative corrections to this with a parton shower approximation. The $2 \to n$ scatter is traditionally calculated by summing Feynman diagrams, however the number of Feynman diagrams has a stronger than factorial growth with the number of final-state particles, hence this method quickly becomes infeasible. We can simplify this calculation by considering helicity amplitudes, in which each particle has its spin either aligned or anti-aligned with its direction of motion i.e. each particle has a specific helicity. In particular, it is well-known that the helicity amplitude for the maximally helicity violating (MHV) configuration is remarkably simple to calculate. In this thesis we describe the physics of the MHV amplitude, how we could use it within a MC event generator, and describe a program we wrote called VinciaMHV which calculates the MHV amplitude for the process $qg \to q + ng$ for $n = 1, 2, 3, 4$. We tested the speed of VinciaMHV against MadGraph4 and found that VinciaMHV calculates the MHV amplitude significantly faster, especially for high particle multiplicities. We also tested the precision of VinciaMHV by comparing its MHV amplitudes to those of MadGraph4. We found that the two programs agree to better than one part in a billion over 99% of the time, thus validating our program.

Acknowledgements

Thank you to my supervisor Associate Professor Peter Skands for his guidance and support which allowed me to grow as both a physicist and a writer of physics. I would also like to thank Peter's PhD student Nadine Fischer for always being happy to help me, particularly for taking time to explain many of the more basic aspects of this project to me. Additionally, I must give a very big thank you my parents for ensuring that this year was as stress-free as possible. Their role cannot be understated. To my fellow honours students I say thank you for keeping me sane during stressful moments, and congratulations on successfully completing your honours. Finally I would like to thank my friends and loved ones for tolerating my general disappearance this year.

Contents

1 Introduction **1**

2 Background Theory **2**
2.1 QCD . . . 2
2.2 Crossing symmetry . . . 4
2.3 Colour factors . . . 4
2.3.1 All-gluon amplitudes . . . 4
2.3.2 Squared all-gluon amplitudes . . . 7
2.3.3 Quark-gluon amplitudes . . . 8
2.3.4 Squared quark-gluon amplitudes . . . 10
2.4 Spinor-helicity formalism . . . 11
2.4.1 Weyl-spinor algebra . . . 11
2.4.2 Spinor inner products . . . 13
2.5 All-gluon helicity amplitudes . . . 15
2.6 Supersymmetry - a quick aside . . . 17
2.7 Helicity amplitudes with a single quark anti-quark pair . . . 19
2.8 Explicit formulae for MHV amplitudes . . . 20

3 Monte Carlo event generators **21**
3.1 Modelling particle collisions . . . 21
3.2 Parton showers . . . 23
3.2.1 Final-state radiation . . . 24
3.2.2 Improving parton showers with matrix elements . . . 28

4 Calculating the MHV amplitude **29**
4.1 MHV frequency . . . 29
4.2 Structure of VinciaMHV . . . 31

5 Comparing VinciaMHV to MadGraph4 **34**
5.1 Validation at specific phase-space points . . . 34
5.2 Singularity structure . . . 37
5.3 Precision tests . . . 39
5.4 Speed tests . . . 39

6 Summary and outlook **41**

Appendix A Conventions **42**

Appendix B QCD Feynman rules **43**

Appendix C Proofs of Weyl-spinor identities **45**

Appendix D Gluon polarisation vector **46**

Appendix E Monte Carlo integration **47**

Appendix F Parton energy fractions **48**

Appendix G Working for all-gluon squared colour matrix **49**

Appendix H VinciaMHV colour matrices **51**

1 Introduction

The majority of processes at the Large Hadron Collider (LHC) are accounted for by the scattering of quarks and gluons (partons) via the strong interaction (quantum chromodynamics, QCD) [1, 2]. Therefore, to understand LHC data we need a thorough understanding of pure QCD processes, each of which produces collimated sprays of energetic hadrons called jets [3, 4]. One of the aims of a Monte Carlo (MC) event generator is to calculate ("predict") the spectrum of jet multiplicities, their structure, and their transverse momenta by calculating the QCD high energy (hard) process and subsequent parton showers which created them. Due to the unprecedented energies and luminosities of the incoming protons at the LHC, we are able to create more numerous and energetic jets than ever before. However, there is still a discrepancy between the number of jets which can be created at the LHC and the number of jets which can be simulated with high precision using a MC event generator. For example, run 1 at the LHC contained collisions which produced 9 jets [1], while the combination of a specialist hard-process program such as ALPGEN [5], interfaced to a general purpose MC event generator such as PYTHIA [6] or HERWIG [7] can only accurately simulate up to 6 jets. A key reason for this is the long computational time needed to calculate the squared scattering amplitude at leading order of the QCD perturbative expansion, also called the tree-level matrix element.

Traditionally, MC event generators calculate the tree-level matrix element by summing over all possible Feynman diagrams at leading order of the perturbative expansion. In this approach, the helicities, i.e. each particle's spin projected onto its direction of motion, are averaged for initial-state particles and summed for final-state particles. This method is implemented in programs such as PYTHIA [6], HERWIG [7], SHERPA [8] and MadGraph [9], however in the past 30 years theorists have shown that QCD amplitudes can be calculated more elegantly using a helicity basis, i.e. by classifying each particle according to its helicity [10–18]. In this basis many amplitudes vanish due to a supersymmetry obeyed by tree amplitudes [19, 20]. There are also remarkably simple formulae for the amplitudes of the so called Maximally Helicity Violating (MHV) configuration, first conjectured by Parke and Taylor in 1986 for an all-gluon amplitude [13], later extended by Mangano and Parke to include amplitudes with a massless quark pair [21], and proven by Berends and Giele a year later [22]. Excitingly, it was recently shown that the MHV amplitude is the dominant helicity amplitude for certain cases [23]. Therefore, it is possible that the MHV amplitude is both the simplest, and most dominant of helicity amplitudes, and may help extend the number of jets a MC event generator can accurately simulate.

In this project we created a fast and reliable program called VinciaMHV which calculates full colour-summed MHV squared amplitudes for the process $qg \to q + ng$ for $n = 1, 2, 3, 4$, along with other $2 \to n$ crossing-related processes. VinciaMHV is meant to be embedded in the parton-shower program VINCIA [24], improving it by partially replacing the MadGraph4 tree-level matrix elements [25]. In Section 2 we briefly explain QCD and crossing symmetry, give a more detailed explanation of QCD colour factors and the spinor-helicity formalism, before finally describing MHV amplitudes for both the case of n gluon scattering, and for the process involving a single quark anti-quark pair with $n - 2$ gluons. In Section 3 we summarised how to use a MC event generator to simulate a proton-proton collision at the LHC, highlighting in which sections of the event generation we can use VinciaMHV. In Section 4 we consider the frequency with which we use the MHV amplitude for 4 to 7 partons, and give instructions upon how to use VinciaMHV. In Section 5 we tested the accuracy and speed of VinciaMHV relative to MadGraph4. We summarise and propose possible future extensions to this thesis in Section 6.

2 Background Theory

The original perturbative method, that of summing all possible Feynman diagrams contributing to each order of the expansion, quickly becomes infeasible as the number of particles increases. For example, the number of $2 \to n$ all-gluon tree diagrams grows alarmingly quickly with the number of final state gluons (see Table 1) [26]. Hence a less demanding method of calculating fixed-order perturbative QCD is required to extend to large multiplicities (i.e. to a large numbers of final state particles). One such method is to use the helicity basis, in which each external particle has a specific helicity. The helicity of a particle is defined as its spin projected onto its direction of motion and for massless particles is normalised such that the helicity equals $+1$ if the spin is aligned with the momentum, and equals -1 if anti-aligned. Note that, for a massless particle, we cannot boost to a reference frame in which the particle's direction of motion switches, Therefore the helicity of a massless particle is equal to its chirality (i.e. it's handedness) and is a conserved quantity. An amplitude calculated in the helicity basis is then referred to as a helicity amplitude. However not all helicity amplitudes were created equally, and we find that helicity amplitudes of massless particles obey a hierarchy of simplicity [2, 27, 28]. If all of the particles are considered to be outgoing, and all have the same helicity, or each particle except one has the same helicity, then the helicity amplitudes vanish. The next most simple helicity configuration, that for which all particles except two have the same helicity, is called the MHV configuration,and has a magnificently simple formula at tree level. For example, if in the MHV configuration, the kinematic part of the 9-gluon MHV amplitude is given by:

$$A_9 = i\frac{\langle ij\rangle^4}{\langle 12\rangle\langle 23\rangle\dots\langle 91\rangle} \ , \tag{1}$$

where we used the term kinematic to imply that the colour information has been factorised out of the amplitude. Here $1, 2, \dots 9$ refers to the 9 particles, i, j are the two particles with negative helicity, all other particles have positive helicity, and $\langle ij\rangle$ is a specific spinor inner product which is simple to calculate and to which we return in section 2.4.2. While we have not yet motivated equation (1), or properly explained its meaning, it is shown here in order to motivate the purpose of the thesis, that being to change a sum of many terms (in this case $559,405$ terms) into a simple product. The purpose of the Background Theory section is therefore to outline the theory needed to understand MHV amplitudes such as equation (1). Note that a different approach used to simplify helicity amplitude calculations is the BCFW recursion relation [29], which has been successfully implemented in the MC event generator Comix [30]. This recursion relation is outside the scope of this thesis and won't be discussed here.

2.1 QCD

In order to make sense of MHV amplitudes we must first understand the quantum field theory in which we are calculating them. In this thesis, the quantum field theory in which we are interested is QCD, due to its abundance at

Number of External Gluons	Number of Feynman Diagrams	Relative Growth
4	4	-
5	25	6.3
6	220	8.8
7	2485	11.3
8	34300	13.8
9	559405	16.3
10	10525900	18.8

Table 1: The number of Feynman diagrams needed to calculate an n-gluon scattering amplitude at tree level [26]. The relative growth is the number of Feynman diagrams in that row divided by the number of Feynman diagrams in the previous row. Notice that the number of diagrams grows like a factorial, but stronger.

the LHC. QCD is a somewhat counter-intuitive theory. At very short distances, (i.e. smaller than $\approx 1\text{fm} = 10^{-15}\text{m}$, the size of the proton), QCD is a theory of asymptotically free quarks and gluons (partons) which only scatter off one another through relatively small quantum corrections[1]. At longer wavelengths (about 1fm) we see strongly bound towers of multiple partons called hadrons, implying that QCD is an interaction which becomes stronger at larger distances.

QCD is a non-abelian $SU(3)_C$ gauge theory of coloured quarks and gluons. Quarks, which we will associate with colour indices from middle of the alphabet ($i, j, k, \cdots = 1, 2, 3$), are in the fundamental representation of $SU(3)_C$, while gluons are in the adjoint representation. We will give adjoint colour indices letters from the start of the alphabet $a, b, c, \cdots = 1, 2, \ldots 8$. The QCD Lagrangian is [35, 36]:

$$\mathcal{L} = \sum_q i\bar{\psi}_q^i \not{D}_{ij} \psi_q^j - m_q \bar{\psi}_q^i \psi_{qi} - \frac{1}{4} F_{\mu\nu}^a F^{a\mu\nu} \ , \tag{2}$$

where repeated indices are implicitly summed, ψ_q^i denotes a quark field with fundamental colour index i, m_q is the quark mass, the sum is over quark flavours q, $\not{D}_{ij}$ is the gamma contracted covariant derivative and is defined as:

$$\not{D}_{ij} \equiv \gamma^\mu D_{\mu ij} = \gamma^\mu \left(\delta_{ij} \partial_\mu - i\sqrt{2} g_s t_{ij}^a A_\mu^a \right) \ , \tag{3}$$

where γ^μ is the Dirac matrix with spacetime index μ, δ_{ij} the Kronecker delta, g_s the strong coupling with $g_s^2 = 4\pi\alpha_s$, A_μ^a the gluon field with adjoint colour index a and t_{ij}^a are the t matrices which are proportional to the Hermitian and traceless Gell-Mann matrices λ_{ij}^a, the generators of $SU(3)_C$:

$$\begin{gathered}
\lambda^1 = \begin{pmatrix} 0 & 1 & 0 \\ 1 & 0 & 0 \\ 0 & 0 & 0 \end{pmatrix} \ , \quad \lambda^2 = \begin{pmatrix} 0 & -i & 0 \\ i & 0 & 0 \\ 0 & 0 & 0 \end{pmatrix} \ , \quad \lambda^3 = \begin{pmatrix} 1 & 0 & 0 \\ 0 & -1 & 0 \\ 0 & 0 & 0 \end{pmatrix} \ , \\
\lambda^4 = \begin{pmatrix} 0 & 0 & 1 \\ 0 & 0 & 0 \\ 1 & 0 & 0 \end{pmatrix} \ , \lambda^5 = \begin{pmatrix} 0 & 0 & -i \\ 0 & 0 & 0 \\ i & 0 & 0 \end{pmatrix} \ , \quad \lambda^6 = \begin{pmatrix} 0 & 0 & 0 \\ 0 & 0 & 1 \\ 0 & 1 & 0 \end{pmatrix} \ , \\
\lambda^7 = \begin{pmatrix} 0 & 0 & 0 \\ 0 & 0 & -i \\ 0 & i & 0 \end{pmatrix} \ , \quad \lambda^8 = \frac{1}{\sqrt{3}} \begin{pmatrix} 1 & 0 & 0 \\ 0 & 1 & 0 \\ 0 & 0 & -2 \end{pmatrix} \ ,
\end{gathered} \tag{4}$$

such that:

$$t_{ij}^a = \frac{1}{\sqrt{2}} \lambda_{ij}^a \ . \tag{5}$$

The field strength tensor in equation (2) $F_{\mu\nu}^a$ is:

$$F_{\mu\nu}^a = \partial_\mu A_\nu^a - \partial_\nu A_\mu^a - g_s f^{abc} A_\mu^b A_\nu^c \ , \tag{6}$$

where f^{abc} are the QCD fine structure constants, related to the t matrices by:

$$t^a t^b - t^b t^a \equiv [t^a, t^b] = i\sqrt{2} f^{abc} t_c \ , \tag{7}$$

or equivalently:

$$f^{abc} = -\frac{i}{\sqrt{2}} \text{Tr}\{t^a [t^b, t^c]\} \ . \tag{8}$$

Note that it is the third term of equation (6) which governs the self-interaction of gluons and creates showers of gluons at the LHC. In perturbative QCD calculations it is useful to know the Fierz identity:

$$t_{ij}^a t_{kl}^a = \delta_{il}\delta_{jk} - \frac{1}{3}\delta_{ij}\delta_{kl} \ , \tag{9}$$

as well as some convention independent trace relations of the t matrices:

$$\text{Tr}\{t^a t^b\} = T_R \delta^{ab} \ , \quad \sum_{a,j} t_{ij}^a t_{jk}^a = C_F \delta_{ik} \ , \quad \sum_{c,d} f^{acd} f_{bcd} = C_A \delta^{ab} \ , \tag{10}$$

[1] This surprising and strange property is called asymptotic freedom, and was the subject of the 2004 Nobel Prize in physics, awarded to David Gross, Hugh Politzer and Frank Wilczek [31–34].

where $a, b, c, d = 1, 2, ..., 8$, $i, j, k = 1, 2, 3$, and $T_R = 1$, $C_F = 8/3$ and $C_A = 3$ are the convention dependent Casimirs of $SU(3)_C$. Note that this convention follows that most used in the spinor helicity community [18, 27, 28] and is different to the convention often used in QCD literature [35–38]. The difference is the normalisation of the t matrices, usually normalised such that $t^a = 1/2\lambda^a$, and hence $T_R = 1/2$, $C_F = 4/3$ and $C_A = 3$. To move from the standard convention to our convention we transform $t \to \sqrt{2}t$ and hence $t^2 \to 2t^2$, or equivalently $C_F \to 2C_F$, with C_A left unchanged. Consequently the colour-ordered Feynman rules (i.e. the QCD Feynman rules stripped of colour information) contain factors of $\sqrt{2}$.

2.2 Crossing symmetry

To calculate kinematic MHV amplitudes we use the convention that every external particle is considered to be outgoing, i.e. each particle is considered to be in the final state. Therefore, before we calculate the MHV amplitude we must first move initial-state particles into the final state. To do this we use crossing symmetry, which states that the amplitude for a process with a left (right) handed particle of momentum k in the initial state is equal to the amplitude for the same process with a right (left) handed anti-particle of momentum $-k$ in the final state [36]. For example, the amplitude for the following two processes is the same:

$$e_L^-(k) + q_L(p) \to e_L^-(k') + q_L(p') \ ,$$
$$e_R^+(-k') + e_L^-(k) \to \bar{q}_R(-p) + q_L(p') \ ,$$

where e_L^- and e_R^+ correspond to a left-handed electron and a right-handed positron, $q_L, \bar{q}_R$ correspond to a left handed-quark and a right-handed anti-quark, and k, k', p and p' are four-momentum of each particle.

In the all-outgoing convention, we note that due to fermion charge conservation, and because massless fermions always conserve chirality when interacting with a gluon or photon, that any QCD fermion pair will be a quark anti-quark pair of opposite chiralities [2]. In this thesis we only consider the light quarks (i.e. not the top quark). Since our quarks are moving near the speed of light, we consider them to be effectively massless, hence in this thesis we have that any quark anti-quark pair must have opposite helicities.

Finally we note that momentum conservation in the all-outgoing formalism takes the form:

$$\sum_{i=1}^{n} k_i = 0 \ , \tag{11}$$

and particles with negative energy are those which have been crossed from the initial state into the final state. Unless otherwise noted we will now use only massless particles with outgoing momenta.

2.3 Colour factors

It is well-known that a QCD scattering amplitude can be factorised into a colour factor and a gauge invariant kinematic colour-ordered amplitude [2, 16, 18, 27, 28, 39, 40]. The colour factors provide a complete (almost) orthogonal basis[2] at tree level for the full colour amplitude. They also fix the order in which gluons are contracted in colour space, and hence the order in which gluons are emitted. Meanwhile the kinematic colour-ordered amplitude (hereafter kinematic amplitude) is stripped of all colour information and is composed of all Feynman diagrams which have the relevant colour ordering. In fact, as we shall see in sections 2.5 and 2.7 there is a far simpler method than summing Feynman diagrams which one can use to calculate the kinematic amplitudes.

In the next two sections we outline this factorisation in the all-gluon case, and then describe the colour factor at both the amplitude level and at the amplitude squared level in detail. Section 2.3.3 and 2.3.4 repeats this for the case of a single quark anti-quark pair, together with $n - 2$ gluons.

2.3.1 All-gluon amplitudes

At tree level, the n gluon scattering amplitude M_n is [14, 27, 28, 39]:

$$M_n(g_1, g_2, \ldots, g_n) = g_s^{n-2} \sum_{\sigma \in S_n/Z_n} \mathrm{Tr}(t^{a_{\sigma(1)}} \ldots t^{a_{\sigma(n)}}) A_n(\sigma(k_1^{h_1}), \ldots, \sigma(k_n^{h_n})) \ , \tag{12}$$

[2]The all-gluon colour factor in equation (12) for example is only orthogonal at leading order in the power of N_C = number of colours. The basis is still however complete, and ensures gauge invariance of the kinematic amplitudes. For alternate orthogonal bases see e.g. [40, 41].

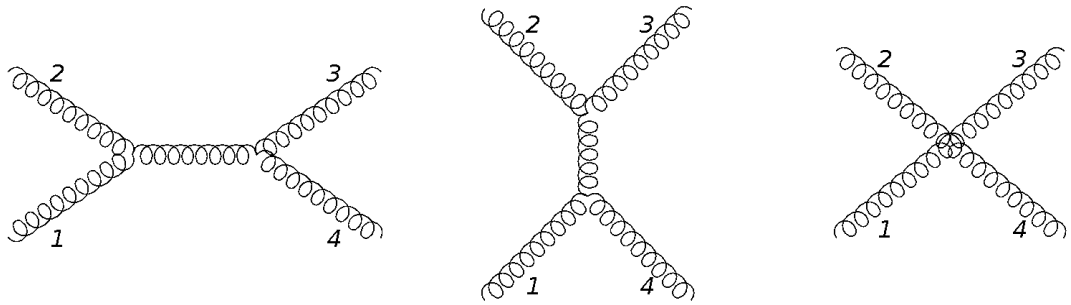

Figure 1: Three of the four diagrams which contribute to 4 gluon interactions at tree level. The omitted diagram is related to the middle diagram by a swap of momenta 3 and 4.

where g_s is the strong coupling ($g_s^2 = 4\pi\alpha_s$), $t^{a_{\sigma(i)}}$ is the t matrix defined in equation (5) with $a = 1, 2, \ldots 8$, k_i is the gluon momentum, h_i, the gluon helicity, $\mathrm{Tr}(t^{a_{\sigma(1)}} \ldots t^{a_{\sigma(1)}})$ the colour factor and $A_n(\sigma(k_1^{h_1}), \ldots, \sigma(k_n^{h_n}))$ the kinematic amplitude. The sum is over all non-cyclic permutations of σ (S_n is the set of all permutations of n objects while Z_n is the subset of cyclic permutations, i.e. S_n/Z_n is the subset set of all non-cyclic permutations) such that, for example, swapping $\sigma(1)$ and $\sigma(2)$ implies that we swap particles 1 and 2 in the colour order. Mathematically, this corresponds to swapping the order of the t matrices, and swapping particles $\sigma(1)$ and $\sigma(2)$ in the kinematic amplitude in equation (12).

To motivate equation (12) we will show that this equation holds for 4-gluon scattering, for which the relevant Feynman Diagrams are shown in Figure 1. We will work in $SU(N_C)$, a generalisation of the $SU(3)_C$ group used in QCD, to show the structure of the group algebra. In $SU(N_C)$ we can re-write the Fierz identity (equation (9)) in the adjoint representation as [28]

$$(t^a)^{\bar{j}_1}_{i_1}(t^a)^{\bar{j}_2}_{i_2} = \delta^{\bar{j}_2}_{i_1}\delta^{\bar{j}_1}_{i_2} - \frac{1}{N_C}\delta^{\bar{j}_1}_{i_1}\delta^{\bar{j}_2}_{i_2} \ , \tag{13}$$

which can be represented pictorially as:

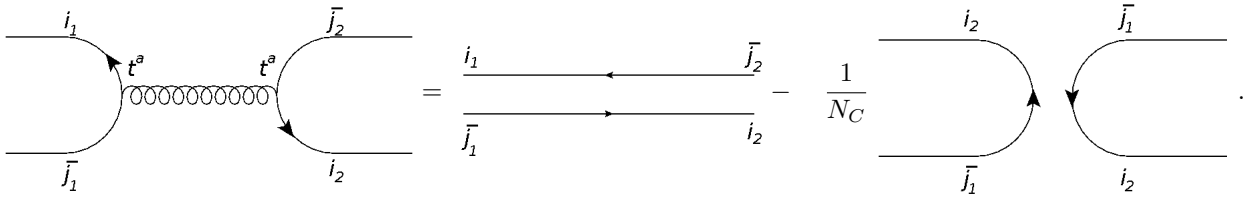

Before continuing we note that the $U(1)$ generator $(t^{a_{U(1)}})^{\bar{j}}_i$ is given by[3] [28]:

$$(t^{a_{U(1)}})^{\bar{j}}_i = \frac{1}{\sqrt{N_C}}\delta^{\bar{j}}_i \ , \tag{14}$$

and hence the second term of equation (13) is the product of two $U(1)$ generators. However since gluons do not carry $U(1)$ charge, and therefore do not couple to the $U(1)$ field, we are free to remove this second term in the all-gluon case. The Fierz identity for gluons is then:

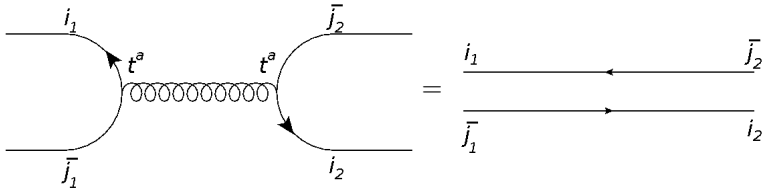

(15)

The standard Feynman rules for QCD (See Appendix B) entangle the colour and kinematic components of the amplitude. We wish to decouple the colour from the kinematics. To do so we first consider just the colour

[3]The $U(1)$ field is often called the photon, but in this case it is not strictly true. This $U(1)$ field is a photon field with QCD coupling strength.

component of the all-gluon 3-vertex:

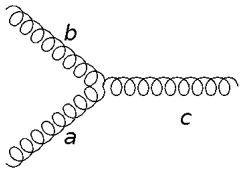

$$= f^{abc} = -\frac{i}{\sqrt{2}}(\mathrm{Tr}(t^a t^b t^c) - \mathrm{Tr}(t^a t^c t^b)) \,, \tag{16}$$

where we used equation (8) on the right-hand side. The traces can be represented pictorially as:

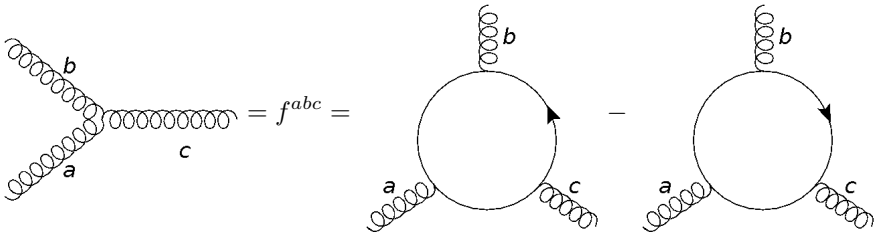

(17)

where closed circles with an arrow represent a trace. Now we have all of the tools required to factorise the colour from the full amplitude, and we are ready to tackle this example. Consider just the colour of the first Feynman diagram in Figure 1. Using equation (17) we can decompose the colour of this diagram into a sum of four traces:

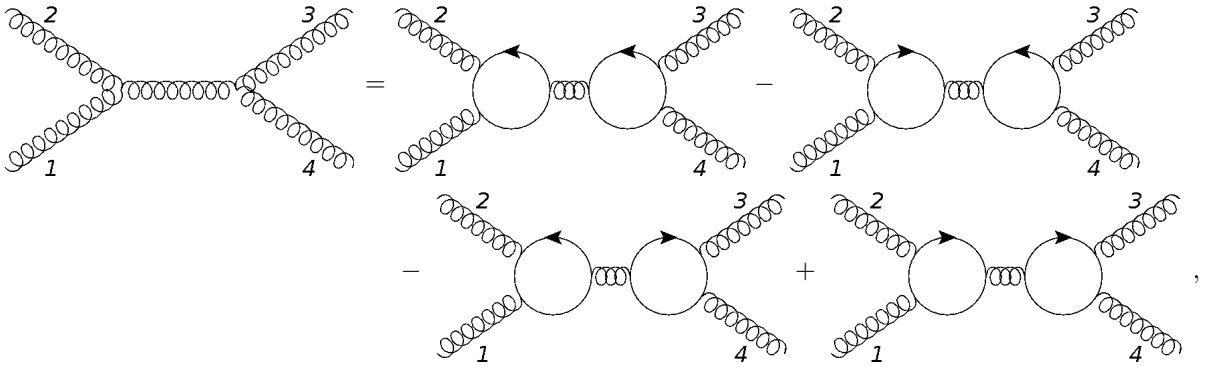

(18)

where the numbers indicate the colours, polarisations and momenta of the particles as per equation (12), and the direction of the arrow is given by equation (17). Notice that the propagator in each term is just the left hand side of equation (15). Therefore we rewrite the colour structure of the diagram as:

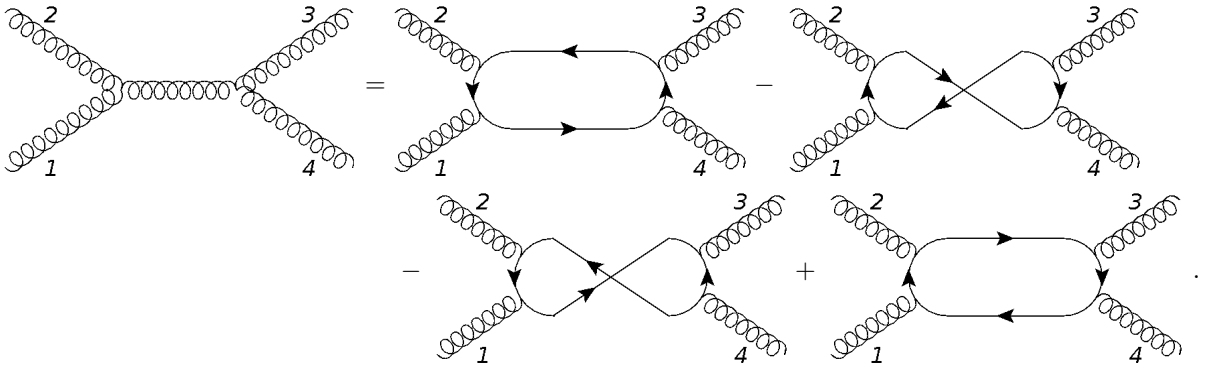

(19)

Note that the direction of the arrow is important, so for example the first and last terms are not equivalent. The final step is to untangle the middle two diagrams, and flip the last diagram so that the arrow in each trace points in the same direction. This step is mostly a visual one, so that we see exactly what order the gluons are colour

contracted. We get that:

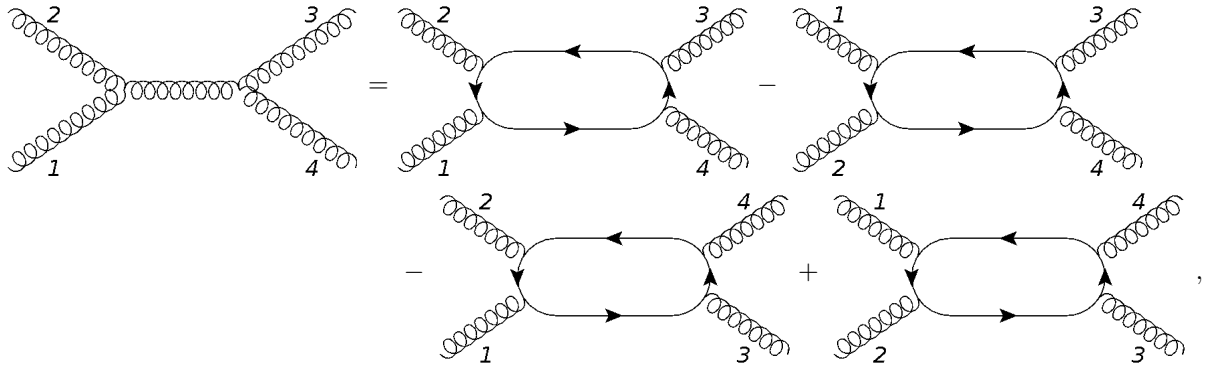

(20)

which is the sum of four independent traces of colour matrices. The relative minus signs are unimportant as they will be absorbed into the kinematic amplitudes. The two remaining non-cyclic permutations of the colour ordering can be obtained from the second diagram in Figure 1. By repeating the above steps on the second diagram we find that:

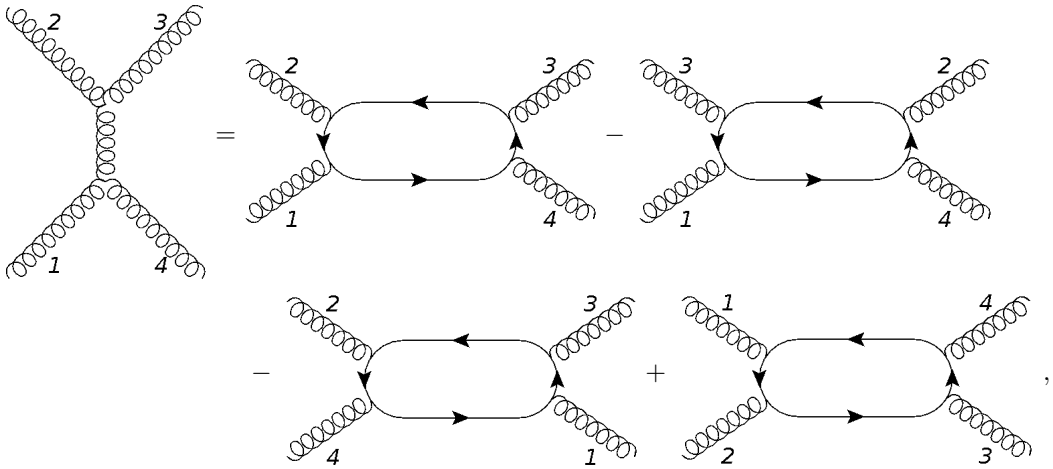

(21)

from which we obtain the remaining two independent non-cyclic permutations in colour space. Note that the third diagram in Figure 1 evaluates to zero (see section 2.5 for details) so does not need to be considered.

2.3.2 Squared all-gluon amplitudes

To calculate the scattering cross section we must first square the scattering amplitude and then sum over colours. This means that we will have to calculate:

$$|M_n(g_1, g_2, \ldots, g_n)|^2 = \sum_{\text{colours}} g_s^{2n-4} \sum_{\sigma_1 \in S_n/Z_n} \text{Tr}(t^{a_{\sigma_1(1)}} \ldots t^{a_{\sigma_1(n)}}) A_n(\sigma_1(k_1^{h_1}), \ldots, \sigma_1(k_n^{h_n})) \times \sum_{\sigma_2 \in S_n/Z_n} \text{Tr}(t^{b_{\sigma_2(1)}} \ldots t^{b_{\sigma_2(n)}})^* A_n(\sigma_2(k_1^{h_1}), \ldots, \sigma_2(k_n^{h_n}))^\dagger \ , \tag{22}$$

where each σ_i is a specific permutation of the colour-ordered gluons. We can represent equation (22) as a matrix equation of the form:

$$|M_n(g_1, g_2, \ldots, g_n)|^2 = g_s^{2n-4} A^\dagger_{\sigma_i} C_{ij} A_{\sigma_j} \ , \tag{23}$$

where C_{ij} is a colour matrix which relates the kinematic amplitude for gluons ordered by the permutation σ_i to the kinematic amplitude for gluons ordered by permutation σ_j. Before we calculate C_{ij} we note that:

$$[\text{Tr}(t^{a_{\sigma_1(1)}} t^{a_{\sigma_1(2)}} \ldots t^{a_{\sigma_1(n)}})]^* = \text{Tr}(t^{a_{\sigma_1(n)}} t^{a_{\sigma_1(n-1)}} \ldots t^{a_{\sigma_1(1)}}) \ , \tag{24}$$

and we introduce the notation:

$$\begin{aligned} (a_1 a_2 \ldots a_n) &= \text{Tr}(t^{a_{\sigma_1(1)}} t^{a_{\sigma_1(2)}} \ldots t^{a_{\sigma_1(n)}}) \ , \\ (b_1 b_2 \ldots b_n) &= \text{Tr}(t^{b_{\sigma_2(1)}} t^{b_{\sigma_2(2)}} \ldots t^{b_{\sigma_2(n)}}) \ , \end{aligned} \tag{25}$$

which means that the colour matrix C_{ij} can be re-written as:

$$C_{ij} = \sum_{a_1,\ldots,a_n=1}^{N_C^2-1} (a_1 a_2 \ldots a_n)(b_1 b_2 \ldots b_n)^* \ . \tag{26}$$

Since σ_2 is some permutation of σ_1, and since the trace is cyclic we can re-write equation (26) as:

$$C_{ij} = \sum_{a_1,\ldots,a_n=1}^{N_C^2-1} (a_1 a_2 \ldots a_n)(b_1 b_2 \ldots b_n)^* = \sum_{a_1,\ldots,a_{n-1}=1}^{N_C^2-1} \sum_{a_n} (a_1 a_2 \ldots a_n)(a_n a_{m_{n-1}} \ldots a_{m_1}) \ , \tag{27}$$

where $\{a_m\}$ is the remaining ordered set of t matrices in the σ_2 permutation. We can then write the traces in component notation and use the Fierz identity (equation (13)) to get that[4]:

$$\begin{aligned} C_{ij} &= \sum_{a_1,\ldots,a_{n-1}=1}^{N_C^2-1} \sum_{a_n} (a_1 a_2 \ldots a_n)(a_n a_{m_{n-1}} \ldots a_{m_1}) \\ &= \sum_{a_1,\ldots,a_{n-1}=1}^{N_C^2-1} \left[(a_1 a_2 \ldots a_{n-1} a_{m_{n-1}} \ldots a_{m_1}) - \frac{1}{N_C} (a_1 a_2 \ldots a_{n-1})(a_{m_{n-1}} \ldots a_{m_1}) \right] . \end{aligned} \tag{28}$$

The first term in the final line of equation (28) can have either of the following forms:

$$\sum_{\Lambda, a_{n-1}} (\Lambda_1 a_{n-1} a_{n-1} \Lambda_2) \ , \quad \text{or} \quad \sum_{\Lambda, a_{n-1}} (\Lambda_1 a_{n-1} \Lambda_2 a_{n-1}) \ ,$$

where Λ_i is some string of t matrices. Note that in the second expression it is likely that we have had to cyclically permute a_{n-1} to the final position, such that Λ_1 has more t matrices than Λ_2. If we have the first form, then we use equation (10) to get that:

$$\sum_{\Lambda, a_{n-1}} (\Lambda_1 a_{n-1} a_{n-1} \Lambda_2) = \sum_{\Lambda} (\Lambda_1 \Lambda_2) \ , \tag{29}$$

and if we have the second form then we again use the Fierz identity to get that:

$$\sum_{\Lambda, a_{n-1}} (\Lambda_1 a_{n-1} \Lambda_2 a_{n-1}) = \sum_{\Lambda} (\Lambda_1)(\Lambda_2) - \frac{1}{N_C} (\Lambda_1 \Lambda_2) \ . \tag{30}$$

We can keep doing this until we find terms proportional to:

$$(a_1 a_1) = \frac{N_C^2 - 1}{N_C} \delta_{ii} = N_C^2 - 1 \ , \tag{31}$$

which allows us to calculate the colour factors C_{ij}. Note that we used that in $SU(N_C)$ we must generalise C_F from $C_F = 8/3$ to $C_F = (N_C^2 - 1)/N_c$. Further note that the leading contribution to the colour matrix comes from the diagonal, i.e. when permutations $\sigma_1 = \sigma_2$. Following through with the algebra, it is possible to show that the leading contribution to the colour factor is [27]:

$$C_{ii} = \sum_{a_1,\ldots,a_n=1}^{N_C^2-1} (a_1 a_2 \ldots a_n)(a_1 a_2 \ldots a_n)^* = N_C^{n-2}(N_C^2 - 1)[1 + \mathcal{O}(1/N_C^2)] \ . \tag{32}$$

Finally, we note that the colour matrix C_{ij} is symmetric, since each vector A contains the same ordered set of gluon permutations σ, and that each diagonal term C_{ii} is identical since we sum over all colours and the order of contractions between t matrices is identical for each C_{ii}.

2.3.3 Quark-gluon amplitudes

At tree level, for a pair of massless quarks and $n-2$ gluons, it is sufficient to consider the basis in which all gluons propagate directly from a single quark anti-quark line such as in Figure 2 [2, 21, 27, 28, 42, 43]. To see why, consider

[4] A more complete derivation is shown in Appendix G.

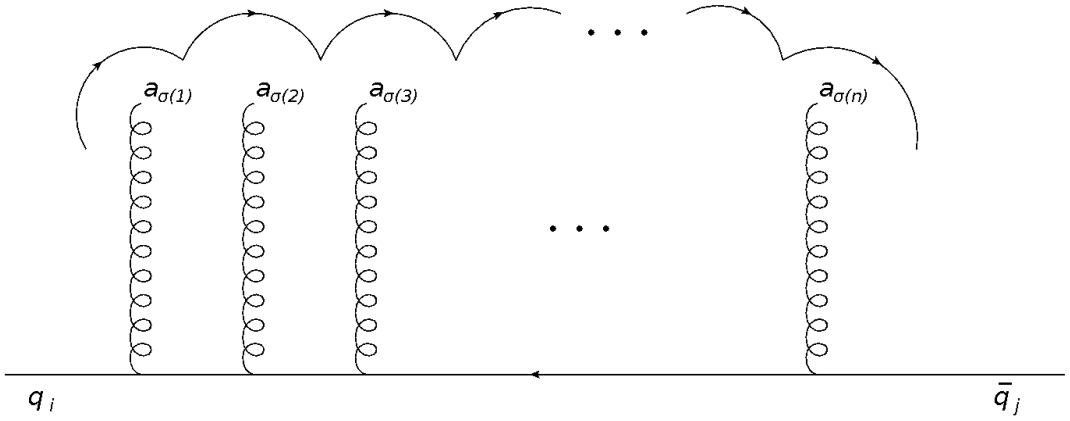

Figure 2: The structure of the quark anti-quark colour basis. The quark q has colour index i, the anti-quark $\bar{q}$ has colour index j, and the permutations over σ permute the order in which gluons are emitted (or equivalently the order in which they are colour connected). The curved lines above the diagram is the colour flow, i.e it shows which partons are colour connected.

the possible Feynman diagrams which can contribute to a given process. If a diagram has a three-gluon vertex connected to a quark line, then we use that:

$$i\sqrt{2}f^{abc}t_c = [t^a, t^b] \ , \tag{33}$$

which up to constants can be described pictorially as:

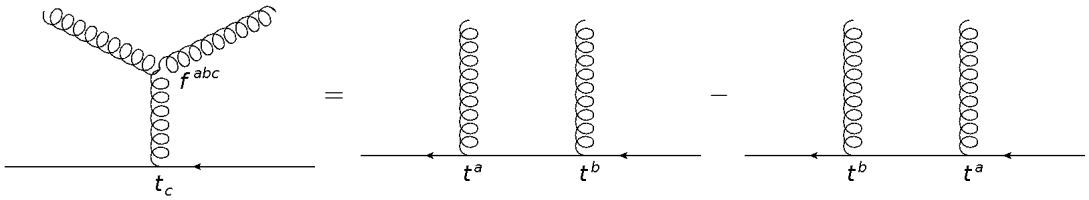

, (34)

and shows that any diagram with a three-gluon vertex can be decomposed into a colour basis in which the external gluons propagate directly from the quark line. The remaining type of diagram has a quark line which emits a gluon, which then emits 3 other gluons. The extra gluons may release more gluons, leading to a tree of gluons propagating off the quark line. The colour factor of this tree is:

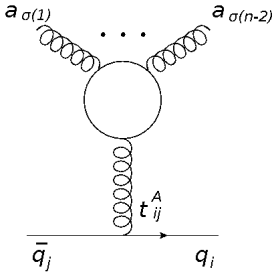

$$= t^A_{ij}\mathrm{Tr}\left[t^A(t^{a_{\sigma(1)}}\dots t^{a_{\sigma(n-2)}}\right] \ , \tag{35}$$

and we can use the Fierz identity (equation (13)) to show that:

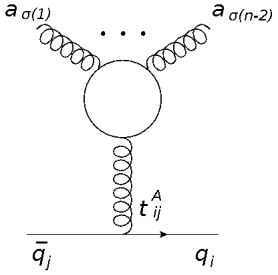

$$= t^A_{ij}t^A_{kl}t^{a_{\sigma(1)}}_{lm}\dots t^{a_{\sigma(n-2)}}_{nk} = \left(\delta_{il}\delta_{jk} - \frac{1}{N_C}\delta_{ij}\delta_{kl}\right)t^{a_{\sigma(1)}}_{lm}\dots t^{a_{\sigma(n-2)}}_{nk} \ .$$

However we know that the second term of the Fierz identity only couples to quarks, and the string of $t^{a_{\sigma(i)}}$ matrices is an all-gluon string, hence the second term in the brackets vanishes, leaving:

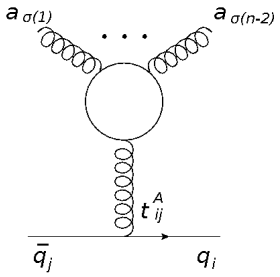

$$= (t^{a_{\sigma(1)}} \dots t^{a_{\sigma(n-2)}})_{ij} \ , \tag{36}$$

which is the same basis as before. Therefore, we can write any amplitude with a single quark pair and $n-2$ gluons in a basis with no gluon self coupling. We say that the colour order always starts at the quark, moves through the gluons, and ends at the anti-quark. The amplitude can be written as:

$$M_n(q, g_1, g_2, \dots g_{n-2}\bar{q}) = g_s^{n-2} \sum_{\sigma \in S_{n-2}} (t^{a_{\sigma(1)}} \dots t^{a_{\sigma(n-2)}})_{ij} A_n(q^{h_q} \sigma(k_1^{h_1}), \sigma(k_2^{h_2}) \dots, \sigma(k_{n-2}^{h_{n-2}}) \bar{q}^{h_{\bar{q}}}) \ , \tag{37}$$

where q, h_q, and i ($\bar{q}$, $h_{\bar{q}}$, and j) is the quark (anti-quark) momentum, helicity, and colour index, and all other symbols the same as equation (12). Note that in equation (37) it is only the gluons which are permuted, and the cyclic permutation is present.

2.3.4 Squared quark-gluon amplitudes

In the cross section we need to calculate the squared amplitude:

$$\begin{aligned}
&\sum_{\text{colours}} |M_n(q, g_1, g_2, \dots, \bar{q})|^2 \\
&\quad = g_s^{2n-4} \sum_{\text{colours}} \sum_{\sigma_1 \in S_{n-2}} (t^{a_{\sigma_1(1)}} \dots t^{a_{\sigma_1(n-2)}})_{ij} A_n(q^{h_q} \sigma_1(k_1^{h_1}), \sigma_1(k_2^{h_2}) \dots, \sigma_1(k_{n-2}^{h_{n-2}}) \bar{q}^{h_{\bar{q}}}) \\
&\qquad \times \sum_{\sigma_2 \in S_{n-2}} (t^{a_{\sigma_2(1)}} \dots t^{a_{\sigma_2(n-2)}})^\dagger_{ji} A_n(q^{h_q} \sigma_2(k_1^{h_1}), \sigma_2(k_2^{h_2}) \dots, \sigma_2(k_{n-2}^{h_{n-2}}) \bar{q}^{h_{\bar{q}}})^\dagger \ ,
\end{aligned} \tag{38}$$

where σ_1 and σ_2 are two permutations of the $n-2$ gluons. Note that we can once again write this as the matrix equation:

$$\sum_{\text{colours}} |M_n(q, g_1, g_2, \dots, \bar{q})|^2 = g_s^{2n-4} A^\dagger_{\sigma_i} C_{ij} A_{\sigma_j} \ , \tag{39}$$

where σ_i and σ_j are two permutations of the gluons. Further note that the colour matrix C_{ij} is once again symmetric, and that each diagonal term C_{ii} is once again identical since we sum over all colours and the order of contractions between t matrices is identical C_{ii}. For example, in the two-gluon case, there are two distinct terms in the colour matrix. Either the two permutations are the same, in which case we calculate $C_{11} = C_{22}$, or they are different in which case we calculate $C_{12} = C_{21}$. If they are the same, we see that the colour factor can be written as:

$$\begin{aligned}
C_{11} = C_{22} &= \sum_{a_1, a_2 = 1}^{N_C^2 - 1} (t^{a_1})_{ij} (t^{a_2})_{jk} [(t^{a_1})_{kl} (t^{a_2})_{li}]^\dagger \\
&= \sum_{a_1, a_2 = 1}^{N_C^2 - 1} (t^{a_1})_{ij} (t^{a_2})_{jk} (t^{a_2})_{kl} (t^{a_1})_{li} \\
&= \sum_{a_1 = 1}^{N_C^2 - 1} \frac{N_C^2 - 1}{N_C} \delta_{jl} (t^{a_1})_{ij} (t^{a_1})_{li} \\
&= \frac{(N_C^2 - 1)^2}{N_C} = \frac{64}{3} \ ,
\end{aligned} \tag{40}$$

where in the second line we used that the t matrices are Hermitian, and used equation (10) in the next two lines. Similarly, we can show that the off-diagonal element is:

$$\begin{aligned} C_{12} = C_{21} = &\sum_{a_1,a_2=1}^{N_C^2-1} (t^{a_1})_{ij}(t^{a_2})_{jk}(t^{a_1})_{kl}(t^{a_2})_{li} \\ =&(t^{a_2})_{jk}(t^{a_2})_{li}[\delta_{il}\delta_{jk} - \frac{1}{N_C}\delta ij\delta_{kl}] \\ =&(t^{a_2})_{kk}(t^{a_2})_{ll} - \frac{1}{N_C}(t^{a_2})_{ik}(t^{a_2})_{ki} \\ =&0 - \frac{N_C^2-1}{N_C} = -\frac{8}{3} \ , \end{aligned} \tag{41}$$

where we used the Fierz identity (equation (13)) in the third line, and the tracelessness of the t matrices along with equation (10) in the last line. We therefore have that:

$$\sum_{\text{colours}} |M_4(q, g_1, g_2, \bar{q})|^2 = g_s^4 \begin{pmatrix} A_4(1,2)^* & A_4(2,1)^* \end{pmatrix} \frac{1}{3} \begin{pmatrix} 64 & -8 \\ -8 & 64 \end{pmatrix} \begin{pmatrix} A_4(1,2) \\ A_4(2,1) \end{pmatrix} \ , \tag{42}$$

where $A_4(1,2)$ is shorthand for $A_4(q^{h_q}, g(k_1^{h_1}), g(k_2^{h_2}), \bar{q}^{h_q})$. More colour matrices are given in Appendix H.

2.4 Spinor-helicity formalism

We now wish to move from colour factors to kinematic amplitudes. While most calculations in high energy physics use the four-component Dirac spinors [44,45] which describe quarks and charged leptons, MHV amplitudes are often best described using two-component Weyl-van der Waerden spinors[5] (commonly known as and hereafter referred to as Weyl spinors) [46,47]. Weyl spinors are described using a different algebra to Dirac spinors, hence it is useful to first describe this algebra, which we will do in section 2.4.1. In Section 2.4.2 we explain how to use Weyl-spinor algebra to build spinor inner products, which are the building blocks used to calculate MHV amplitudes in sections 2.5 and 2.7.

2.4.1 Weyl-spinor algebra

We will use indices in the middle of the Greek alphabet ($\mu, \nu, \rho, ... = 0, 1, 2, 3$) to indicate spacetime indices[6], while indices from the start of the Greek alphabet ($\alpha, \beta, \gamma, ... = 1, 2$) are spinor indices. A right-handed spinor is associated with undotted spinor indices, while a left-handed spinor has dotted spinor indices. It is important to distinguish between the two types of indices because they represent two separate representations of the Lorentz group and therefore it is not possible to contract a dotted index with an undotted index to form a Lorentz invariant quantity [49]. A right-hand massless spinor is defined as [2,28]:

$$U_+(k_i) \equiv |i^+\rangle \equiv (\lambda_i)_\alpha = \begin{pmatrix} \sqrt{k_i^+} \\ e^{i\phi_i} \end{pmatrix} \ , \tag{43}$$

$$\overline{U}_-(k_i) \equiv \langle i^-| \equiv (\lambda_i)^\alpha = \begin{pmatrix} e^{i\phi_i} & -\sqrt{k_i^+} \end{pmatrix} \ , \tag{44}$$

where $U_+(k_i)$ is a four-component Dirac spinor with four-momentum k_i, $(\lambda_i)_\alpha$ is the same particle in the two-component Weyl-spinor formalism, $k^+ = k^0 + k^3$ where the raised index for each k is the spacetime index, and:

$$e^{\pm i\phi_i} = \frac{k_i^1 \pm ik_i^2}{\sqrt{k_i^+}} \ . \tag{45}$$

Note that in matrix notation a lowered undotted index is a row index (i.e. it implies that λ_α is a column vector), while a raised undotted index is a column index. Further note that if $k_i^+ = 0$, then $k_i^1 = k_i^2 = 0$ (since $k^2 = 0$),

[5] Both Weyl and van der Waerden independently decomposed the Dirac equation into two coupled differential equations of 2 two-spinors, however in the literature it is usually only Weyl who is given this credit. Indeed it was van der Waerden who first investigated the application of tensor calculus to spinor analysis and introduced the notation of dotted and undotted indices described in section 2.4.1.

[6] for a pedagogical treatment of spacetime indices see the textbook by Riley, Hobson and Bence [48].

and naively we have that $e^{i\phi_i} = 0/0$. In this case we must instead use the well-known formula for a right-handed particle moving along the z axis:

$$U_+(k_i) \equiv |i^+\rangle \equiv (\lambda_i)_\alpha = \begin{pmatrix} 0 \\ \sqrt{2E_i} \end{pmatrix} \ , \tag{46}$$

$$\overline{U}_-(k_i) \equiv \langle i^-| \equiv (\lambda_i)^\alpha = \begin{pmatrix} \sqrt{2E_i} & 0 \end{pmatrix} \ . \tag{47}$$

Similarly, a left-handed massless spinor is defined as:

$$\overline{U}_+(k_i) \equiv \langle i^+| \equiv (\tilde{\lambda}_i)_{\dot{\alpha}} = \begin{pmatrix} e^{-i\phi_i} & -\sqrt{k_i^+} \end{pmatrix} \ , \tag{48}$$

$$U_-(k_i) \equiv |i^-\rangle \equiv (\tilde{\lambda}_i)^{\dot{\alpha}} = \begin{pmatrix} \sqrt{k_i^+} \\ e^{-i\phi_i} \end{pmatrix} \ , \tag{49}$$

or if $k_i^+ = 0$, then we similarly have:

$$\overline{U}_+(k_i) \equiv \langle i^+| \equiv (\tilde{\lambda}_i)_{\dot{\alpha}} = \begin{pmatrix} -\sqrt{2E_i} & 0 \end{pmatrix} \ , \tag{50}$$

$$U_-(k_i) \equiv |i^-\rangle \equiv (\tilde{\lambda}_i)^{\dot{\alpha}} = \begin{pmatrix} 0 \\ -\sqrt{2E_i} \end{pmatrix} \ . \tag{51}$$

Note that for dotted indices, a raised index is a row index, while a lowered dotted index is a column index. Further note that $(\tilde{\lambda}_i)_{\dot{\alpha}} = [(\lambda_i)_\alpha]^\dagger = [(\lambda_i)^\alpha]^*$. Spinor indices are raised or lowered using the two-index antisymmetric Levi-Cevita symbol:

$$\epsilon^{12} = -\epsilon^{21} = -\epsilon_{12} = \epsilon_{21} = 1 \ , \tag{52}$$

which written in matrix notation is:

$$\epsilon^{\alpha\beta} = \begin{pmatrix} 0 & 1 \\ -1 & 0 \end{pmatrix} \quad \text{and} \quad \epsilon_{\alpha\beta} = \begin{pmatrix} 0 & -1 \\ 1 & 0 \end{pmatrix} \ . \tag{53}$$

Note that the Levi-Cevita symbol is sometimes referred to as the spinor metric, or just the epsilon, and that some epsilon identities are included in Appendix A. Also note that in raising or lowering a spinor index, adjacent indices are summed over when multiplied on the left by the appropriate spinor metric. Thus one can write:

$$\lambda_\alpha = \left[\epsilon_{\alpha\beta}\lambda^\beta\right]^T \quad \text{and} \quad \lambda^\alpha = \left[\epsilon^{\alpha\beta}\lambda_\beta\right]^T \ , \tag{54}$$

$$\tilde{\lambda}_{\dot{\alpha}} = \left[\epsilon_{\dot{\alpha}\dot{\beta}}\tilde{\lambda}^{\dot{\beta}}\right]^T \quad \text{and} \quad \tilde{\lambda}^{\dot{\alpha}} = \left[\epsilon^{\dot{\alpha}\dot{\beta}}\tilde{\lambda}_{\dot{\beta}}\right]^T \ , \tag{55}$$

where we have included the transpose sign to make it explicit that raising or lowering a spinor index changes a row vector to a column vector and vice versa.

We construct Lorentz invariant objects by first contracting spinor indices to make objects that transform as Lorentz tensors [49]. A Lorentz scalar is created by taking the spinor inner product (see section 2.4.2), a Lorentz vector is obtained using the Pauli matrices in spinor notation, while higher rank Lorentz tensors are outside the scope of this thesis. We first consider Lorentz vectors. The Pauli matrices (see Appendix A) can be written in spinor notation as:

$$\begin{aligned} (\sigma^\mu)^{\dot{\beta}\alpha} \equiv \overline{\sigma}^\mu \equiv \sigma_+ &= (\mathbb{1}_{2\times 2}, -\vec{\boldsymbol{\sigma}}) \ , \\ (\sigma^\mu)_{\alpha\dot{\beta}} \equiv \sigma^\mu \equiv \sigma_- &= (\mathbb{1}_{2\times 2}, \vec{\boldsymbol{\sigma}}) \ , \end{aligned} \tag{56}$$

and are used to construct both Lorentz vectors and Lorentz scalars. Each Lorentz vector A^μ has a one-to-one correspondence with its bi-spinor $\not{A}_{\alpha\dot{\beta}}$ [47, 50, 51] such that:

$$A^\mu = \frac{1}{2}(\sigma^\mu)^{\dot{\beta}\alpha}\not{A}_{\alpha\dot{\beta}} \ , \quad \text{and} \quad \not{A}_{\alpha\dot{\beta}} = A^\mu(\sigma_\mu)_{\alpha\dot{\beta}} \ , \tag{57}$$

hence the Pauli matrices are the analogue of the Dirac matrices in two-component notation. Note that the bi-spinors are 2×2 matrices, such that:

$$(\not{A}^T)_{\alpha\dot{\beta}} = \not{A}_{\beta\dot{\alpha}} \ , \tag{58}$$

$$\not{A}_{\alpha\dot{\beta}} = (\not{A}_{\dot{\alpha}\beta})^* \ , \tag{59}$$

$$(\not{A}^\dagger)_{\alpha\dot{\beta}} = (\not{A}_{\beta\dot{\alpha}})^* \ , \tag{60}$$

where equation (59) shows that changing between dotted and undotted indices is equivalent to complex conjugating each term. Also, if $\not{A}$ is Hermitian, then $\not{A} = \not{A}^\dagger$, or equivalently $\not{A}_{\alpha\dot{\beta}} = \not{A}_{\dot{\alpha}\beta}$. Using this we can manoeuvre between the four-momentum k^μ and its bi-spinor $\not{k}_{\alpha\dot{\alpha}}$:

$$(\not{k}_i)_{\alpha\dot{\alpha}} = k_i^\mu(\sigma_\mu)_{\alpha\dot{\alpha}} = (\lambda_i)_\alpha(\tilde{\lambda}_i)_{\dot{\alpha}} = \begin{pmatrix} k_i^+ & k_i^1 - ik_i^2 \\ k_i^1 + ik_i^2 & k_i^- \end{pmatrix} , \tag{61}$$

where $k_i^- = k_i^0 - k_i^3$. It is useful to also have an expression for $(\not{k}_i)^{\dot{\alpha}\alpha}$:

$$(\not{k}_i)^{\dot{\alpha}\alpha} = k_i^\mu(\sigma_\mu)^{\dot{\alpha}\alpha} = \tilde{\lambda}^{\dot{\alpha}}\lambda^\alpha = \begin{pmatrix} k^- & -k^1 + ik^2 \\ -k^1 - ik^2 & k^+ \end{pmatrix} . \tag{62}$$

Note that $\det\left[(\not{k}_i)^{\dot{\alpha}\alpha}\right] = \det\left[(\not{k}_i)_{\alpha\dot{\alpha}}\right] = 0$. To move the other way, we use:

$$2k_i^\mu = (\sigma^\mu)^{\dot{\alpha}\alpha}(\not{k}_i)_{\alpha\dot{\alpha}} = (\sigma^\mu)^{\dot{\alpha}\alpha}(\lambda_i)_\alpha(\tilde{\lambda}_i)_{\dot{\alpha}} = (\tilde{\lambda}_i)_{\dot{\alpha}}(\sigma^\mu)^{\dot{\alpha}\alpha}(\lambda_i)_\alpha \equiv \langle i^+|\gamma^\mu|i^+\rangle . \tag{63}$$

Similarly, we also have that:

$$2k_i^\mu = (\lambda_i)^\alpha(\sigma^\mu)_{\alpha\dot{\alpha}}(\tilde{\lambda}_i)^{\dot{\alpha}} \equiv \langle i^-|\gamma^\mu|i^-\rangle . \tag{64}$$

It follows that there are 4 Dirac equations in two-component notation:

$$\langle i^\mp|k\cdot\sigma_\pm = 0 \quad \text{and} \quad k\cdot\sigma_\pm|i^\mp\rangle \ = 0, \tag{65}$$

Or equivalently:

$$\not{k}_{\alpha\dot{\alpha}}\tilde{\lambda}^{\dot{\alpha}} = 0 , \quad \lambda^\alpha\not{k}_{\alpha\dot{\alpha}} = 0 , \quad \not{k}^{\dot{\alpha}\alpha}\lambda_\alpha = 0 , \quad \tilde{\lambda}_{\dot{\alpha}}\not{k}^{\dot{\alpha}\alpha} = 0 . \tag{66}$$

Finally, it is useful to know some relations between $(\sigma^\mu)_{\alpha\dot{\alpha}}$ and $(\sigma^\mu)^{\dot{\beta}\beta}$:

$$(\sigma^\mu)_{\alpha\dot{\alpha}} = \epsilon_{\alpha\beta}\epsilon_{\dot{\alpha}\dot{\beta}}(\sigma^\mu)^{\dot{\beta}\beta} , \qquad (\sigma^\mu)^{\dot{\alpha}\alpha} = \epsilon^{\alpha\beta}\epsilon^{\dot{\alpha}\dot{\beta}}(\sigma^\mu)_{\beta\dot{\beta}} , \tag{67}$$

$$\epsilon^{\alpha\beta}(\sigma^\mu)_{\beta\dot{\alpha}} = \epsilon_{\dot{\alpha}\dot{\beta}}(\sigma^\mu)^{\dot{\beta}\alpha} , \qquad \epsilon^{\dot{\alpha}\dot{\beta}}(\sigma^\mu)_{\alpha\dot{\beta}} = \epsilon_{\alpha\beta}(\sigma^\mu)^{\dot{\alpha}\beta} , \tag{68}$$

along with the Fierz identities:

$$(\sigma^\mu)_{\alpha\dot{\alpha}}(\sigma_\mu)^{\dot{\beta}\beta} = 2\delta_\alpha{}^\beta\delta^{\dot{\beta}}{}_{\dot{\alpha}} , \tag{69}$$

$$(\sigma^\mu)_{\alpha\dot{\alpha}}(\sigma_\mu)_{\beta\dot{\beta}} = 2\epsilon_{\alpha\beta}\epsilon_{\dot{\alpha}\dot{\beta}} , \tag{70}$$

$$(\sigma^\mu)^{\dot{\alpha}\alpha}(\sigma_\mu)^{\dot{\beta}\beta} = 2\epsilon^{\alpha\beta}\epsilon^{\dot{\alpha}\dot{\beta}} , \tag{71}$$

where we wrote the Kronecker delta as $\delta_\alpha{}^\beta$ to show explicitly which index is the row index and which the column index. This separation is useful when it is necessary to remember the origin of the indices.

2.4.2 Spinor inner products

To create a Lorentz scalar from Weyl spinors we need to contract the indices to form an inner product. Spinor inner products are the building blocks from which helicity amplitudes, and ultimately the MHV amplitudes upon which this thesis is based, are created. Due to the two types of spinor indices, there are two types of inner products. The first type, using undotted indices is defined as[7]:

$$\langle ij\rangle = \langle i^-|j^+\rangle = (\lambda_i)^\alpha(\lambda_j)_\alpha = \epsilon^{\alpha\beta}(\lambda_i)_\beta(\lambda_j)_\alpha = -(\lambda_i)_\alpha(\lambda_j)^\alpha . \tag{72}$$

It is useful for numerical calculations to have an expression for $\langle ij\rangle$ in terms of four-momenta. To do this, combine the definitions of λ (equations (43) and (44)) with equation (72) to get that:

$$\langle ij\rangle = \sqrt{k_j^+}e^{i\phi_i} - \sqrt{k_i^+}e^{i\phi_j} , \tag{73}$$

[7]Our definition of $\langle ij\rangle$ follows the old convention as found in [28]. In the new convention (which can be found in [16] and [2]), the undotted inner product is defined as $\langle ij\rangle = (\lambda_i)_\alpha(\lambda_j)^\alpha$. To move between the two conventions one must multiply each factor of $\langle ij\rangle$ by -1 in every equation, or swap the upstairs and downstairs indices if working in the spinor index notation.

where $e^{i\phi_i}$ and k^+ are defined as before. In the special case that $k_i^+ = 0$, we must substitute equations (47) and (43) into equation (72) to get:

$$\langle ij\rangle = \sqrt{2E_i k_j^+}\ , \tag{74}$$

while in the special case that both particles are parallel, such that $k_j = zk_i$ for some (real) factor z, we have that:

$$\langle ij\rangle = \langle i(zi)\rangle = \sqrt{z}\left[\sqrt{k_i^+}e^{i\phi_i} - \sqrt{k_i^+}e^{i\phi_i}\right] = 0\ . \tag{75}$$

We therefore conclude that the inner product of two parallel spinors vanishes[8]. Similarly, the dotted inner product is defined as:

$$[ij] = \langle i^+|j^-\rangle = (\tilde{\lambda}_i)_{\dot{\alpha}}(\tilde{\lambda}_j)^{\dot{\alpha}} = \epsilon^{\dot{\alpha}\dot{\beta}}(\tilde{\lambda}_i)_{\dot{\alpha}}(\tilde{\lambda}_j)_{\dot{\beta}} = -(\tilde{\lambda}_i)^{\dot{\alpha}}(\tilde{\lambda}_j)_{\dot{\alpha}}\ . \tag{76}$$

Combining equations (48), (49) and (76) gives the numerical form of $[ij]$:

$$[ij] = \sqrt{k_i^+}e^{-i\phi_j} - \sqrt{k_j^+}e^{-i\phi_i}\ , \tag{77}$$

while for the special case $k_i^+ = 0$ we have:

$$[ij] = -\sqrt{2E_i k_j^+}\ , \tag{78}$$

and the collinear case again vanishes. From equations (73) and (77) it is immediately obvious that:

$$\langle ij\rangle = [ji]^*\ , \tag{79}$$
$$\langle ij\rangle = -\langle ji\rangle\ , \tag{80}$$
$$[ij] = -[ji]\ , \tag{81}$$
$$\langle ii\rangle = [ii] = 0\ , \tag{82}$$

where equations (80) - (82) show that the inner products are anti-symmetric. Using equations (63), (64) and (69) it is possible to construct the momentum invariant $s_{ij} = (k_i + k_j)^2 = 2k_i \cdot k_j$ in terms of spinor inner products[9]:

$$s_{ij} = 2k_i \cdot k_j = \langle ij\rangle[ji]\ , \tag{83}$$

and combining equation (83) with equation (79) gives that:

$$s_{ij} = \langle ij\rangle\langle ij\rangle^* = [ij][ij]^* = |\langle ij\rangle|^2 = |[ij]|^2\ .$$

Hence we can re-write the inner products as complex square roots of the momentum-invariant:

$$\langle ij\rangle = \sqrt{|s_{ij}|}e^{i\phi_{ij}}\ , \qquad [ij] = -\sqrt{|s_{ij}|}e^{-i\phi_{ij}}\ , \tag{84}$$

for some phase ϕ_{ij}. Other useful properties of the inner product include charge conjugation:

$$\langle i^+|\gamma^\mu|j^+\rangle = \langle j^-|\gamma^\mu|i^-\rangle\ , \tag{85}$$

or equivalently:

$$(\tilde{\lambda}_i)_{\dot{\alpha}}(\sigma^\mu)^{\dot{\alpha}\alpha}(\lambda_j)_\alpha = (\lambda_j)^\alpha(\sigma^\mu)_{\alpha\dot{\alpha}}(\tilde{\lambda}_i)^{\dot{\alpha}}\ ; \tag{86}$$

the Fierz rearrangement:

$$\begin{aligned}\langle i^+|\gamma^\mu|j^+\rangle\langle k^+|\gamma_\mu|l^+\rangle &\equiv (\tilde{\lambda}_i)_{\dot{\alpha}}(\sigma^\mu)^{\dot{\alpha}\alpha}(\lambda_j)_\alpha(\tilde{\lambda}_k)_{\dot{\beta}}(\sigma_\mu)^{\dot{\beta}\beta}(\lambda_l)_\beta = 2[ik]\langle lj\rangle\ ,\\ \langle i^-|\gamma^\mu|j^-\rangle\langle k^-|\gamma_\mu|l^-\rangle &\equiv (\lambda_i)^\alpha(\sigma^\mu)_{\alpha\dot{\alpha}}(\tilde{\lambda}_i)^{\dot{\alpha}}(\lambda_k)^\beta(\sigma_\mu)_{\dot{\beta}\beta}(\tilde{\lambda}_l)^{\dot{\beta}} = 2[kj]\langle il\rangle\ ;\end{aligned} \tag{87}$$

and the Schouten identities:

$$\langle ij\rangle\langle kl\rangle = \langle ik\rangle\langle jl\rangle + \langle il\rangle\langle kj\rangle\ , \tag{88}$$
$$[ij][kl] = [ik][jl] + [il][kj]\ , \tag{89}$$
$$\langle i^-|\not{k}_m|j^-\rangle = \langle im\rangle[mj]\ , \tag{90}$$
$$\langle i^+|\not{k}_m|j^+\rangle = [jm]\langle mj\rangle\ . \tag{91}$$

[8]Note that this is a very important result which leads to the collinear singularity of QFT, as we shall see in section 3.2.

[9]For a full derivation of equation (83), as well as equations (85), (87), (88) and (90) see appendix C.

2.5 All-gluon helicity amplitudes

We now have all of the tools needed to calculate any helicity amplitude, and specifically to calculate the MHV amplitude. To apply the spinor-helicity formalism to gluons we must associate the gluon polarisation with its helicity. We can do this because a gluon is massless, hence it has no longitudinal polarisation, and its spin is either aligned or anti-aligned with its motion. The gluon polarisation vector ϵ is best given by[10]

$$\epsilon_\mu^\pm(k,p) = \pm\frac{\langle k^\pm|\gamma^\mu|p^\pm\rangle}{\sqrt{2}\langle p^\mp|k^\pm\rangle} \ , \tag{92}$$

where k is the gluon momentum, p is a reference momentum which we are free to choose (so long as the spinor $|p^\pm\rangle$ obeys the massless Dirac equation $\not{p}|p^\pm\rangle = 0$), and the spinors are defined in equations (43) - (49). Note that the polarisation vector is gauge invariant, i.e. we can choose a different reference momentum p for each gluon. It is easy to show that equation (92) is indeed the polarisation. Firstly, the polarisation is always transverse:

$$\epsilon_\mu^\pm(k,p)\ k^\mu = \pm\frac{\langle k^\pm|\not{k}|p^\pm\rangle}{\sqrt{2}\langle p^\mp|k^\pm\rangle} = 0 \ , \tag{93}$$

which follows from the Dirac equation $\langle k^\pm|\not{k} = 0$. The polarisation is also an orthonormal basis:

$$\epsilon^\pm(k,p)\cdot\epsilon^\pm(k,p) = \epsilon^\pm(k,p)\cdot(\epsilon^\mp(k,p))^* = 0 \ , \tag{94}$$

$$\epsilon^\pm(k,p)\cdot(\epsilon^\pm(k,p))^* = -1 \ , \tag{95}$$

which can both be proven using the Fierz rearrangement (equation (87)).

Now that we know how to describe the polarisation of each gluon, we can consider the different choices of reference momentum p. In every all-gluon helicity amplitude we must contract the polarisation vectors either with a propagator momentum, or with another polarisation vector. It is convenient to choose reference momenta of like-helicity gluons to be the same, and to coincide with the momentum of an opposite-helicity gluon. This is because:

$$\epsilon^\pm(k,p)\cdot\epsilon^\pm(k',p) = \epsilon^\pm(k,p)\cdot\epsilon^\mp(p,p') = 0 \ . \tag{96}$$

Similarly, it is convenient to choose the reference momenta to be the propagator momentum, or external quark momentum, since:

$$\epsilon^\pm(k,p)\cdot p = 0 \ , \tag{97}$$

which vanishes because the reference momentum must obey the massless Dirac equation. We will now show that equations (96) and (97) imply that many helicity amplitudes vanish. First, consider the 4-gluon process shown in Figure 1. Let each gluon have the same helicity such that we want to solve $A_4(1^\pm,2^\pm,3^\pm,4^\pm)$. Choose the reference momentum of each particle to be p. Using the colour-ordered Feynman rules (see Appendix B) and equation (96) we see that every term must have $\epsilon^\pm(k_i,p)\cdot\epsilon^\pm(k_j,p) = 0$, and hence the helicity amplitude vanishes.

Similarly, we can show that if all but one particle has the same helicity then the helicity amplitude vanishes. In this case we solve $A_4(1^\mp,2^\pm,3^\pm,4^\pm)$, and choose reference momentum $p_1 = k_2$, and $p_i = k_1$ for $i = 2,3,4$. Each term has either $\epsilon^\mp(k_1,k_2)\cdot\epsilon^\pm(k_i,k_1) = 0$, or $\epsilon^\pm(k_i,k_1)\cdot\epsilon^\pm(k_j,k_1) = 0$ for $j = 2,3,4,\ j \neq i$. This argument also holds for all permutations of the gluons such that, e.g. $A_4(4^\pm,2^\mp,3^\pm,1^\pm)$ also vanishes. Note that this vanishing property is not exclusive to a 4-gluon amplitude. This argument still holds for the n-gluon amplitude, hence:

$$A_n(1^\pm,2^\pm,3^\pm,\dots n^\pm) = 0 \tag{98}$$

$$A_n(1^\mp,2^\pm,3^\pm,\dots n^\pm) = 0 \ . \tag{99}$$

The only remaining 4-gluon helicity amplitude up to permutations is $A_4(1^\mp,2^\mp,3^\pm,4^\pm)$. For simplicity we will restrict ourselves to carefully calculating the helicity amplitude for $A_4(1^-,2^-,3^+,4^+)$. The physical process we are considering is:

$$g^+(-k_1)g^+(-k_2) \to g^+(k_3)g^+(k_4) \ , \tag{100}$$

and the relevant diagrams shown in Figure 3. Note that the colour order is 1234 and that the first two particles are considered incoming, so their helicities have been flipped, and their momenta are negative so that momentum conservation takes the crossed form:

$$k_1 + k_2 + k_3 + k_4 = 0 \ . \tag{101}$$

[10] A more complete discussion of the polarisation vector, including a derivation of equations (92) - (96) is given in Appendix D.

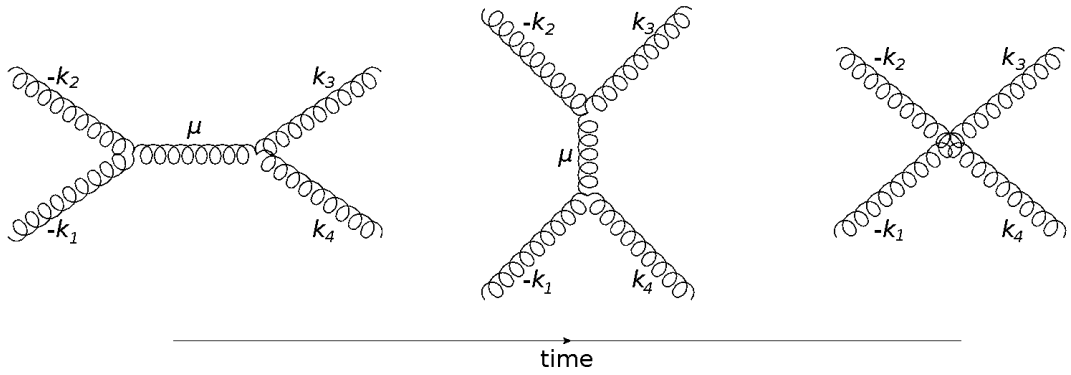

Figure 3: The three diagrams with colour order 1234 contributing to $g^+(-k_1)g^+(-k_2) \to g^+(k_3)g^+(k_4)$. Particles on the left side of a vertex are considered ingoing. Note that the fourth $gg \to gg$ diagram does not have the correct colour order, hence is not shown.

Written more carefully, the helicity amplitude for this process is:

$$\mathcal{A}\left(g^+(-k_1)g^+(-k_2) \to g^+(k_3)g^+(k_4)\right) = A_4\left((k_1)^-, (k_2)^-, (k_3)^+, (k_4)^+\right) \equiv A_4(1^-, 2^-, 3^+, 4^+) \ . \tag{102}$$

To calculate this helicity amplitude choose the reference momenta $p_1 = p_2 = k_4$ and $p_3 = p_4 = k_1$. Equation (96) implies that the only non-zero ϵ contraction is $\epsilon^{\mp}(k_2, k_4) \cdot \epsilon^{\pm}(k_3, k_1) \equiv \epsilon_2 \cdot \epsilon_3$. The third diagram in Figure 3 is still zero because each term contains at least one of the vanishing ϵ contractions. The bottom vertex of the middle diagram is given by:

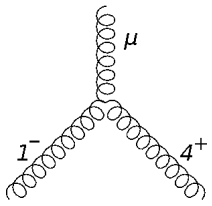

$$= \quad \epsilon_1^- \cdot \epsilon_4^+ (k_1 - k_4)^\mu + \epsilon_1^\mu (-2k_1 - k_4) \cdot \epsilon_4^+ + \epsilon_4^\mu (2k_4 + k_1) \cdot \epsilon_1^- = 0 \ , \tag{103}$$

where each term individually is 0. The first term is trivially 0 by construction of our reference momenta (equation (96)). The second term has two separate contractions, $\epsilon_4 \cdot k_1$ and $\epsilon_4 \cdot k_4$ which are both 0 due to the Dirac equation $\not{k}_i |k_i^\pm\rangle = 0$. To see this, substitute the definition of the polarisation vector (equation (92)) into the contraction $\epsilon_4 \cdot k_1$. This gives that:

$$\epsilon^+(k_4, k_1) \cdot k_1 = \frac{\langle k_4^+ | \gamma^\mu | k_1^+ \rangle}{\sqrt{2}\langle k_1^- | k_4^+ \rangle} \ (k_1)_\mu = \frac{\langle k_4^+ | \not{k}_1 | k_1^+ \rangle}{\sqrt{2}\langle k_1^- | k_4^+ \rangle} = 0 \ . \tag{104}$$

This can be done for each of the remaining terms on the right hand side, and hence the second diagram vanishes. The helicity amplitude is therefore equal to the remaining Feynman diagram in Figure 3, and is calculated using the colour-ordered Feynman rules (see appendix B) as follows:

$$\begin{aligned} A_4(1^-, 2^-, 3^+, 4^+) = &\left(\frac{i}{\sqrt{2}}\right)^2 \frac{-i}{(-k_1 - k_2)^2} \\ &\times \left[\epsilon_1^- \cdot \epsilon_2^- (k_1 - k_2)^\mu + \left(\epsilon_2^-\right)^\mu \epsilon_1^- \cdot (2k_2 + k_1) + \left(\epsilon_1^-\right)^\mu \epsilon_2^- \cdot (-2k_1 - k_2)\right] \\ &\times \left[\epsilon_3^+ \cdot \epsilon_4^+ (k_3 - k_4)_\mu + \left(\epsilon_4^+\right)_\mu \epsilon_3^+ \cdot (2k_4 + k_3) + \left(\epsilon_3^+\right)_\mu \epsilon_4^+ \cdot (-2k_3 - k_4)\right] \\ = &\frac{-2i}{s_{12}} \left(\epsilon_2^- \cdot \epsilon_3^+\right) \left(\epsilon_1^- \cdot k_2\right) \left(\epsilon_4^+ \cdot k_3\right) \ , \end{aligned} \tag{105}$$

where we put the propagator at the front of the equation and rewrote the momentum invariant $(k_1 + k_2)^2 = s_{12}$ in the last line. To get to the last line we removed all quantities which were zero either from the choice of reference momenta (equation (96)) or the Dirac equation (equation (104)). Note that each polarisation vector is gauge dependent, hence equation (105) is currently gauge dependent. To make this gauge invariant we use equation (87)

for the first term and equation (90) for the latter two terms to write all polarisations and momenta in terms of spinor inner products. Hence:

$$\epsilon_2^- \cdot \epsilon_3^+ = -\frac{\langle 4^+|\gamma^\mu|2^+\rangle\langle 1^-|\gamma_\mu|3^-\rangle}{\sqrt{2}[42]\langle 13\rangle} = -\frac{[43]\langle 12\rangle}{[42]\langle 13\rangle} \ , \tag{106}$$

$$\epsilon_1^- \cdot k_2 = \frac{-1}{\sqrt{2}}\frac{[42]\langle 21\rangle}{[41]} \ , \tag{107}$$

$$\epsilon_4^+ \cdot k_3 = \frac{1}{\sqrt{2}}\frac{\langle 13\rangle[34]}{\langle 14\rangle} \ . \tag{108}$$

Substituting these equations into equation (105), cancelling common factors and using equation (83) to write that $s_{12} = \langle 12\rangle[21]$ gives that:

$$A_4(1^-, 2^-, 3^+, 4^+) = -i\frac{\langle 12\rangle[34]^2}{[12]\langle 14\rangle[14]} \ . \tag{109}$$

This is a perfectly acceptable (i.e. gauge invariant) equation, but we can make it more elegant. Multiply and divide by $\langle 23\rangle\langle 34\rangle$ to get that:

$$A_4(1^-, 2^-, 3^+, 4^+) = -i\frac{\langle 12\rangle(\langle 23\rangle[34])(\langle 34\rangle[34])}{[12]\langle 23\rangle\langle 34\rangle\langle 14\rangle[14]} \ , \tag{110}$$

which at first sight doesn't look elegant. However using the equations for invariant mass (equation (83)) and momentum conservation (equation (101)) we have that:

$$[34]\langle 34\rangle = -s_{34} = -s_{12} = [12]\langle 12\rangle \ , \tag{111}$$

and using the Schouten identity (equation (90)), momentum conservation (equation (101)) and the Dirac equation we see that:

$$\begin{aligned}\langle 23\rangle[34] =& \langle 2^-|\not{k}_3|4^-\rangle \\ =& -\langle 2^-|\not{k}_1 + \not{k}_2 + \not{k}_4|4^-\rangle \\ =& -\langle 2^-|\not{k}_1|4^-\rangle \\ =& -\langle 21\rangle[14] \ .\end{aligned} \tag{112}$$

Substituting these into equation (110) gives that:

$$\begin{aligned}A_4(1^-, 2^-, 3^+, 4^+) =& -i\frac{\langle 12\rangle(-\langle 21\rangle[14])(\langle 12\rangle[12])}{[12]\langle 23\rangle\langle 34\rangle\langle 14\rangle[14]} \\ =& i\frac{\langle 12\rangle^4}{\langle 12\rangle\langle 23\rangle\langle 34\rangle\langle 41\rangle} \ ,\end{aligned} \tag{113}$$

which is the famous Parke Taylor formula for 4-gluon scattering[11] [13]. Incredibly, all n-gluon helicity amplitudes with the form $A_n(1^-, 2^-, 3^+, \ldots, n^+)$ have the same simple form:

$$A_n(1^-, 2^-, 3^+, \ldots, n^+) = i\frac{\langle 12\rangle^4}{\langle 12\rangle\langle 23\rangle \ldots \langle n1\rangle} \ , \tag{114}$$

and can be evaluated without summing diagrams. Note that if particles i and j had negative helicity (instead of 1 and 2), then we must replace the numerator in equation (114) with $\langle ij\rangle^4$. Note that to prove equation (114) requires recursion relations which are outside the scope of this thesis [22].

2.6 Supersymmetry - a quick aside

To derive the MHV amplitude for the process which contains a single quark anti-quark pair it is possible to once again use the colour-ordered Feynman rules as above, however this MHV amplitude is more elegantly derived using

[11] Actually, Parke and Taylor wrote their formula in terms of momentum inner products. The use of spinor inner products was first used by Mangano and Parke a year later [21].

supersymmetry (SUSY), which is the theoretical symmetry that relates fermions and bosons [52]. It contains an operator Q, also called the supersymmetry charge, which generates this transformation such that:

$$Q|\text{Boson}\rangle = |\text{Fermion}\rangle \ , \qquad Q|\text{Fermion}\rangle = |\text{Boson}\rangle \ . \tag{115}$$

The single-particle supersymmetric states fall into irreducible representations of the supersymmetric algebra, called supermultiplets [53–55]. Each supermultiplet contains an equal number of fermionic and bosonic degrees of freedom of equal mass, called the superpartners of each other. Every particle within a supermultiplet is in the same representation of the gauge group, and hence each particle has the same electric charge, colour charge and weak isospin as its superpartners. A particular example of a supermultiplet (one which we will use) is the gluon supermultiplet. The fermionic superpartner of the gluon is called the gluino, and by construction is massless (for unbroken SUSY), has an adjoint colour index and is spin 1/2. Note that if we are only considering strong interactions, the gluino is identical to the previously considered massless quarks up to the colour. Additionally, tree-level QCD is effectively supersymmetric [20, 56]. To see this in the n-gluon case is trivial: there are no loops, so there are no fermions. Therefore any fermions in our theory may as well be gluinos, i.e. we may as well be calculating a SUSY amplitude. Similarly, if we have quarks, up to the colour index of the fermion the two theories are the same. Therefore we expect that the purely kinematical amplitude involving 2 gluinos and $n-2$ gluons should be identical to that involving a massless quark anti-quark pair and $n-2$ gluons. However SUSY amplitudes are easier to calculate due to the extra relationships between them. One such relationship is the supersymmetric Ward identities (SWI) [19, 27, 28, 57], which we now describe below.

Denote the polarised gluon as before by $g^\pm$ and a gluino by $\Lambda^\pm$, where $\pm$ denotes the gluino helicity. Let $Q(\eta)$ be the supersymmetry charge with η being some fermionic parameter of the transformation. We then have the following relationships [27, 28]:

$$[Q(\eta), g^\pm(k)] = \mp\, \Gamma^\pm(k,\eta)\Lambda^\pm \ , \tag{116}$$

$$[Q(\eta), \Lambda^\pm(k)] = \mp\, \Gamma^\mp(k,\eta) g^\pm \ , \tag{117}$$

where k is the gluon or gluino momentum and $\Gamma^\pm$ is a complex function which satisfies:

$$\Gamma^+(k,\eta) = \bar{\eta} U_-(k) \ , \quad \text{and} \quad \Gamma^-(k,\eta) = \bar{\eta} U_+(k) \ , \tag{118}$$

for $U_-(k)$ ($U_+(k)$) being a negative (positive) helicity spinor with momentum k which satisfies the massless Dirac equation. We are allowed to choose the supersymmetric parameter η arbitrarily, so we choose it to be a negative-helicity spinor of momentum p obeying the massless Dirac equation times a (real) Grassmann variable[12] θ. The Grassmann variable reminds us that $\Gamma^\pm$ anti-commutes with the fermion creation and annihilation operators, and commutes with the bosonic operators. We then write that:

$$\begin{aligned} \Gamma^+(k,\eta(p)) \equiv \Gamma^+(k,p) &= \bar{\eta}(p) U_-(k) \\ &= \theta \langle p^+ | k^- \rangle \\ &= \theta [pk] \ , \end{aligned} \tag{119}$$

where we used the bra-ket notation for spinors defined in Section 2.4.1 along with the definition of the spinor inner product equation (76). Note that we can choose Γ^+ to vanish by letting $p = k$. Using equation (118) we similarly have that:

$$\Gamma^-(k,p) = \theta \langle pk \rangle \ , \tag{120}$$

and we can similarly make Γ^- vanish by choosing $p = k$. A useful property in unbroken SUSY (which we are considering) is that the operator $Q(\eta) \equiv Q(p)$ annihilates the vacuum[13] [28, 58]. Therefore the commutator of $Q(k)$ with any string of operators creating or annihilating gluons or gluinos has a vanishing vacuum expectation value. That is:

$$0 = \langle 0 | \left[Q, \phi_1^\pm \phi_2^\pm \dots \phi_n^\pm \right] | 0 \rangle = \sum_{i=1}^{n} \langle 0 | \phi_1^\pm \dots \left[Q, \phi_i^\pm \right] \dots \phi_n^\pm | 0 \rangle \ , \tag{121}$$

where each $\phi_i^\pm$ creates or annihilates a gluon or gluino helicity eigenstate. Equation (121) is what we call the supersymmetric Ward identity (SWI) and will be used throughout the next section.

[12] The key property of Grassmann variables is that they anticommute with themselves and commute with ordinary (i.e. non-Grassmann) variables. Specifically this means that if θ_1 and θ_2 are Grassmann variables, then $\theta_1\theta_2 = -\theta_2\theta_1$ and that $\theta_1^2 = \theta_2^2 = 0$. For more details see e.g. [37]

[13] If $Q(p)$ did not annihilate the vacuum then we would be using broken SUSY. Note that because we do not see low mass superpartners in nature, SUSY must be a broken symmetry (if it exists at all) [58].

2.7 Helicity amplitudes with a single quark anti-quark pair

We are now ready to use (unbroken) SUSY to calculate helicity amplitudes involving a single quark anti-quark pair and $n-2$ gluons. The simplest helicity configuration occurs when every particle has the same helicity. For this configuration the relevant helicity amplitude is the SUSY amplitude $A_n(\Lambda_1^{\pm}, g_2^{\pm}, g_3^{\pm}, \ldots, g_{n-1}^{\pm}, \Lambda_n^{\pm})$ (Recall that the position of the quark and anti-quark are fixed from the colour structure (see section 2.3.3)). However, in SUSY helicity is still conserved along a fermion line, so that in our all outgoing convention each pair of gluinos must have opposite helicities [27, 28]. Hence this amplitude vanishes and due to the equivalence of the kinematic amplitudes:

$$A_n(q^{\pm}, g_1^{\pm}, \ldots g_{n-2}^{\pm}, \bar{q}^{\pm}) = 0 \ , \tag{122}$$

where the gluons in equation (122) are relabelled so that the first gluon's index is 1. Note that we can use helicity conservation along a fermion line to again prove that the all-gluon amplitude $A_n(g_1^{\pm}, \ldots, g_n^{\pm})$ vanishes. To do so we consider the following all positive helicity SWI:

$$\begin{aligned}
0 =& \langle 0| \left[Q(p), \Lambda_1^+ g_2^+ g_3^+ \ldots g_n^+\right] |0\rangle \\
=& \langle 0| \left[Q(p), \Lambda_1^+\right] g_2^+ g_3^+ \ldots g_n^+ |0\rangle + \langle 0|\Lambda_1^+ \left[Q(p), g_2^+\right] g_3^+ \ldots g_n^+ |0\rangle \\
&+ \cdots + \langle 0|\Lambda_1^+ g_2^+ g_3^+ \ldots g_{n-1}^+ \left[Q(p), g_n^+\right] |0\rangle \\
=& -\Gamma^-(k_1,p)\langle 0|g_1^+ g_2^+ \ldots g_n^+|0\rangle + \Gamma^+(k_2,p)\langle 0|\Lambda_1^+\Lambda_2^+ g_3^+ \ldots g_n^+|0\rangle \\
&+ \cdots + \Gamma^+(k_n,p)\langle 0|\Lambda_1^+ g_2^+ \ldots g_{n-1}^+\Lambda_n^+|0\rangle \\
=& -\Gamma^-(k_1,p)A_n(g_1^+, g_2^+, \ldots, g_n^+) + \Gamma^+(k_2,p)A_n(\Lambda_1^+, \Lambda_2^+, g_3^+, \ldots, g_n^+) \\
&+ \cdots + \Gamma^+(k_n,p)A_n(\Lambda_1^+, g_2^+, \ldots g_{n-1}^+, \Lambda_n^+) \\
=& -\Gamma^-(k_1,p)A_n(g_1^+, g_2^+, \ldots, g_n^+) \ ,
\end{aligned} \tag{123}$$

where we used the SWI (equation (121)) in the second line and equations (116) and (117) to express the commutators in terms of $\Gamma^{\pm}$ in the third line. In the fourth line we used the definitions of the kinematic amplitudes A_n, and we used helicity conservation along a fermion line in the last line. Choosing $p \neq k_1$ implies that the all-gluon amplitude vanishes as expected. We can show that the next simplest helicity configuration also vanishes by changing the helicity of the final gluon at the top of equation (123). Doing so gives that:

$$\begin{aligned}
0 =& \langle 0| \left[Q(p), \Lambda_1^+ g_2^+ \ldots g_{n-1}^+ g_n^-\right] |0\rangle \\
=& -\Gamma^-(k_1,p)\langle 0|g_1^+ g_2^+ \ldots, g_{n-1}^+ g_n^-|0\rangle + \cdots + \Gamma^+(k_2,p)\langle 0|\Lambda_1^+\Lambda_2^+ g_3^+ \ldots g_n^+|0\rangle \\
&+ \cdots + \Gamma^+(k_n,p)\langle 0|\Lambda_1^+ g_2^+ \ldots g_{n-1}^+\Lambda_n^-|0\rangle \\
=& -\Gamma^-(k_1,p)A_n(g_1^+, g_2^-, \ldots, g_n^+) + \Gamma^+(k_n,p)A_n(\Lambda_1^+, g_n^+, \ldots, g_{n-1}^+, \Lambda_n^-) \ .
\end{aligned} \tag{124}$$

To get the last line we recognised that every term except for the first and last violates helicity conservation along a fermion line. Setting $p = k_1$ gives that the second amplitude must vanish, while setting $p = k_n$ implies that the first amplitude vanishes (something which we already proved in equation (99)). We can swap all of the helicities and follow the same procedure as for equation (124) to conclude that:

$$A_n(q^{\pm}, g_1^{\pm}, \ldots g_{n-2}^{\pm}, \bar{q}^{\mp}) = A_n(\Lambda_1^{\pm}, g_n^{\pm}, \ldots, g_{n-1}^{\pm}, \Lambda_n^{\mp}) = 0 \ . \tag{125}$$

Now let us consider the first non-vanishing amplitude, i.e. the MHV amplitude. To calculate this consider the following SWI:

$$\begin{aligned}
0 =& \langle 0| \left[Q(p), g_1^-, g_2^- g_3^+ \ldots g_{n-1}^+ \Lambda_n^+\right] |0\rangle \\
=& \Gamma^-(k_1,p)\langle 0|\Lambda_1^- g_2^- g_3^+ \ldots \Lambda_n^+|0\rangle + \Gamma^-(k_2,p)\langle 0|g_1^- \Lambda_2^- g_3^+ \ldots g_{n-1}^+\Lambda_n^+|0\rangle \\
&- \Gamma^+(k_3,p)\langle 0|g_1^- g_2^- \Lambda_3^+ g_4^+ \ldots g_{n-1}^+\Lambda_n^+|0\rangle + \cdots - \Gamma^-(k_n,p)\langle 0|g_1^- g_2^- g_3^+ \ldots g_n^+|0\rangle \\
=& \Gamma^-(k_1,p)A_n(\Lambda_1^-, g_2^-, g_3^+, \ldots, g_{n-1}^+, \Lambda_n^+) + \Gamma^-(k_2,p)A_n(g_1^-, \Lambda_2^-, g_3^+, \ldots, g_{n-1}^+, \Lambda_n^+) \\
&- \Gamma^-(k_n,p)A_n(g_1^-, g_2^-, g_3^+, \ldots, g_n^+) \ ,
\end{aligned} \tag{126}$$

where we once again removed amplitudes which vanish due to fermion helicity conservation. Now let $p = k_2$, so that the only remaining amplitude with gluinos is in the same colour order as the quark amplitude. Rearranging gives that:

$$\Gamma^-(k_1,k_2)A_n(\Lambda_1^-, g_2^-, g_3^+, \ldots, g_{n-1}^+, \Lambda_n^+) = \Gamma^-(k_n,k_2)A_n(g_1^-, g_2^-, g_3^+, \ldots, g_n^+) \ , \tag{127}$$

while substituting equation (120) for each Γ^- and equation (114) for the all-gluon MHV amplitude gives:

$$\theta\langle 21\rangle A_n(\Lambda_1^-, g_2^-, g_3^+, \ldots, g_{n-1}^+, \Lambda_n^+) = \theta\langle 2n\rangle i \frac{\langle 12\rangle^4}{\langle 12\rangle\langle 23\rangle \ldots \langle n1\rangle} \ . \tag{128}$$

Cancelling common factors and using that the inner products are antisymmetric gives that:

$$A_n(\Lambda_1^-, g_2^-, g_3^+, \ldots, g_{n-1}^+, \Lambda_n^+) = i \frac{\langle 12\rangle^3\langle n2\rangle}{\langle 12\rangle\langle 23\rangle \ldots \langle n1\rangle} \ . \tag{129}$$

A final step is to relabel the particles so that only the gluons are numbered, and turn the gluinos into a quark anti-quark pair, giving that:

$$A_n(q^-, g_1^-, g_2^+, \ldots, g_{n-2}^+, \bar{q}^+) = i \frac{\langle q1\rangle^3\langle \bar{q}1\rangle}{\langle q1\rangle\langle 12\rangle \ldots \langle (n-2)\bar{q}\rangle\langle \bar{q}q\rangle} \ , \tag{130}$$

which is the MHV formula for an amplitude with $n-2$ gluons of mostly positive helicities, a single negative helicity quark, and a single positive helicity anti-quark. If we swap the helicities of the quark and the anti-quark we simply have to exchange the quark with the anti-quark in the numerator of equation (130). To see why, consider the SWI:

$$\begin{aligned} 0 &= \langle 0| \left[Q(p), \Lambda_1^+, g_2^- g_3^+ \ldots g_{n-1}^+ g_n^-\right] |0\rangle \\ &= -\Gamma^-(k_1, k_2)\langle 0|g_1^+ g_2^- g_3^+ \ldots g_{n-1}^+ g_n^-|0\rangle + \Gamma^-(k_n, k_2)\langle 0|\Lambda_1^+ g_2^- g_3^+ \ldots g_{n-1}^+ \Lambda_n^-|0\rangle \ , \end{aligned} \tag{131}$$

where we again chose the reference momentum $p = k_2$. If we proceed as before we find that:

$$\langle 21\rangle A_n(g_1^+, g_2^-, g_3^+, \ldots, g_{n-1}^+, g_n^-) = \langle 2n\rangle A_n(\Lambda_1^+, g_2^-, g_3^+, \ldots, g_{n-1}^+, \Lambda_n^-) \ , \tag{132}$$

or that:

$$A_n(q^+, g_1^-, g_2^+, \ldots, g_{n-2}^+, \bar{q}^-) = i \frac{\langle \bar{q}1\rangle^3\langle q1\rangle}{\langle q1\rangle\langle 12\rangle \ldots \langle (n-2)\bar{q}\rangle\langle \bar{q}q\rangle} \ . \tag{133}$$

2.8 Explicit formulae for MHV amplitudes

In this section we summarise the two key MHV amplitudes used in this thesis. The n-gluon MHV amplitude with negative helicity gluons at positions i and j is given by the Parke Taylor formula [13]:

$$A_n(1^+, \ldots, (i-1)^+, i^-, (i+1)^+, \ldots, (j-1)^+, j^-, (j+1)^+, \ldots, n^+) = i \frac{\langle ij\rangle^4}{\langle 12\rangle\langle 23\rangle \ldots \langle n1\rangle} \ , \tag{134}$$

while flipping all of the helicities implies that we must flip each $\langle ij\rangle \to [ji]$. Hence:

$$\begin{aligned} A_n(1^-, \ldots, (i-1)^-, i^+, (i+1)^-, \ldots, (j-1)^-, j^+, (j+1)^-, \ldots, n^-) &= i \frac{[ij]^4}{[1n][n(n-1)] \ldots [21]} \\ &= i(-1)^n \frac{[ij]^4}{[12][23] \ldots [n1]} \ . \end{aligned} \tag{135}$$

There is an equally compact MHV formula for the process involving $n-2$ gluons and a quark anti-quark pair. If the quark and gluon i each have negative helicity (hence the anti-quark and all other gluons have positive helicity) then the amplitude is [21, 22]:

$$A_n(q^-, 1^+, \ldots, (i-1)^+, i^-, (i+1)^+, \ldots, (n-2)^+, \bar{q}^+) = \frac{\langle qi\rangle^3\langle \bar{q}i\rangle}{\langle \bar{q}q\rangle\langle q1\rangle\langle 12\rangle \ldots \langle (n-2)\bar{q}\rangle} \ , \tag{136}$$

where the numbers refer to the (colour ordered) gluons. If we exchange the helicities on the quarks, it is sufficient to exchange the exponents in the numerator:

$$A_n(q^+, 1^+, \ldots, (i-1)^+, i^-, (i+1)^+, \ldots, (n-2)^+, \bar{q}^-) = \frac{\langle qi\rangle\langle \bar{q}i\rangle^3}{\langle \bar{q}q\rangle\langle q1\rangle\langle 12\rangle \ldots \langle (n-2)\bar{q}\rangle} \ , \tag{137}$$

while flipping the helicity of each particle again implies that we must change $\langle ij\rangle \to [ji]$. Finally we note that at the amplitude squared level it does not matter whether we consider the mostly-plus or the mostly-minus MHV amplitude. This is because $\langle ij\rangle = -[ij]^*$, and hence $A_n(+) = (-1)^n A_n(-)^*$, or that:

$$|A_n(+)|^2 = A_n(+)^* A_n(+) = (-1)^n A_n(-) \times (-1)^n A_n(-)^* = |A_n(-)|^2 \ , \tag{138}$$

where $A_n(+)$ is a mostly-plus MHV kinematic amplitude, and $A_n(-)$ is the same amplitude with all of the helicities flipped.

3 Monte Carlo event generators

To use the results of the previous section to make predictions at the LHC we must place them within a general purpose Monte Carlo (MC) event generator such as PYTHIA [6], HERWIG [7] or SHERPA [8]. This is because the $2 \to n$ scatter for which we just calculated the squared amplitude is only a small part of any proton-proton collision. To understand how we use the MHV formulae to help make predictions we must therefore understand a MC event generator. The following sections will first give a basic overview of an LHC particle collision, and then discuss how a MC event generator simulates this collision. There will be a particular focus on how and where we can use the MHV formulae within the MC event generator VINCIA [24], since we aim to include these formulae within this program. For a more detailed review on MC event generators see e.g. [59].

3.1 Modelling particle collisions

At the LHC, each collision typically produces hundreds of composite colour-neutral particles, an example of which is shown in Figure 4. At first glance this appears to be in direct opposition to fixed-order perturbation which tells us how to produce $n \lesssim 10$ coloured partons[14]. Nonetheless fixed-order perturbation is a key component of the MC event generator, and we build the structure of a proton-proton collision at the LHC by factorising the collision into several distinct processes with the fixed-order expansion at its core [59–62]. This structure can be summarised as follows:

- **Hard process**: This is the $2 \to n$ collision between two partons, one from each incoming proton. We calculate the hard scatter cross section using the fixed-order perturbative amplitudes of the previous section. Note that hard refers to the high energy of each incoming particle, (while soft processes are those in which the particles have low energy). Hence in any hard process either a large momentum transfer occurs, or heavy particles are created. Further, note that we choose the hard process of interest, which for this thesis will be a QCD process.
- **Heavy resonance decay**: If heavy particles such as the top quark, or the $W^{\pm}$ or Z^0 bosons are produced, their decay is viewed as part of the hard process.
- **Parton shower**: Accelerated colour and electromagnetic charges emit bremsstrahlung. Note that the gluon is itself colour charged and therefore emits further bremsstrahlung, hence a shower of colour-charged particles is created. Emissions associated with the two incoming partons is called initial-state radiation, while final-state radiation describes the parton showers associated with final-state partons.
- **Multiple parton interactions**: Secondary interactions between the remaining partons within the colliding hadrons can occur. Each of these secondary interactions has its own parton showers.
- **Hadronisation**: Colour confinement becomes significant as partons become softer through bremsstrahlung radiation, and they move apart in spacetime. Partons bunch into colour-neutral primary hadrons, which are often unstable and decay further to lighter, more stable particles.
- **Use a detector simulator**: At this stage, the MC event generator finishes and we switch to a different program to simulate the interaction of the produced particles with the detector material. It is only at this point that we mimic the experimental information that can be obtained and used to reconstruct what happened at the core of this collision.

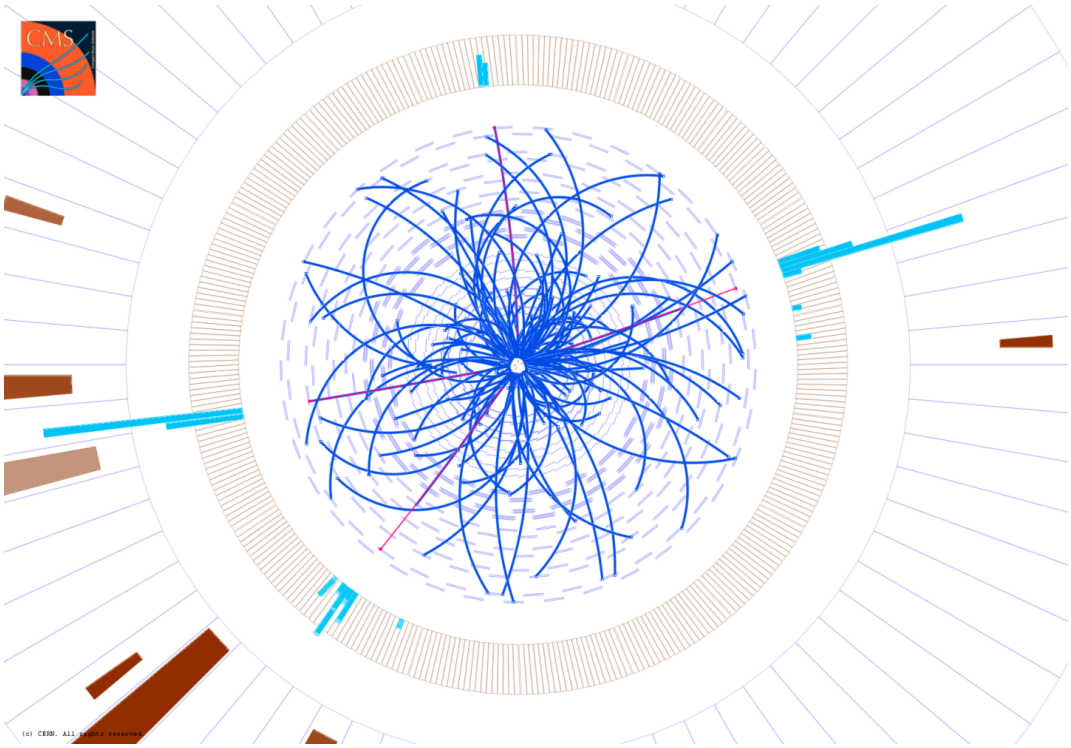

Figure 4: Actual data from the CMS detector at the LHC showing production of many hadrons (the blue curved lines) and four high energy electrons (the purple lines). It is the aim of the MC event generator to predict the complex spectrum of resultant particles in LHC collisions such as this. Figure courtesy of [60].

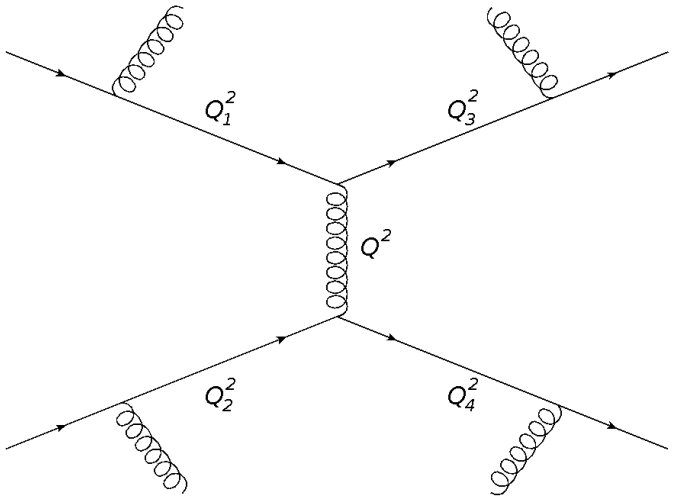

Figure 5: The virtualities Q^2 of each particle in an LHC collision. We choose the hard process to be the one with the largest Q^2 (in this case the central gluon), and approximate all other virtualities as vanishing.

3.2 Parton showers

The idea of a parton shower is to iteratively build up a cascade of coloured partons, using simple dipole expressions for transitions such as $q\bar{q} \to qg\bar{q}$, $gg \to ggg$, $gg \to gq\bar{q}$, $qg \to qq'\bar{q}'$, and $qg \to qgg$ [63, 64]. Note that we use the "dipole" or "antenna" shower since this is what VINCIA uses. Readers may be more familiar with conventional "parton" showers which are based on the so-called DGLAP formalism, however we show below that the former includes the latter, hence there is no fundamental incompatibility between them. The starting point for this shower is the hard process, usually a simple $2 \to 2$ scatter in which each external particle is approximated as on shell. This means that the virtuality of each external massless particle Q^2 is approximately 0, where Q^2 is defined as:

$$Q^2 = |k^2| = \left| E^2 - |\vec{\mathbf{k}}|^2 \right| \ . \tag{139}$$

Since each hard coloured particle emits bremsstrahlung, we must realise that the external particles aren't actually external, and have non-zero virtualities. Therefore, there is some ambiguity as to which process is the hard scatter. For example, consider Figure 5 in which two quarks scatter via exchange of a gluon, and also emit bremsstrahlung gluons. Since we choose the hard process based on the largest virtuality, for the hard scatter to be $qq \to qq$ we must have that $Q^2 > Q_i^2$ $(i = 1, 2, 3, 4)$ [61]. We approximate each $Q_i^2 \approx 0$, and then use expressions for $qq \to qgq$ to correct each of these on-shell approximations. Note that if for example Q_1^2 had the largest virtuality, then the hard process would be $qg \to qg$.

After we have chosen the hard process we then calculate its differential cross section $d\sigma_{ME}$ using the squared matrix elements $|M_n|^2$ from section 2 [37]:

$$d\sigma_{ME} = \frac{1}{4E_1E_2} \frac{1}{|\vec{v}_1 - \vec{v}_2|} |M_n|^2 \, d\Phi_n \ , \tag{140}$$

where E_1 (E_2) is the energy of the first (second) incoming particle and $\vec{v}_1$ ($\vec{v}_2$) the incoming velocity of the first (second) particle as viewed from the lab frame, and $d\Phi_n$ is defined as:

$$d\Phi_n = (2\pi)^4 \delta^{(4)} (k_F - k_I) \prod_{i=1}^{n} \frac{d^3k_i}{(2\pi)^3} \frac{1}{2E_{\vec{k}_i}} \ , \tag{141}$$

where n is the number of final-state particles, k_F is the sum of final-state four-momenta, and k_I the sum of initial-state four-momenta. Note that every quantity in equation (140) is Lorentz invariant except for the velocities and the energies, and that $d\Phi_n$ is what we call relativistically invariant n-body phase space, or just phase space for short, and has $3n - 4$ dimensions. Note that integrals over phase space are often of dimension $d \gg 2$, hence we must use an integration method which is independent of dimensionality, such as the MC method. For more details see Appendix E.

Before moving on to the shower we must first recognise that the amplitudes which make up this cross section diverge. For example consider a mostly-positive-helicity MHV amplitude with a single quark pair, and $n-2$ gluons. This amplitude is given by equation (130):

$$A_n(q^-, g_1^-, g_2^+, \ldots, g_{n-2}^+, \bar{q}^+) = i \frac{\langle q1 \rangle^3 \langle \bar{q}1 \rangle}{\langle q1 \rangle \langle 12 \rangle \ldots \langle (n-2)\bar{q} \rangle \langle \bar{q}q \rangle} \ . \tag{142}$$

Further, recall equation (84), which relates the inner products to the momentum invariants:

$$s_{ij} = (p_i + p_j)^2 = 2p_i \cdot p_j = 2E_iE_j(1 - \cos\theta_{ij}) = |\langle ij \rangle|^2 \ , \tag{143}$$

or equivalently that:

$$\langle ij \rangle = e^{i\phi_{ij}} \sqrt{|s_{ij}|} = e^{i\phi_{ij}} \sqrt{2E_iE_j(1 - \cos\theta_{ij})} \ , \tag{144}$$

where $e^{i\phi_{ij}}$ is some phase factor, E_i (E_j) is the energy of particle i (j) and θ_{ij} the angle between the two particles in some frame. While the final form of the momentum invariant in equation (144) isn't actually Lorentz invariant, it does give us valuable insight. It implies that there are two ways that the momentum invariant, and hence the

[14] In practice most MC event generators only use fixed-order calculations for processes with a few particles in the final state. For example PYTHIA only uses fixed-order perturbation in $2 \to 2$ or $2 \to 3$ processes (with some higher multiplicity states available via decays of heavy resonances), while a more specialised program such as MadGraph5 can calculate QCD amplitudes at leading order for processes with up to 7 particles in the final state [9].

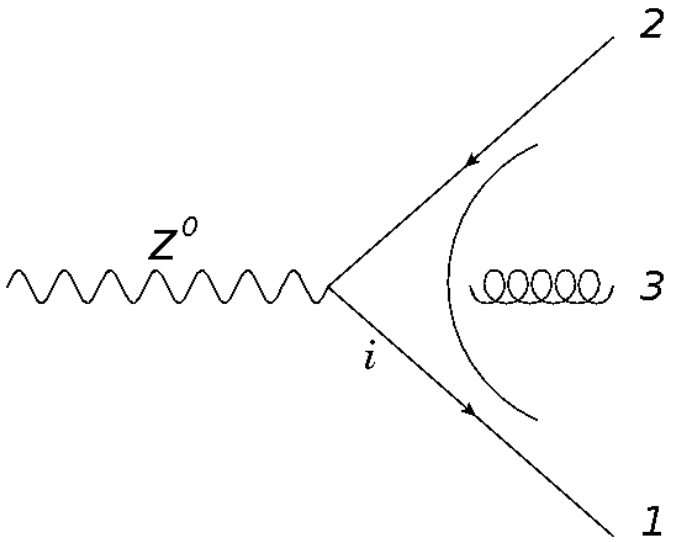

Figure 6: The $q\bar{q}$ dipole in $Z^0 \to q\bar{q} \to qg\bar{q}$. The dipole itself is represented by the curved line between the $q\bar{q}$ pair, and the gluon can be emitted by either the quark or anti-quark in the dipole. Note that the Z^0 is considered to have come from a lepton pair, say e^+e^-, so that there is no ISR.

denominator in equation (142), can vanish. One of the particles can either be soft (i.e. $E_i \to 0$) or two colour-connected particles can become collinear ($\theta_{ij} \to 0$). These are unsurprisingly called the soft singularity and the collinear singularity. Note that the physical reasons for these singularities are the following: the soft singularity occurs because the emitted particle has so little energy that it is impossible to detect, while the collinear singularity occurs because at a small angular separation the two particles are so close together that we can no longer distinguish between them. We must therefore be mindful of which areas of phase space we want to access, and somehow remove these singularities. Note that to properly remove the singularities we must use that tree-level diagrams with a soft or collinear parton are exactly equal and opposite to those diagrams involving a soft or collinear virtual parton [65,66]. However, virtual, or loop-level QCD, is notoriously difficult [18], so we instead tame these singularities using a computationally cheap method which we describe in the next section.

3.2.1 Final-state radiation

The aim of the parton shower is to add soft and/or collinear gluon radiation to the incoming and outgoing partons. To demonstrate how this works, consider the scenario in which two leptons annihilate into a Z^0, which creates a $q\bar{q}$ pair (as studied at the LEP collider). Since the incoming particles are leptons, we only encounter final-state QCD radiation in this scenario. The first radiated gluon must therefore come from the $q\bar{q}$ dipole, as shown in Figure 6. Note that the Z^0 is at rest in the centre-of-mass frame. Denote the cross section of the original process to be σ_0, along with its matrix element $|M_{q\bar{q}}|^2$ and phase space $d\Phi_0$, and denote the cross section of the new process (i.e. with radiation) as σ, along with its matrix element $|M_{qg\bar{q}}|^2$ and phase space $d\Phi$. The new cross section is then related to the old one by [35, 63, 64]:

$$\frac{d\sigma}{\sigma_0} = \frac{|M_{qg\bar{q}}|^2}{|M_{q\bar{q}}|^2}\frac{d\Phi}{d\Phi_0} = g_s^2\frac{8}{3}\left[\frac{2s_{12}}{s_{13}s_{23}} + \frac{1}{s}\left(\frac{s_{13}}{s_{23}} + \frac{s_{23}}{s_{13}}\right)\right]\frac{1}{16\pi^2 s}ds_{13}ds_{23} \ , \tag{145}$$

which can be verified by direct substitution of the relevant matrix elements and phase spaces. Here s is the centre-of-mass invariant:

$$s = s_{12} + s_{13} + s_{23} = E_{cm}^2 \ , \tag{146}$$

where the last equality is only true in the centre-of-mass frame, and partons $1, 2$, and 3 are those in Figure 6. Note that the term $2s_{12}/s_{13}s_{23}$ in equation (145) is called the eikonal or soft factor, and is universal, i.e. any ratio of matrix elements $|M_{n+g}|^2/|M_n|^2$ will include this term. The remaining terms within the square brackets on the right of equation (145) are the collinear terms, and are dependent upon whether the emitter was a quark or a gluon.

Substituting into equation (145) the energy fractions x_i of each parton, defined such that[15]:

$$x_1 = \frac{2E_1}{E_{cm}} = 1 - \frac{s_{23}}{s} \ , \qquad x_2 = \frac{2E_2}{E_{cm}} = 1 - \frac{s_{13}}{s} \ , \qquad x_3 = \frac{2E_3}{E_{cm}} = 1 - \frac{s_{12}}{s} \ , \tag{147}$$

re-writing $g_s^2 = 4\pi\alpha_s$ and cancelling gives that:

$$\frac{d\sigma}{\sigma_0} = \frac{2\alpha_s}{3\pi} \frac{x_1^2 + x_2^2}{s(1-x_1)(1-x_2)} \frac{1}{s} ds_{13} ds_{23} \ . \tag{148}$$

Finally we note that $dx_1 = -ds_{23}/s$ and $dx_2 = -ds_{13}/s$ to get the result:

$$\frac{d\sigma}{\sigma_0} = \frac{2\alpha_s}{3\pi} \frac{x_1^2 + x_2^2}{(1-x_1)(1-x_2)} dx_1 dx_2 \ . \tag{149}$$

We could similarly derive expressions describing gluon emission from the remaining possible dipoles. These expressions are given by [63]:

$$gg \text{ dipole:} \qquad \frac{d\sigma}{\sigma_0} = \frac{3\alpha_s}{4\pi} \frac{x_1^3 + x_2^3}{(1-x_1)(1-x_2)} dx_1 dx_2 \ , \tag{150}$$

$$qg \text{ dipole:} \qquad \frac{d\sigma}{\sigma_0} = \frac{3\alpha_s}{4\pi} \frac{x_1^2 + x_2^3}{(1-x_1)(1-x_2)} dx_1 dx_2 \ . \tag{151}$$

Note that each gluon emitter corresponds to a term x_i^3, while each quark (or anti-quark) emitter corresponds to a term x_i^2. We mention here for completeness that if the emitted gluon is collinear to the particle which emitted it, we can change from "dipole" showers to "parton" showers, and use the so-called Altarelli-Parisi splitting functions to describe the emission. We can relate the dipoles in equations (149) - (151) to the Altarelli-Parisi splitting in the limit that $x_2 \to 1$, by making the following substitutions:

$$\begin{aligned} k_\perp^2 =& E_{cm}^2 (1-x_1)(1-x_2) \Rightarrow dk_\perp^2 = -E_{cm}^2 dx_2 \\ z =& 1 - x_1 \Rightarrow dz = -dx_1 \ , \end{aligned} \tag{152}$$

where $k_\perp$ is the transverse momentum of the gluon relative to the dipole axis, $z = E_g/E_i$ is the energy fraction carried by the gluon (see Figure 7), and the limit $x_2 \to 1$ corresponds to the limit that the gluon is collinear to the quark (see Figure 8). Substituting equation (152) into equation (149) gives that:

$$\frac{d\sigma}{\sigma_0} = \frac{2\alpha_s}{3\pi} \frac{dk_\perp^2}{k_\perp^2} \frac{dz}{z} \left[1 + (1-z)^2\right] \ . \tag{153}$$

We can similarly take the collinear limit for the other two dipole cross sections (equations (150) and (151)) to obtain the famous DGLAP equations [67–69]:

$$\frac{d\sigma}{\sigma_0} = \frac{\alpha_s}{4\pi} \frac{dk_\perp^2}{k_\perp^2} P_{a\to bc}(z) dz \ , \tag{154}$$

where:

$$\begin{aligned} P_{q\to qg}(z) =& \frac{1 + (1-z)^2}{z} \\ P_{g\to gg}(z) =& \frac{\left[1 - z(1-z)\right]^2}{z(1-z)} \ , \end{aligned} \tag{155}$$

are called the DGLAP splitting kernels. What we have described so far has seen us make no approximations. However, in general we will have for gluon emission that:

$$\frac{|M_{n+g}|^2}{|M_n|^2} = g_s^2 N_C \left(\frac{2s_{12}}{s_{13}s_{23}} + \text{collinear terms} + \text{finite} \right) \ , \tag{156}$$

where the finite term for Z^0 decay just happens to be 0. If the finite term is not zero, then we make the approximation [35]:

$$a = g_s^2 N_C \left(\frac{2s_{12}}{s_{13}s_{23}} + \text{collinear terms} \right) \approx \frac{|M_{n+g}|^2}{|M_n|^2} \ , \tag{157}$$

[15] For a more in depth discussion of the energy fractions x_i along with a more thorough derivation of equation (149), see Appendix F.

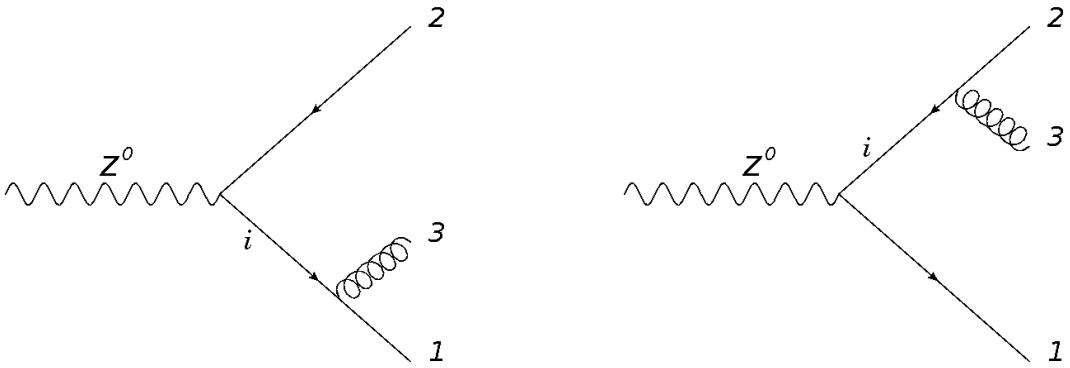

Figure 7: The two Feynman diagrams which contribute to $Z^0 \to qg\bar{q}$. Momentum i is the off-shell quark (anti-quark) momentum. In the limit that the gluon is collinear to either the quark or the anti-quark, we must no longer consider the dipole, and instead must consider only one of these diagrams. For example, if the gluon is collinear to the quark we consider only the first diagram with the gluon carrying energy $E_3 = zE_i$, and the quark carrying energy $E_1 = (1-z)E_i$, $0 < z < 1$.

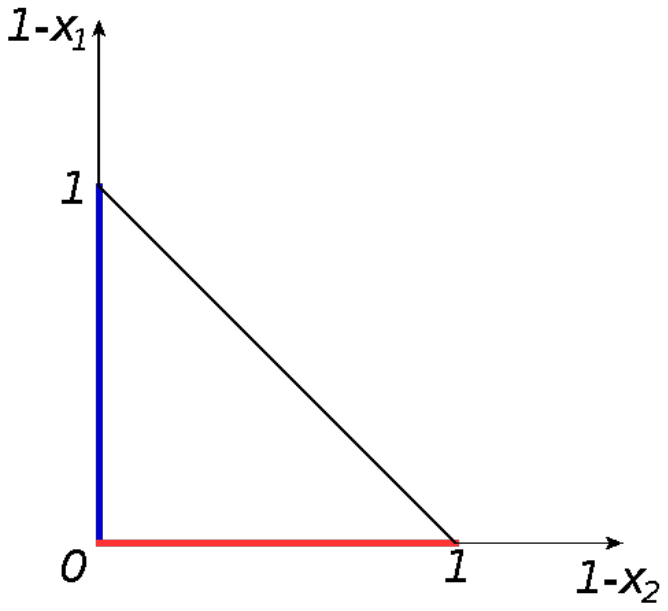

Figure 8: Two-dimensional phase space. When $x_2 \to 1$ we have that $s_{13} \to 0$, possibly with $E_1, E_3 \neq 0$. This implies that the gluon and quark are collinear and corresponds to the blue line. Similarly if the anti-quark and gluon are collinear we are on the red line.

where a is called the antenna function. Similarly, if a gluon splits into a quark anti-quark pair, then the antenna function is given by [64]:

$$a = \frac{1}{s^2}\left(\frac{s_{1q}^2 + s_{1\bar{q}}^2}{s_{q\bar{q}}}\right) \approx \frac{|M_{n+q\bar{q}}|^2}{|M_{n+g}|^2} \ , \tag{158}$$

where particle 1 is the remaining particle in the original dipole. In the limit in which the quark and anti-quark become collinear we obtain the final DGLAP splitting kernel:

$$P_{g\to q\bar{q}}(z) = \left[z^2 + (1-z)^2\right] \ . \tag{159}$$

At this point we use the antenna function to calculate the new differential cross-section using (for gluon emission):

$$\frac{d\sigma}{\sigma_0} \approx a\frac{1}{16\pi^2 s} ds_{13} ds_{23} \ . \tag{160}$$

This approximation is therefore only valid near the soft and collinear singularities, where we can ignore finite terms. However, since the amplitude for soft and collinear bremsstrahlung is higher than that for a hard, well-separated emission, we expect the majority of our radiation to be soft and/or collinear. If the radiation is hard and well separated, we must make corrections to this approximation, which we will outline in Section 3.2.2.

We now have the cross sections, but we don't quite have the probability of the dipole emitting a gluon. While we normally have that the probability of emission from a dipole is $d\mathcal{P}_0 = d\sigma/\sigma_0$, we need to ensure that an emission has not already occurred, i.e. we want the first emission. The probability that the first emission occurs at time T is the probability that something happens at T multiplied by the probability that nothing has already happened before T:

$$d\mathcal{P}_{\text{first}}(T) = d\mathcal{P}_{\text{something happens}}(T)\mathcal{P}_{\text{nothing happens}}(0 \le t \le T) \ . \tag{161}$$

To find a useful formula for the probability that an emission already happened we consider:

$$\mathcal{P}_{\text{nothing}}(0 \le t \le T) = 1 - \mathcal{P}_{\text{something}}(0 \le t \le T) \ , \tag{162}$$

and divide the probability of something happening into n equal sections. Taking the limit that $n \to \infty$ we get:

$$\mathcal{P}_{\text{nothing}}(0 \le t \le T) = \lim_{n\to\infty}\prod_{i=0}^{n}\left[1 - \frac{\mathcal{P}_{\text{something}}(T_i \le t \le T_{i+1})}{n}\right]^n = \exp\left(-\int_0^T \frac{d\mathcal{P}_{\text{something}}(t)}{dt}dt\right) \ . \tag{163}$$

Substituting this into equation (161) gives:

$$d\mathcal{P}_{\text{first}}(T) = d\mathcal{P}_{\text{something}}(T)\exp\left(-\int_0^T \frac{d\mathcal{P}_{\text{something}}(t)}{dt}dt\right) \ . \tag{164}$$

We now need to relate the time variable to one of our two variables $dk_\perp$ or z. To do so we must consider what we mean by the first emission. Earlier we said that the hard process is the one which has the largest virtuality Q^2, and that with each emission the emitting particle loses some virtuality (because it has lost four-momentum). Therefore, an earlier emission is associated with a larger Q^2 than a later emission. This ties nicely into equation (164), since time is inversely related to energy, and therefore earlier times are associated with larger four-momenta, or equivalently larger Q^2. We can relate the virtuality to the energy fractions using [61]:

$$Q^2 = E_{cm}^2(1-x_2) \ , \tag{165}$$

and from equation (152) we know that:

$$k_\perp^2 = E_{cm}^2(1-x_1)(1-x_2) = (1-x_1)Q^2 \ . \tag{166}$$

Therefore we see that:

$$\frac{dk_\perp^2}{k_\perp^2} = \frac{dQ^2}{Q^2} \ , \tag{167}$$

which relates $k_\perp^2$ to Q^2 and hence to the first emission. Therefore the probability of a process in our shower occurring in terms of $k_\perp^2$ is [63]:

$$d\mathcal{P} = d\mathcal{P}_0\exp\left(-\int_{k_\perp^2}^{k_{\perp\max}^2}\frac{d\mathcal{P}_0}{dk_\perp^2}dk_\perp^2\right) = \frac{d\sigma}{\sigma_0}\exp\left(-\int_{k_\perp^2}^{k_{\perp\max}^2}\frac{1}{\sigma_0}\frac{d\sigma}{dk_\perp^2}dk_\perp^2\right) \ , \tag{168}$$

where $d\sigma/\sigma_0$ is given by the equations above, $k^2_{\perp_{\max}}$ corresponds to the earliest possible emission and $k^2_\perp$ corresponds to the actual emission. We therefore describe the order of emissions as going from the largest $k^2_\perp$ to the smallest $k^2_\perp$. Note that the exponential in equation (168) is called the Sudakov factor, and that in the regions of phase space where $d\sigma/\sigma_0 \to \infty$, the Sudakov factor approaches 0 exponentially, ensuring a finite answer. Therefore, including the Sudakov factor is a computationally cheap method of approximating all cancellations between loop level and tree level, hence the parton shower is better than matrix elements at handling the soft and collinear regions of phase space [35, 61, 62].

3.2.2 Improving parton showers with matrix elements

We can improve parton showers by including correction factors. We give here a brief outline of one such approach, without explaining any of its details. In this method we calculate the parton-shower approximation and correct the antenna function with a multiplicative correction factor [35, 59, 61]. This can be sketched as:

$$\text{Exact} = \frac{\text{Exact}}{\text{Approximate}} \times \text{Approximate} \ , \tag{169}$$

where "approximate" refers to the parton shower approximation, and the fraction is the correction factor. This factor is, in more detail:

$$\frac{\text{Exact}}{\text{Approximate}} = \frac{|M_{n+1}|^2}{\sum a |M_n|^2} \ , \tag{170}$$

where the sum is over all possible shower histories which could create the final state. We have therefore replaced the antenna function with the exact ratio of matrix elements, and the corrected emission is thus correct to leading order in the perturbative expansion. To do this obviously requires us to be able to calculate the fixed-order matrix element, for which we can use VinciaMHV.

4 Calculating the MHV amplitude

We wrote a C++ program called VinciaMHV which uses the techniques described in section 2 to calculate the full colour-summed MHV squared amplitude (hereafter called the FC MHV squared amplitude) for $qg \to q + ng$, $n = 1, 2, 3, 4$, or any other crossing-related $2 \to n$ process. VinciaMHV can also calculate the kinematic colour-ordered n-gluon amplitude, however we did not have enough time to add the colour information. We can use our program to help calculate the basic hard scatter matrix element and to help correct parton showers using matching (see section 3.2.2). In Section 4.1 we consider the frequency with which we can use VinciaMHV. We then give an overview of the structure of VinciaMHV in Section 5, including what the program can calculate, how it does this, and instructions on how to use it. Note that since VinciaMHV uses header files from PYTHIA, it will not work on a computer on which PYTHIA is not installed. For instructions on how to install PYTHIA see [6] .

4.1 MHV frequency

It is worthwhile to ask what fraction of the time we will sample the MHV configuration for $qg \to q+ng$, $n = 1, 2, 3, 4$, and hence how often we will use VinciaMHV to calculate the amplitude for this process. The first thing to notice is that for 4 or 5 partons, the only non-vanishing amplitude is the MHV amplitude, hence we can use VinciaMHV to calculate the entire matrix element for these multiplicities. How about for 6 or 7 partons? A naive method of calculating how often we are in the MHV configuration i.e. of calculating the MHV frequency, would be to calculate the ratio of MHV configurations to all non-vanishing helicity configurations. For the 6 parton mostly-plus MHV configuration, we have 2 different ways to choose the quark and anti-quark helicities, and 4 possible choices for position of the remaining negative helicity gluon. Since we can also do this for the mostly-minus MHV configuration, we find that there are $2 \times 2 \times 4 = 16$ possible MHV configurations. The non-MHV configuration for 6 partons, also called the NMHV configuration, has 3 positive and 3 negative helicity partons. The quark and anti-quark have opposite helicities, and there are 2 ways of this occurring. We now have ${}^4C_2 = 4!/(2!2!) = 6$ ways in which to choose the positions of the 2 remaining positive helicity gluons, and hence 12 ways of obtaining the NMHV configuration. The ratio of MHV configurations to all non-vanishing helicity configurations for 6 partons is therefore:

$$\frac{\text{MHV}}{\text{All}} = \frac{16}{28} = 0.57 \ . \tag{171}$$

A similar treatment of the 7 parton case shows that there are $2\times2\times5 = 20$ MHV configurations, and $2\times({}^5C_2+{}^5C_3) = 40$ NMHV configurations. Therefore, the ratio of MHV to all non-vanishing helicity configurations is:

$$\frac{\text{MHV}}{\text{All}} = \frac{20}{60} = 0.33 \ . \tag{172}$$

At first glance these do not look promising. However for these ratios to be the MHV frequency, every helicity configuration must contribute equally to the total amplitude. If the MHV configurations contribute more to the total amplitude than non-MHV configurations, then we have an enhanced probability of being in the MHV configuration. To test these contributions we used the RAMBO algorithm to generate a million uniform random phase space points, and used VINCIA's interface with MadGraph4 [25] to calculate the fraction $|M_n^{\text{MHV}}|^2/|M_n|^2$ for each phase space point. We then plotted the probability of each of these fractions occurring, which is shown in Figure 9. The first thing to notice in Figure 9 is that for 4 and 5 partons, we are always in the MHV configuration as expected. More interesting is that for 6 partons, the MHV amplitude contributes $55 - 80\%$ of the amplitude about 90% of the time, while for 7 partons, the MHV amplitude contributes $35 - 60\%$ of the amplitude about 90% of the time. From this we conclude that the naive frequency given by ratios is the lower bound of the true frequency, and that the average MHV frequency is about 15% higher than the simple ratio of possible configurations.

We can find a more accurate MHV frequency by sampling phase space more frequently near the singularities, since the probability of being near them is high. This sampling becomes very interesting when considering the

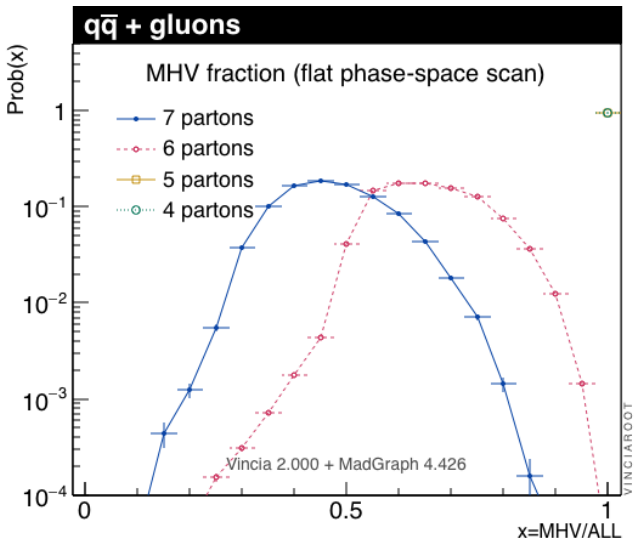

Figure 9: The fractions of the total amplitude given by the MHV amplitudes, and the probability of obtaining these fractions. Phase space was scanned a million times using RAMBO, and amplitudes calculated using VINCIA interfaced with MadGraph4. Notice in the top right-hand corner that for 4 and 5 partons the MHV configuration is the only contributing configuration. Error bars indicate a single standard deviation.

helicity structure of the collinear singularity. Consider the case in which partons a and b become collinear, such that the intermediate momentum $k_P \equiv k_a + k_b$ goes on shell. We have that:

$$k_P^2 = 2k_a \cdot k_b \xrightarrow{a\|b} 0 \ , \tag{173}$$

and:

$$k_a \approx z k_P \ , \qquad k_b \approx (1-z) k_P \ , \tag{174}$$

for $0 < z < 1$. Similarly, since the momenta are (almost) collinear, we have that:

$$\lambda_a \approx \sqrt{z}\lambda_P \ , \qquad \lambda_b \approx \sqrt{1-z}\lambda_P \ , \tag{175}$$

and similar for $\tilde{\lambda}_a$ and $\tilde{\lambda}_b$ where λ_i is a two-spinor as defined in section 2.4. It can be shown that in this case we have [2]:

$$A_n(\dots, a^{h_a}, b^{h_b}, \dots) \xrightarrow{a\|b} \sum_{h_P=\pm} \mathrm{Split}_{-h_P}(a^{h_a}, b^{h_b}; z) A_{n-1}(\dots, P^{h_P}, \dots) \ , \tag{176}$$

where h_i is the helicity of particle i, A_{n-1} is assumed to be an MHV amplitude and $\mathrm{Split}_{-h_P}(a^{h_a}, b^{h_b}; z)$ is a splitting function, which, in the case $q \to qg$, is given by:

$$\begin{aligned} \mathrm{Split}_-(q^+, g^+) &= \frac{1}{\sqrt{1-z}\langle qg\rangle} \ , \quad \mathrm{Split}_-(q^+, g^-) = -\frac{z}{\sqrt{1-z}[qq]} \ , \\ \mathrm{Split}_-(g^+, \bar{q}^+) &= \frac{1}{\sqrt{z}\langle g\bar{q}\rangle} \ , \quad \mathrm{Split}_-(g^-, \bar{q}^+) = -\frac{1-z}{\sqrt{z}[g\bar{q}]} \ , \end{aligned} \tag{177}$$

where the opposite quark helicity case is not shown, and can be calculated using charge conjugation. Note that particle P is going into Split with helicity h_P (see Figure 10), but in the all outgoing convention we must flip the helicity of P, hence we have Split_{-h_P}. For A_n to be MHV we require the positive helicity P to split into two positive helicity particles a and b, which corresponds to the two splitting functions on the left of equation (177). What we notice is that the non-MHV cases on the right of equation (177) are suppressed by z and $1-z$ respectively. If we build up radiation starting from the 5 parton MHV case we find that, in the collinear limit, we obtain the MHV configuration most often. Therefore a weighted scan of phase space may find an even higher MHV frequency than the flat scan in Figure 9. We can therefore use VinciaMHV to calculate significant fractions of the total FC amplitude.

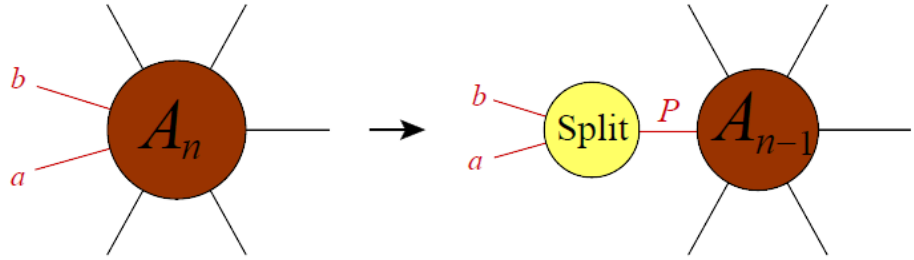

Figure 10: Factorisation of the QCD amplitude when colour-connected partons a and b become collinear. Figure courtesy of [2].

4.2 Structure of VinciaMHV

VinciaMHV is broken up into two classes: `SpinorProducts` and `SPBag`, both contained within a single header file `2_Quarks.h`. The second class inherits spinor products from the first, and calculates the FC MHV squared amplitude for $qg \to q + ng$, $n = 1, 2, 3, 4$, or any other $2 \to n$ crossing-related process. This structure was chosen because spinor products are universal, and we want to retain the flexibility to use different classes to calculate different types of MHV amplitudes. Note that it would be easy to combine these two classes into one. As the name suggests, the main purpose of the former class is to calculate spinor inner products. It requires the input of two four-momenta and should be called as:

- `MHV.spinorProdPos(Vec4 k_i, Vec4 k_j);`, to calculate $\langle ij \rangle$.
- `MHV.spinorProdNeg(Vec4 k_i, Vec4 k_j);`, to calculate $[ij]$.

where `MHV` is an object of class `SpinorProducts` or `SPBag`, `k_i` and `k_j` are the particles' four-momenta, stored as type `Pythia8/Basics::Vec4`, inner products were calculated using equations (73) and (77), and we calculated $k^+ = k^0 + k^3$ using `Pythia8/Basics::pPos()`. Note that the momentum inputs have (natural) units of energy and, while the exact unit is unimportant, for definiteness we will assume that all momentum inputs in this thesis have units of GeV. Further note that we will call all objects of these two classes `MHV` throughout this thesis.

The main purpose of the class `SPBag` is to calculate the FC MHV squared amplitude. It is also possible to use this class to calculate the kinematic amplitude for any colour order, and to calculate the leading-colour (LC) squared amplitude i.e. a single colour-ordered kinematic amplitude squared, multiplied by the diagonal entry of the relevant colour matrix. To calculate the FC MHV squared amplitude we need two functions: one to construct the object of type `SPBag` and calculate all of the spinor inner products; and another to actually calculate the FC MHV squared amplitude. The constructor needs four inputs:

- The (`int`) number of partons in the process.
- A vector of input type `Pythia8/Basics::Vec4` containing the four-momentum of each particle.
- A vector of input type `double` containing the helicities ± 1.0 of each particle.
- A vector of input type `int` containing the particle IDs (see Table 2).

The constructor should be called as follows:

- `SPBag MHV(nPartons, momenta, helicities, IDs);`.

Note that it is important that the i^{th} input of each vector refers to the same particle, and that these inputs are uncrossed (i.e. containing both incoming and outgoing particles).

The first job of the constructor is to cross the two incoming particles into the outgoing formalism of section 2, and rearrange the particles so that they are in the order $q, g_1, g_2, \ldots, g_{n-2}, \bar{q}$, as shown in Table 3. The constructor also checks that we have all of the correct tools to calculate the MHV amplitude. It checks the following: the

Particle	ID
u	1
d	2
s	3
c	4
b	5
g	21

Table 2: The IDs of each particle used in our code. Note that the ID of each anti-quark is just the negative of the quark ID, and that we follow the standard MC particle numbering scheme [70].

Input			Crossed			
particle	4-momentum	Helicities	particle	4-momentum	helicity	Colour order
q	$(5,\ 0,\ 0,\ 5)$	$-$	$\bar{q}$	$(-5,\ 0,\ 0, -5)$	$+$	4
g	$(5,\ 0,\ 0, -5)$	$-$	g	$(-5,\ 0,\ 0,\ 5)$	$+$	2
q	$(5,\ 3,\ 4,\ 0)$	$-$	q	$(\ 5,\ 3,\ 4,\ 0)$	$-$	1
g	$(5, -3, -4,\ 0)$	$-$	g	$(\ 5, -3, -4,\ 0)$	$-$	3

Table 3: An example of input 4-momenta and helicities for VinciaMHV, and the crossed momenta, helicities, particle types and colour-order. The 4-momenta are in units of GeV and given as (E, k^1, k^2, k^3), while the colour order starts at the quark, moves through the gluons in the order in which they appear, and finishes at the anti-quark.

helicity configuration of each particle; that there is exactly one quark and anti-quark with opposite helicities; that all other particles are gluons; and that we are in the MHV configuration. If there is an error, VinciaMHV will output to the screen what the error is, and set all complex variables to the complex error value `pie`, defined as:

$$\text{pie} = -\pi + ei\ . \tag{178}$$

If we ask for the LC or FC squared amplitude VinciaMHV will return the unphysical squared amplitude $|M_n|^2 = -1$.

If there is no error, VinciaMHV begins to calculate spinor inner products. Since the FC MHV squared amplitude requires every possible colour connection, and therefore every possible spinor inner product (see sections 2.3.4 and 2.8), the constructor calculates each unique spinor inner product and store them in an $n \times n$ array which we call `spBag`. This array has the following structure:

$$\begin{pmatrix} \langle qq\rangle & \langle q1\rangle & \dots & \langle q(n-2)\rangle & \langle q\bar{q}\rangle \\ \langle 1q\rangle & \langle 11\rangle & \dots & \langle 1(n-2)\rangle & \langle 1\bar{q}\rangle \\ \vdots & \vdots & \ddots & \vdots & \vdots \\ \langle (n-2)q\rangle & \langle (n-2)1\rangle & \dots & \langle (n-2)(n-2)\rangle & \langle (n-2)\bar{q}\rangle \\ \langle \bar{q}q\rangle & \langle \bar{q}1\rangle & \dots & \langle \bar{q}(n-2)\rangle & \langle \bar{q}\bar{q}\rangle \end{pmatrix}\ , \tag{179}$$

where q and $\bar{q}$ are the quark and anti-quark four-momenta respectively, and $1, 2, \dots, (n-2)$ are the gluon four-momenta in the order of input. Note that since $\langle ij\rangle = -\langle ji\rangle$, and since `SPBag` is symmetric, we only calculate the upper diagonal using `SpinorProducts::spinorProdPos`, and fill the lower diagonal by calculating the negative of the upper diagonal. We also save computational time by not calculating the diagonal inner products, instead pre-setting each $\langle ii\rangle = 0$. For spinor inner products of type $[ij]$ we do the exact same procedure, replacing each $\langle ij\rangle$ with $[ij]$. Note that we often re-use the same inner product to calculate the FC MHV squared amplitude. Therefore, the advantage of this method is that we only have to calculate each spinor inner product once, and then just retrieve their values from this array when needed. Further note that this is not an efficient method if we are only interested in a single LC amplitude squared.

The second important function of class `SPBag` is the function `fullColourAmp`, which calculates either the LC or FC MHV squared amplitude. It takes a single integer input, and is called as:

- `MHV.fullColourAmp(type);`,

where the input `type` tells the computer what to compute:

- `type = 0`: Computes the LC amplitude squared, with the colour-order of the gluons given by the order of input.
- `type = 1`: Computes the FC MHV squared amplitude.

Note that a particular LC amplitude may not diverge, even if the FC amplitude diverges. This would happen if there are two collinear partons i and j which are not colour-connected in the LC amplitude. However, to calculate the FC MHV squared amplitude we sum over every colour connection (see Section 2.3.4), hence the FC MHV squared amplitude diverges, even though the LC amplitude did not. Therefore we should exercise additional caution when interpreting the results of a LC amplitude.

The first task of the `fullColourAmp` function (when `type = 1`) is to calculate each of the kinematic amplitudes, and store them in an array, which we call `ampBag`. This calculation was optimised by noting that the entire numerator, as well as the term $\langle \bar{q}q \rangle$ in the denominator of equation (136), is common to each kinematic amplitude in `ampBag`. Hence we only calculate this common factor once, and then, for each amplitude in `ampBag`, divide this factor by the relevant inner products in the denominator. We use the function `std::next_permutation()` to permute the $n-2$ gluons after each colour-ordered kinematic amplitude is created. This permutes the gluons lexicographically, which means that if we replace the numerical sequence $1, 2, 3, \ldots, n$ with the alphabetical sequence $a, b, c, \ldots, n$, then the set of permutations is in alphabetical order. For example, the lexicographical order of $1, 2, 3$ is:

$$(1,2,3),\ (1,3,2),\ (2,1,3),\ (2,3,1),\ (3,1,2),\ (3,2,1),$$

and `ampBag` would have the following entries:

$$\texttt{ampBag} = [A_5(1,2,3), A_5(1,3,2), A_5(2,1,3), A_5(2,3,1), A_5(3,1,2), A_5(3,2,1)] \ ,$$

where $A_5(1,2,3)$ refers to the kinematic MHV amplitude with gluons given by colour-order $(1,2,3)$. If amplitude i has a singularity, then `ampBag[i]= pie`, `fullColourAmp(type)` returns -1, (i.e. $|M_n|^2 = -1$), and an error message is output to the screen. If there is no error we use the matrix equation (see equation (39)):

$$|M_n|^2 = A_i^* (C_n)_{ij} A_j \ , \tag{180}$$

to calculate the FC MHV squared amplitude (without the factor of g_s^{2n-4}), where A_i is the i^{th} component of `ampBag`, and $(C_n)_{ij}$ is the colour matrix for n partons given in Appendix H. We used a MadGraph4 interface to calculate each colour matrix, corrected for both the difference in t-matrix and gluon-permutation conventions, and stored each C_n in the header file `2_Quarks.h`. Since equation (180) is symmetric, we optimised VinciaMHV by calculating:

$$|M_n|^2 = \sum_{i>j} 2[\mathrm{Re}(A_i^*)\mathrm{Re}(A_j) + \mathrm{Im}(A_i^*)\mathrm{Im}(A_j)](C_n)_{ij} + \sum_k |A_k|^2 (C_n)_{kk} \ , \tag{181}$$

instead of equation (180). Note that equation (181) is independent of the running coupling, and is therefore scale invariant. Further note that the squared amplitude has (natural) units of E^{8-2n}, where E is energy. Other useful functions in the class `SPBag` are:

- `printMatrix()`: Prints `spBag` (equation (179)).
- `printAmps()`: Prints all of the colour-ordered kinematic amplitudes in `ampBag`.
- `amplitude(type)`: Calculates colour-ordered kinematic amplitudes. If `type = 0`, it calculates the colour-ordered kinematic amplitude $A_n(1, 2, \ldots, n-2)$, and if `type = 1`, it calculates all colour-ordered kinematic amplitudes and stores them in `ampBag`.

5 Comparing VinciaMHV to MadGraph4

We used an existing interface to MadGraph4 to compare VinciaMHV's output with a known, conventional solution for the process $qg \to q + ng$, $n = 1, 2, 3, 4$. We tested both the LC and FC MHV squared amplitudes for accuracy, and compared the time it takes each program to calculate the FC MHV squared amplitude.

5.1 Validation at specific phase-space points

We compared the VinciaMHV 4-parton LC squared amplitude against MadGraph4 for pre-determined phase-space points. One such point is shown in Table 4, and shows that we successfully crossed and re-ordered our partons, and calculated the correct LC squared amplitude. It additionally validates equation (138), which states that the mostly-plus and mostly-minus squared MHV amplitudes are equivalent. Note that we will only include unique MHV squared amplitudes from this point on.

We tested the VinciaMHV 4-parton FC MHV squared amplitude against MadGraph4 for three different momentum configurations. The configurations and their results are given in Tables 5 - 7, and show agreement between the two programs up to at least 8 significant figures. Notice that for the second momentum configuration, shown in Table 6, the quark and gluon scatter mostly in the forwards direction, leading to an enhanced amplitude, while for the third momentum configuration, shown in Table 7, the quark and gluon scatter mostly in the backwards direction, hence dampening the amplitude as expected. We also chose specific phase-space points for the 5-parton and 6-parton processes and validated VinciaMHV for these multiplicities, as shown in Tables 8 and 9 respectively.

To validate VinciaMHV for the 7-parton process we used RAMBO to provide ten million uniform random four-momenta, and at each of these compared the FC MHV squared amplitude calculated by VinciaMHV to that calculated by MadGraph4. In Table 10, we show two such comparisons which demonstrate the divergent nature of MHV amplitudes. In the first configuration, each particle has roughly an equal share of the incoming energy, and is well separated. Therefore the FC MHV squared amplitude has the relatively small value of 1.457×10^3 GeV^{-6}. In the second configuration, the final gluon is soft compared to every other particle, and is approximately collinear to the incoming gluon, hence the FC MHV squared amplitude has the much larger value of 2.878×10^{11} GeV^{-6}.

Helicities	MadGraph4	VinciaMHV
$----$	170.7	170.7
$-+-+$	42.67	42.67
$+-+-$	42.67	42.67
$++++$	170.7	170.7

Table 4: Validation of VinciaMHV LC squared amplitude, and the equivalence of the mostly-minus and mostly-plus squared amplitudes. Four-momenta are taken from Table 3, and helicities are uncrossed. Note that the 4-parton squared amplitude is dimensionless.

Particle	E	k^1	k^2	k^3
q	5	0	0	5
g	5	0	0	-5
q	5	3	4	0
g	5	-3	-4	0
Helicities	MadGraph4		VinciaMHV	
$----$	234.66667		234.66667	
$-+-+$	58.666667		58.666667	

Table 5: VinciaMHV 4-parton FC MHV squared amplitude for transverse scattering. Momentum is uncrossed and in units of GeV and the 4-parton squared amplitudes are dimensionless.

Particle	E	k^1	k^2	k^3
q	5	0	0	5
g	5	0	0	-5
q	5	4	0	3
g	5	-4	0	-3
Helicities	MadGraph4		VinciaMHV	
$----$	1226.6667		1226.6667	
$-+-+$	785.06667		785.06667	

Table 6: VinciaMHV 4-parton FC MHV squared amplitude for mostly forward scattering. Momentum is uncrossed and in units of GeV and the 4-parton squared amplitudes are dimensionless.

Particle	E	k^1	k^2	k^3
q	5	0	0	5
g	5	0	0	-5
q	5	-4	0	-3
g	5	4	0	3
Helicities	MadGraph4		VinciaMHV	
$----$	181.66667		181.66667	
$-+-+$	7.2666667		7.2666667	

Table 7: VinciaMHV 4-parton FC MHV squared amplitudes for mostly backward scattering. Momentum is uncrossed and in units of GeV and the 4-parton squared amplitudes are dimensionless.

Particle	E	k^1	k^2	k^3
q	5	0	0	5
g	5	0	0	-5
q	4.167	2.5	3.333	0
g	3.333	0	-3.333	0
g	2.5	-2.5	0	0
Helicities	MadGraph4		VinciaMHV	
$-----$	442.5		442.5	
$----+$	44.25		44.25	
$---+-$	9.834		9.834	
$-+--+$	5.532		5.532	
$-+-+-$	19.67		19.67	
$-+-++$	76.83		76.83	

Table 8: VinciaMHV 5-parton FC MHV squared amplitude for a chosen phase-space point. Momentum is uncrossed and in units of GeV and the 5-parton FC MHV squared amplitude has units of GeV^{-2}

Particle	E	k^1	k^2	k^3
q	5	0	0	5
g	5	0	0	-5
q	3	1	2.333	1.599
g	2	1	0.667	-1.599
g	2	-2	0	0
g	3	0	-3	0
Helicities	MadGraph4		VinciaMHV	
$------$	1.348×10^4		1.348×10^4	
$-----++$	18.22		18.22	
$----+-+$	24.01		24.01	
$----++-$	288.1		288.1	
$-+---+$	253.2		253.2	
$-+---+-$	37.51		37.51	
$-+-+--$	163.9		163.9	
$-+-+++$	2850		2850	

Table 9: VinciaMHV 6-parton FC MHV squared amplitude for a chosen phase-space point. Momentum is uncrossed and in units of GeV and the 6-parton squared amplitudes have units of GeV^{-4}

Particle	E	k^1	k^2	k^3
q	5	0	0	5
g	5	0	0	-5
q	1.347	-0.041	-0.305	-1.312
g	1.389	-1.134	-0.504	-0.624
g	2.341	2.020	-1.071	0.505
g	2.812	0.656	2.726	0.214
g	2.110	-1.501	-0.846	1.218
Helicities	MadGraph4		VinciaMHV	
$-------$	1.457×10^3		1.457×10^3	

Particle	E	k^1	k^2	k^3
q	5	0	0	5
g	5	0	0	-5
q	4.066	-2.204	-3.203	1.192
g	1.782	-0.865	1.450	-0.572
g	2.318	1.668	0.886	-1.345
g	1.810	1.402	0.866	0.748
g	2.3×10^{-2}	-4×10^{-4}	4×10^{-4}	-2.3×10^{-2}
Helicities	MadGraph4		VinciaMHV	
$-------$	1.872×10^{15}		1.872×10^{15}	

Table 10: VinciaMHV 7-parton FC MHV squared amplitudes for two phase-space points. Momentum is uncrossed and in units of GeV, and the 7-parton squared amplitude has units GeV^{-6}.

5.2 Singularity structure

A region in which it is possible to lose numerical precision is the collinear region. For VinciaMHV, this loss would occur because the spinor inner product is defined numerically as:

$$\langle ij\rangle = \sqrt{k_j^+}e^{i\phi_i} - \sqrt{k_i^+}e^{i\phi_j} \ , \tag{182}$$

along with a similar expression for $[ij]$. If the two partons i and j are almost collinear, we will subtract similar terms in equation (182), and hence lose numerical precision. Since the collinear spinor inner product gives the dominant contribution to the FC MHV squared amplitude, any loss in numerical precision will be significant. Similarly, it is possible for MadGraph4 to lose numerical precision in the collinear region of phase space since the cancellations between diagrams may be very significant in this region.

To test the relative precision of the two programs in the collinear limit we used a simple 5-parton collinear phase-space point, and used `Pythia8/Basics::Vec4::rot(`ϵ`,0)` to rotate the final-state partons by a small polar angle ϵ. We used both programs to calculate the FC MHV squared amplitude, and plotted the relative precision between them for decreasing values of ϵ. We used two different helicity configurations, one in which the two collinear partons have the same helicity, and one in which their helicities differ. This plot is shown in Figure 11. Note that the relative precision is defined as:

$$\text{Relative VinciaMHV Precision} = \frac{|\text{VinciaMHV} - \text{MadGraph4}|}{\text{VinciaMHV} + \text{MadGraph4}} \ , \tag{183}$$

and that the specific momentum configuration is shown in Table 11. From Figure 11, we see that the two programs diverge from one another in the collinear limit, and if the two collinear helicities differ in the all-outgoing convention, then this divergence is enhanced. The two programs diverge from one another at $\epsilon < 10^{-5}$ for the opposite helicity case, while for the same helicity case this divergence occurs for $\epsilon < 10^{-7}$. Further, Table 12 shows that MadGraph4 gives the more singular result at the asymptote. Figure 11 also shows that any loss of precision in VinciaMHV will occur beyond any phase space cuts, which are typically at the order of 1GeV, which corresponds to $\epsilon \approx 10^{-3}$. Finally, we also see that the two programs appear to converge in the region in which they will be used, something which will be confirmed in the next section.

Particle	E	k^1	k^2	k^3
q	1	0	0	1
g	1	0	0	-1
q	0.417	0.333	0.250	0
g	0.333	-3.333	0	0
g	0.250	0	0	-0.250

Table 11: Uncrossed momentum inputs for Figure 11.

ϵ	MadGraph4	VinciaMHV
1.00×10^{-7}	3.53×10^{29}	1.78×10^{19}
5.62×10^{-7}	7.75×10^{22}	5.63×10^{17}
1.00×10^{-6}	7.91×10^{20}	1.78×10^{17}
5.62×10^{-5}	5.64×10^{13}	5.64×10^{13}

Table 12: MadGraph4 and VinciaMHV FC MHV squared amplitudes in the collinear limit for the $(-,+,+,-,-)$ helicity configuration. These values are all from the asymptotic region of Figure 11.

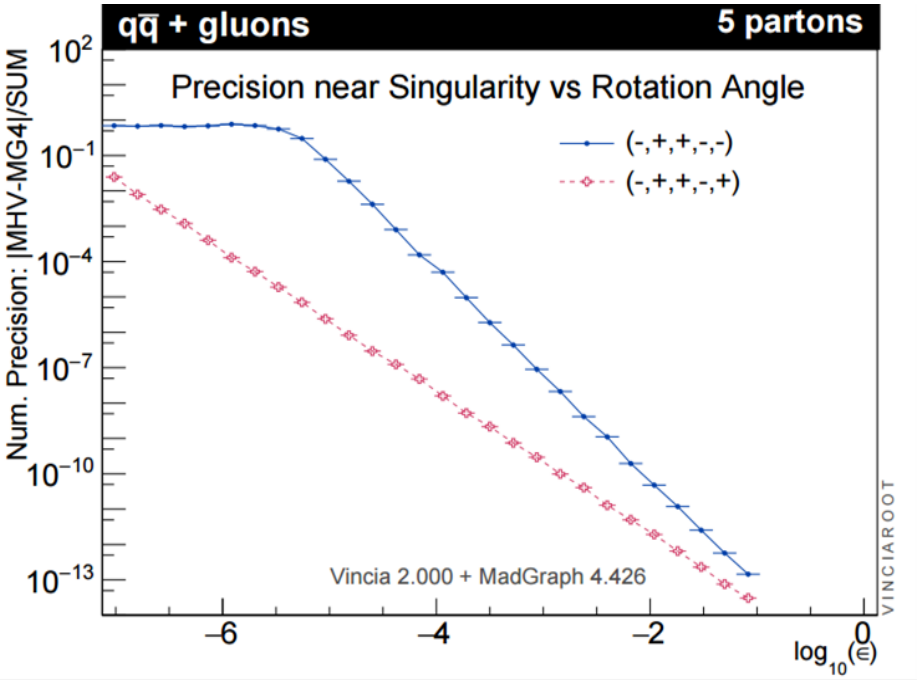

Figure 11: Relative numerical precision of VinciaMHV compared to MadGraph4 near the singularities. The helicities are given in the order $q, \bar{q}, g_1, g_2, g_3$, and are in the all-outgoing formalism. Error bars indicate a single standard deviation.

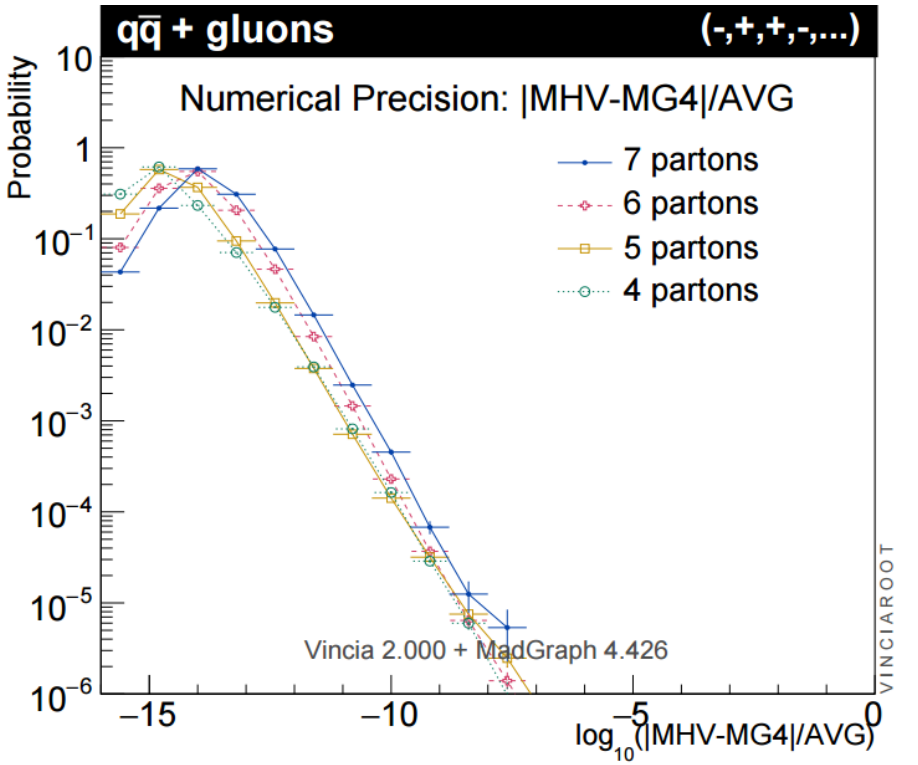

Figure 12: Relative numerical precision of VinciaMHV compared to MadGraph4. Error bars indicate a single standard deviation.

5.3 Precision tests

We used RAMBO to generate ten million n-parton phase-space points for $n = 4, 5, 6, 7$, and calculated the FC MHV squared amplitude using both VinciaMHV and MadGraph4. We calculated the relative numerical precision of VinciaMHV, in this case normalised such that:

$$\text{Relative VinciaMHV Precision} = \frac{|\text{VinciaMHV} - \text{MadGraph4}|}{\text{Average}} , \tag{184}$$

and plotted its probability distribution in Figure 12. We see that the two programs agree to better than one part in a trillion 96% of the time, and to better than one part in a billion over 99% of the time, thus validating our implementations. Additionally, we see that the difference between the two programs becomes slightly larger as we increase the number of partons. This is as expected, because at increasing multiplicities MadGraph4 sums over more diagrams, cancelling an increasing number of terms, and hence losing numerical precision in the kinematic amplitude. Conversely, VinciaMHV uses multiplication to calculate this value, and therefore does not lose stability with additional partons. For this reason we expect the very small observed difference between the two programs to be in favour of VinciaMHV. Figure 12 also shows that one (or both) of the programs becomes numerically unstable at certain phase space points, however this is rare, and the two programs are in near-perfect agreement in almost all of phase space, hence we can use either program to calculate the same result.

5.4 Speed tests

In this thesis we aimed to increase the speed with which we calculate QCD amplitudes, especially those of high multiplicity. Many programs use Feynman diagrams to calculate the squared amplitude, however the stronger than factorial growth of the number of diagrams makes these programs very slow for high multiplicities. To test just how slow, we tested the speed that it takes a single 3 GHz CPU (Mac Pro) to calculate an MHV amplitude using MadGraph4, and, for comparison, tested the time it takes VinciaMHV to calculate the same amplitude. To do this we used RAMBO to generate 10 million uniform random n-parton phase space points for $n = 4, 5, 6, 7$, and calculated the average time it took each program to calculate each amplitude. The results are shown in Table 13. For 4 and 5 partons MadGraph4 takes only a few microseconds per phase-space point, while for 6 partons we need 55.8 microseconds per phase-space point, and for 7 partons we decrease the speed per phase-space point by a factor of 11.77 to 651.5 microseconds per phase space point. Excluding RAMBO, it took 108 minutes for MadGraph4 to calculate the 7-parton FC MHV squared amplitude for every phase-space point generated.

Using VinciaMHV, the speed increases by a factor of 2.2 and 3.5 for 4 and 5-parton amplitudes respectively, and because the MHV configuration is the only contributing configuration, we will always experience this gain. We saw in Section 4.1 that for 6 partons the MHV configuration occurs between about $55 - 80\%$ of the time. Therefore, if we use VinciaMHV to calculate the MHV amplitudes and MadGraph4 to calculate the non-MHV amplitudes, we would expect the efficiency increase in calculating the total FC amplitude $|M_n|^2$ to be a factor of about $55 - 80\%$ of 10.2, i.e. a factor of about $5.6 - 8.2$. Similarly, since for the 7 parton amplitude we are in the MHV configuration between about $35 - 60\%$ of the time, we expect the efficiency increase in calculating $|M_n|^2$ to be a factor of about $8.2 - 14$. If we use both programs to calculate ten million random phase space points using a weighted helicity sample, we therefore expect the total time taken to be between 8 and 13 minutes. This is compared to the pure MadGraph4 value of 108 minutes calculated earlier. Note that while MadGraph5 is the latest version, we still expect that a speed test of MadGraph4 will be representative of the loss of speed at high multiplicities, since both versions of MadGraph use Feynman diagrams to calculate their amplitude.

nParticles	RAMBO	MadGraph4	VinciaMHV	Ratio
4	0.32	4.16	2.04	2.2
5	0.42	9.84	3.14	3.5
6	0.51	55.8	5.94	10.2
7	0.62	651.5	28.3	23.5

Table 13: Time it takes in microseconds to calculate a single FC MHV squared amplitude (including RAMBO). The ratio is excluding RAMBO, and all speeds were benchmarked with a single 3GHz CPU (Mac Pro) using clang++ v3.6 -02.

It is interesting to note that the speed of VinciaMHV also decreases noticeably with particle multiplicity. This is because the number of kinematic amplitudes grows factorially. Recall that to calculate the FC MHV squared

amplitude we evaluate:

$$|M_n|^2 = \sum_{i>j} 2[\mathrm{Re}(A_i^*)\mathrm{Re}(A_j) + \mathrm{Im}(A_i^*)\mathrm{Im}(A_j)](C_n)_{ij} + \sum_k |A_k|^2 (C_n)_{kk} \ , \tag{185}$$

where for the 4-parton amplitude we evaluate 2 terms in equation (185), for the 6-parton amplitude we evaluate 288 terms, and for the 7-parton amplitude we evaluate 7200 terms, hence why a 7-parton FC MHV squared amplitude is calculated 14 times slower than a 4-parton FC MHV squared amplitude. This leads into our final comment that a speed comparison for a single kinematic amplitude or a LC squared amplitude would yield even more impressive looking results, since VinciaMHV would not have to sum any terms while MadGraph4 still sums its diagrams. However, the LC squared amplitude does not take colour interference into account, and for realistic results we must choose the FC squared amplitudes.

6 Summary and outlook

In this thesis it was shown that the spinor-helicity formalism can be used to calculate the MHV amplitude very efficiently. If put within the context of a MC event generator, it is possible to use this formalism to increase the speed with which we calculate the QCD matrix elements needed for the hard process and matching. We created a program called VinciaMHV which uses this formalism to calculate the MHV FC squared amplitude $qg \to q + ng$ for $n = 1, 2, 3, 4$, or any other $2 \to n$ amplitude related to this process by crossing. We explored the frequency with which we can use VinciaMHV, explained how VinciaMHV calculates its MHV amplitudes, and gave instructions on how to use it. We found that for 6 partons the MHV configuration occurs about $55 - 80\%$ of the time, and for 7 partons this occurs about $35 - 60\%$ of the time. We tested the accuracy and speed of VinciaMHV relative to MadGraph4, with which we had an existing interface. We chose MadGraph4 since we wanted to compare the spinor-helicity method to the method of summing Feynman diagrams. We found that the two programs give the same result for the FC MHV squared amplitude up to at least the 9^{th} significant figure for over 99% of phase space, thus validating VinciaMHV. Using clang++ v3.6 -02 on a single 3 GHz CPU (Mac Pro) to benchmark the speed of both VinciaMHV and MadGraph4, and using RAMBO to generate ten million uniform random phase space points, we found that on average VinciaMHV calculates the 7-parton FC MHV squared amplitude 23.5 times faster than MadGraph4, with decreasing gain for smaller parton multiplicities. Using the fraction of the time we expect to sample the MHV configuration, we found that using VinciaMHV together with MadGraph4 will increase the matrix-element calculation by a factor of $5.6 - 8.2$ times for 6 partons, and by a factor of $8.2 - 14$ times for 7 partons.

In addition to the above, we did extensive work proving the current literature. A major issue was to obtain a set of self-consistent conventions for the spinor-helicity formalism, since no complete set was available in the literature. These conventions are given in Appendix A. To gain a better understanding of the amplitudes at hand, we proved many of the spinor identities which we use to calculate the MHV amplitude. The results can be found in Appendix C. In Appendix D we showed that we can choose reference momenta such that many gluon polarisation contractions vanish. In Appendix F we calculated the parton energy fractions, and used them to reformulate the $q\bar{q} \to qg\bar{q}$ antenna function. Finally, in Appendix G we partially calculated the n-gluon colour factor.

There are several possible extensions to this project. The simplest is to add the colour information to the all-gluon MHV amplitude, and add another gluon to the $qg \to q + ng$ FC amplitude. Since we have a program which converts a MadGraph5 colour matrix into a VinciaMHV colour matrix, these extensions should be trivial. Less trivial is to extend VinciaMHV to calculate the MHV amplitude involving a second quark anti-quark pair, however there is existing literature on this topic [16, 18, 27]. Once this is achieved we can further extend VinciaMHV to include the case in which a massive electroweak boson decays to a lepton pair [12, 15, 18, 27]. Note that the spinor helicity formalism is a natural way to describe electroweak decay since Z^0 couples differently to left and right-handed particles, while the $W^{\pm}$ only couples to left-handed particles. Additionally, we can further extend VinciaMHV by including the process involving a Higgs boson and n partons [71, 72]. Finally, we wish to also use the spinor-helicity formalism to calculate the next-to MHV (NMHV) and next-to next-to MHV (NNMHV) etc. amplitudes so that we can efficiently calculate any FC squared amplitude. We hope that with these extensions we can use VinciaMHV within VINCIA to accurately simulate 7 or more jets at the LHC.

A Conventions

Due to the unfortunately large number of conventions used within physics it is useful to explicitly define those which we use[16]. This thesis uses natural units in which $c = \hbar = 1$. The metric tensor is defined to be:

$$g_{\mu\nu} = g^{\mu\nu} = \text{diag}(+1, -1, -1, -1) \ , \tag{186}$$

where $\mu, \nu = 0, 1, 2, 3$ are spacetime indices. we will use indices in the middle of the Greek alphabet ($\mu, \nu, \rho, ...$ to indicate spacetime indices[17] while indices from the start of the Greek alphabet ($\alpha, \beta, \gamma, ... = 1, 2$) are spinor indices. Contravariant four-vectors (e.g. position and momentum) are defined with raised indices, while covariant four-vectors (e.g. derivatives) are defined with lowered indices:

$$x^\mu = (t, \vec{\mathbf{x}}) \tag{187}$$

$$k^\mu = (E, \vec{\mathbf{k}}) \tag{188}$$

$$\partial_\mu \equiv \frac{\partial}{\partial x^\mu} = \left(\frac{\partial}{\partial t}, \vec{\boldsymbol{\nabla}}\right) \ . \tag{189}$$

The Pauli matrices σ^i, $i = 1, 2, 3$, are defined as:

$$\sigma^1 = \begin{pmatrix} 0 & 1 \\ 1 & 0 \end{pmatrix} \ , \qquad \sigma^2 = \begin{pmatrix} 0 & -i \\ i & 0 \end{pmatrix} \ , \qquad \sigma^3 = \begin{pmatrix} 1 & 0 \\ 0 & -1 \end{pmatrix} \ , \tag{190}$$

and can be put into a two separate four-vectors:

$$\begin{aligned} (\sigma^\mu)^{\dot{\beta}\alpha} \equiv \overline{\sigma}^\mu \equiv \sigma_+ &= (\mathbb{1}_{2\times 2}, -\vec{\boldsymbol{\sigma}}) \\ (\sigma^\mu)_{\alpha\dot{\beta}} \equiv \sigma^\mu \equiv \sigma_- &= (\mathbb{1}_{2\times 2}, \vec{\boldsymbol{\sigma}}) \ , \end{aligned} \tag{191}$$

with $\vec{\boldsymbol{\sigma}} \equiv (\sigma^1, \sigma^2, \sigma^3)$. The Dirac gamma matrices γ^μ follow a Clifford algebra:

$$\{\gamma^\mu, \gamma^\nu\} \equiv \gamma^\mu\gamma^\nu + \gamma^\nu\gamma^\mu = 2g^{\mu\nu}\mathbb{1}_{4\times 4} \ , \tag{192}$$

and are considered to be in the Chiral representation:

$$\gamma^\mu = \begin{pmatrix} 0 & \overline{\sigma}^\mu \\ \sigma^\mu & 0 \end{pmatrix} \ , \tag{193}$$

where each component of the gamma matrices is itself a 2×2 matrix. The Dirac four-spinor U which obeys the four-component massless Dirac equation $\not{k}U = 0$ ($\not{k} = \gamma^\mu k_\mu$) can be defined in terms of 2 independent projections $U_\pm$, where U_+ (U_-) defines a right-handed (left-handed) Dirac spinor, and $U_\pm = P_\pm U$ with:

$$P_\pm = \frac{1}{2}(1 \pm \gamma^5) \ . \tag{194}$$

Here the sign convention of γ^5 is:

$$\gamma^5 = i\gamma^0\gamma^1\gamma^2\gamma^3 = \begin{pmatrix} 1 & 0 \\ 0 & -1 \end{pmatrix} \ . \tag{195}$$

To move from the Dirac spinor to the Weyl spinor it is necessary to first use the projection operator and then re-write $U_\pm$ in two component notation:

$$U_+(k_i) \equiv |i^+\rangle \equiv (\lambda_i)_\alpha = \begin{pmatrix} \sqrt{k_i^+} \\ e^{i\phi_i} \end{pmatrix} \tag{196}$$

$$\overline{U}_-(k_i) \equiv \langle i^-| \equiv (\lambda_i)^\alpha = \begin{pmatrix} e^{i\phi_i} & -\sqrt{k_i^+} \end{pmatrix} \tag{197}$$

$$\overline{U}_+(k_i) \equiv \langle i^+| \equiv (\tilde{\lambda}_i)_{\dot{\alpha}} = \begin{pmatrix} e^{-i\phi_i} & -\sqrt{k_i^+} \end{pmatrix} \tag{198}$$

$$U_-(k_i) \equiv |i^-\rangle \equiv (\tilde{\lambda}_i)^{\dot{\alpha}} = \begin{pmatrix} \sqrt{k_i^+} \\ e^{-i\phi_i} \end{pmatrix} \ . \tag{199}$$

[16] For example, while all of [18, 49, 53–55, 73, 74] explain or use spinor indices, none of them use the same conventions. Fortunately, an excellent review by Dreiner, Haber and Martin explains how to manoeuvre between different conventions [49].

[17] for a pedagogical treatment of spacetime indices see the textbook by Riley, Hobson and Bence [48]).

Note that equations (196) - (199) are just equations (43) - (49), with all symbols as previously defined. Hence we have that:

$$U = \begin{pmatrix} \lambda_\alpha \\ \tilde{\lambda}^{\dot{\alpha}} \end{pmatrix} \ , \tag{200}$$

and similarly:

$$\overline{U} = \begin{pmatrix} \tilde{\lambda}_{\dot{\alpha}} & \lambda^\alpha \end{pmatrix} \ . \tag{201}$$

The Levi-Cevita tensor used to raise or lower spinor indices is defined as:

$$\epsilon^{12} = -\epsilon^{21} = -\epsilon_{12} = \epsilon_{21} = 1 \ , \tag{202}$$

which written in matrix notation is:

$$\epsilon^{\alpha\beta} = \begin{pmatrix} 0 & 1 \\ -1 & 0 \end{pmatrix} \quad \text{and} \quad \epsilon_{\alpha\beta} = \begin{pmatrix} 0 & -1 \\ 1 & 0 \end{pmatrix} \ . \tag{203}$$

The epsilons obey the following identies:

$$\epsilon_{\alpha\beta}\epsilon^{\gamma\delta} = -\delta^\gamma_\alpha\delta^\delta_\beta + \delta^\delta_\alpha\delta^\gamma_\beta \ , \qquad \epsilon_{\dot{\alpha}\dot{\beta}}\epsilon^{\dot{\gamma}\dot{\delta}} = -\delta^{\dot{\gamma}}_{\dot{\alpha}}\delta^{\dot{\delta}}_{\dot{\beta}} + \delta^{\dot{\delta}}_{\dot{\alpha}}\delta^{\dot{\gamma}}_{\dot{\beta}} \ , \tag{204}$$

where δ is the Kronecker delta. From this it follows that:

$$\epsilon_{\alpha\beta}\epsilon^{\beta\gamma} = \epsilon^{\gamma\beta}\epsilon_{\beta\alpha} = \delta^\gamma_\alpha \ , \qquad \epsilon_{\dot{\alpha}\dot{\beta}}\epsilon^{\dot{\beta}\dot{\gamma}} = \epsilon^{\dot{\gamma}\dot{\beta}}\epsilon_{\dot{\beta}\dot{\alpha}} = \delta^{\dot{\gamma}}_{\dot{\alpha}} \ . \tag{205}$$

B QCD Feynman rules

The full (i.e. including colour) Feynman rules for massless QCD with all particles outgoing are [36, 38]

Vertices:

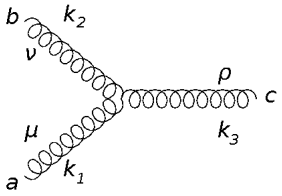

$$= \ ig_s f^{abc}[g_{\mu\nu}(k_1 - k_2)_\rho + g_{\nu\rho}(k_2 - k_3)_\mu + g_{\rho\mu}(k_3 - k_1)_\nu]$$

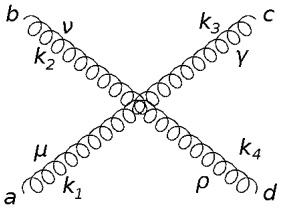

$$= \ ig_s^2[f^{abe}f^{cde}(g_{\mu\gamma}g_{\nu\rho} - g_{\mu\rho}g_{\nu\gamma}) + f^{ace}f^{dbe}(g_{\mu\rho}g_{\nu\gamma} - g_{\mu\nu}g_{\gamma\rho}) + f^{ade}f^{bce}(g_{\mu\nu}g_{\gamma\rho} - g_{\mu\gamma}g_{\nu\rho})]$$

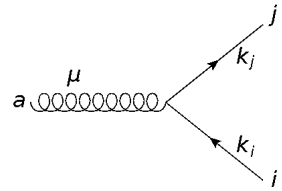

$$= \ -ig_s t^a_{ij}\gamma_\mu$$

Propagators:

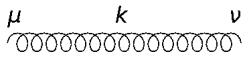

$$= \ -i\frac{g_{\mu\nu}}{k^2}\delta^{ab}$$

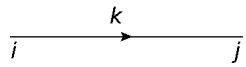

$$= \ \frac{i}{\not{k}}\delta^{ij}$$

External Particles:

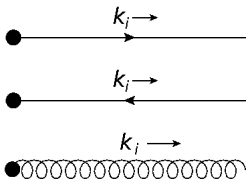

$$= \bar{u}_{\pm}(k_i) = \langle i^{\pm}|$$

$$= v_{\mp}(k_i) = |i^{\pm}\rangle$$

$$= \epsilon^{\pm}_{\mu}(k_i, p_i)$$

where straight lines represent fermions, curly lines represent gluons, all momenta are considered outgoing and we are in the Lorentz-Feynman gauge. By decoupling the colour indices a, b, c, d from the spacetime kinematical indices μ, ν, ρ, γ we are able to factorise the full amplitude into a product of colour factors and kinematical factors (see equations (12) and (37)). The colour factors are trivial (if tedious) to calculate using equations (9) and (10), and the kinematical factors can be calculated in several ways. The brute-force approach is to use the colour-ordered Feynman rules for massless particles [28]:

Vertices:

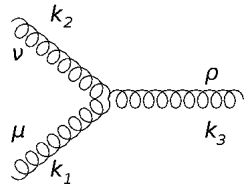

$$= \frac{i}{\sqrt{2}}[g_{\mu\nu}(k_1 - k_2)_\rho + g_{\nu\rho}(k_2 - k_3)_\mu + g_{\rho\mu}(k_3 - k_1)_\nu]$$

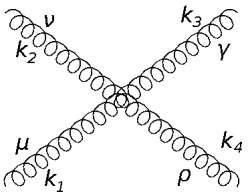

$$= ig_{\mu\gamma}g_{\nu\rho} - \frac{i}{2}(g_{\mu\rho}g_{\nu\gamma} + g_{\mu\nu}g_{\gamma\rho})$$

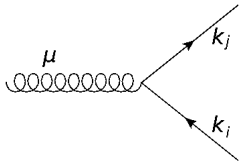

$$= -i\sqrt{2}\gamma_\mu$$

Propagators:

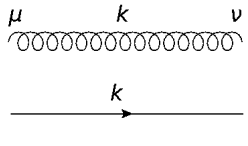

$$= -i\frac{g_{\mu\nu}}{k^2}$$

$$= \frac{i}{\not{k}}$$

External Particles:

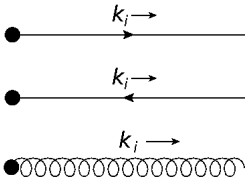

$$= \bar{u}_{\pm}(k_i) = \langle i^{\pm}| = \bar{v}_{\pm}(k_i)$$

$$= v_{\mp}(k_i) = |i^{\pm}\rangle = u_{\pm}(k_i)$$

$$= \epsilon^{\pm}_{\mu}(k_i, p_i)$$

which are just the full Feynman rules above with all colour information removed. Note that the appearance of $\sqrt{2}$ in many of these rules comes from our normalisation convention and that these rules are also in the Lorentz-Feynman gauge. We can use the colour-ordered rules in the helicity basis to confirm the helicity amplitudes calculated in section 2.5.

C Proofs of Weyl-spinor identities

In this section we expand upon some results and statements made in sections 2.4.1 and 2.4.2. Note that these proofs are very rarely recorded in the literature, and hence this appendix (along with appendix F and G) shows evidence of our own work and understanding of the topics in this thesis. The Dirac equation is straightforward to prove using spinor inner products. Recall one of the four massless Dirac equations:

$$(\not{k}_i)_{\alpha\dot{\alpha}}(\tilde{\lambda}_i)^{\dot{\alpha}} = 0 \ , \tag{206}$$

for which we want to prove that the left hand side is indeed 0. Using equation (61) we have that:

$$\begin{aligned}(\not{k}_i)_{\alpha\dot{\alpha}}(\tilde{\lambda}_i)^{\dot{\alpha}} =&(\lambda_i)_\alpha(\tilde{\lambda}_i)_{\dot{\alpha}}(\tilde{\lambda}_i)^{\dot{\alpha}} \\ =&(\lambda_i)_\alpha[ii] \\ =&0 \ ,\end{aligned} \tag{207}$$

where we used that the inner product $[ii]$ is antisymmetric. Next let us consider the momentum invariant $s_{ij} = (k_i + k_j)^2 = 2k_i \cdot k_j = \langle ij\rangle[ji]$. To prove this first recall the Fierz identity (equation (69)):

$$(\sigma_\mu)^{\dot{\alpha}\alpha}(\sigma^\mu)_{\dot{\beta}\beta} = \ 2\delta_\alpha{}^\beta\delta^{\dot{\beta}}{}_{\dot{\alpha}} \ . \tag{208}$$

Next use equations (63) and (64) to write the momentum invariant as:

$$s_{ij} = 2k_i \cdot k_j = \frac{1}{2}(\tilde{\lambda}_i)_{\dot{\alpha}}(\sigma^\mu)^{\dot{\alpha}\alpha}(\lambda_i)_\alpha(\lambda_i)^\beta(\sigma_\mu)_{\beta\dot{\beta}}(\tilde{\lambda}_i)^{\dot{\beta}} \ , \tag{209}$$

and use the Fierz identity (equation (208)) and then the definitions of spinor inner products (equations (72) and (77)) to show that:

$$\begin{aligned}s_{ij} = 2k_i \cdot k_j =&\frac{1}{2}(\tilde{\lambda}_i)_{\dot{\alpha}}(\sigma^\mu)^{\dot{\alpha}\alpha}(\lambda_i)_\alpha(\lambda_i)^\beta(\sigma_\mu)_{\beta\dot{\beta}}(\tilde{\lambda}_i)^{\dot{\beta}} \\ =&(\tilde{\lambda}_i)_{\dot{\alpha}}(\lambda_i)_\alpha(\lambda_i)^\beta(\tilde{\lambda}_i)^{\dot{\beta}}\delta^\alpha_\beta\delta^{\dot{\alpha}}_{\dot{\beta}} \\ =&(\lambda_i)_\beta(\lambda_i)^\beta(\tilde{\lambda}_i)_{\dot{\alpha}}(\tilde{\lambda}_j)^{\dot{\alpha}} \\ =&-\langle ij\rangle[ij] \\ =&\langle ij\rangle[ji] \ ,\end{aligned} \tag{210}$$

where in the last line we used that the inner products are antisymmetric. To prove charge conjugation, recall from equation (67) that:

$$(\sigma^\mu)^{\dot{\alpha}\alpha} = \epsilon^{\alpha\beta}\epsilon^{\dot{\alpha}\dot{\beta}}(\sigma^\mu)_{\beta\dot{\beta}} \ . \tag{211}$$

Inserting this into the 2-component definition of the Lorentz vector gives:

$$\begin{aligned}(\tilde{\lambda}_i)_{\dot{\alpha}}(\sigma^\mu)^{\dot{\alpha}\alpha}(\lambda_j)_\alpha =&(\tilde{\lambda}_i)_{\dot{\alpha}}\epsilon^{\alpha\beta}\epsilon^{\dot{\alpha}\dot{\beta}}(\sigma^\mu)_{\beta\dot{\beta}}(\lambda_j)_\alpha \\ =&(\lambda_j)^\beta(\sigma^\mu)_{\beta\dot{\beta}}(\tilde{\lambda}_i)^{\dot{\beta}} \\ =&(\lambda_j)^\alpha(\sigma^\mu)_{\alpha\dot{\alpha}}(\tilde{\lambda}_i)^{\dot{\alpha}} \ ,\end{aligned} \tag{212}$$

or equivalently that:

$$\langle i^+|\gamma^\mu|j^+\rangle = \langle j^-|\gamma^\mu|i^-\rangle \ . \tag{213}$$

The Fierz rearrangement (equation (87)) follows from charge conjugation and the Fierz identity (equation (69)). It is best shown in 2-component notation that:

$$\begin{aligned}(\tilde{\lambda}_i)_{\dot{\alpha}}(\sigma_\mu)^{\dot{\alpha}\alpha}(\lambda_j)_\alpha(\tilde{\lambda}_k)_{\dot{\beta}}(\sigma^\mu)^{\dot{\beta}\beta}(\lambda_l)_\beta &= (\tilde{\lambda}_i)_{\dot{\alpha}}(\sigma_\mu)^{\dot{\alpha}\alpha}(\lambda_j)_\alpha(\lambda_l)^\beta(\sigma^\mu)_{\beta\dot{\beta}}(\tilde{\lambda}_k)^{\dot{\beta}} \\ &= (\tilde{\lambda}_i)_{\dot{\alpha}}(\lambda_j)_\alpha(\lambda_l)^\beta(\tilde{\lambda}_k)^{\dot{\beta}}(\sigma_\mu)^{\dot{\alpha}\alpha}(\lambda_j)_\alpha(\sigma^\mu)_{\beta\dot{\beta}} \\ &= (\tilde{\lambda}_i)_{\dot{\alpha}}(\lambda_j)_\alpha(\lambda_l)^\beta(\tilde{\lambda}_k)^{\dot{\beta}}\left(2\delta^\alpha_\beta\delta^{\dot{\alpha}}_{\dot{\beta}}\right) \\ &= 2(\tilde{\lambda}_i)_{\dot{\alpha}}(\tilde{\lambda}_k)^{\dot{\alpha}}(\lambda_j)_\beta(\lambda_l)^\beta \\ &= 2[ik]\langle lj\rangle \ ,\end{aligned} \tag{214}$$

where we used charge conjugation in the first line, the Fierz identity in the third line and the definitions of the inner products (equations (72) and (76)) in the last line. The equivalent expression in 4-component notation is:

$$\langle i^+|\gamma^\mu|j^+\rangle\langle k^+|\gamma_\mu|l^+\rangle = \langle i^+|\gamma^\mu|j^+\rangle\langle l^-|\gamma_\mu|k^-\rangle = 2[ik]\langle lj\rangle \ . \tag{215}$$

The first Schouten identity (equation (88)) can be proven by direct substitution of the inner products (equation (73)). First we use that the inner products are antisymmetric to write that:

$$\langle pq\rangle\langle rs\rangle + \langle qr\rangle\langle sq\rangle + \langle ps\rangle\langle qr\rangle = 0 \ , \tag{216}$$

and then use the definition of the inner products to show that the left hand side indeed vanishes:

$$\begin{aligned}\langle pq\rangle\langle rs\rangle + \langle qr\rangle\langle sq\rangle + \langle ps\rangle\langle qr\rangle &= (p_1q_2 - p_2q_1)(r_1s_2 - r_2s_1) + (p_1r_2 - p_2r_1)(s_1q_2 - s_2q_1) \\ &\quad + (p_1s_2 - p_2s_1)(q_1r_2 - q_2r_1) \\ &= p_1q_2r_1s_2 - p_1q_2r_2s_1 - p_2q_1r_1s_2 + p_2q_1r_2s_1 - p_1r_2s_2q_1 - p_2r_1s_1q_2 \\ &\quad - p_1q_2r_1s_2 + p_1q_2r_2s_1 + p_2q_1r_1s_2 - p_2q_1r_2s_1 + p_1r_2s_2q_1 + p_2r_1s_1q_2 \\ &= 0 \ ,\end{aligned} \tag{217}$$

while the second Schouten identity (equation (89)) is proven similarly using equation (77). The third Schouten identity (equation (90)) is easy to prove in 2-component notation:

$$\langle i^-|\not{k}_m|j^-\rangle \equiv (\lambda_i)^\alpha(\not{k}_m)_{\alpha\dot\alpha}(\tilde\lambda_j)^{\dot\alpha} = (\lambda_i)^\alpha(\lambda_m)_\alpha(\tilde\lambda_m)_{\dot\alpha}(\tilde\lambda_j)^{\dot\alpha} = \langle im\rangle[mj] \ , \tag{218}$$

where we used that $\not{k}_{\alpha\dot\alpha} = \lambda_\alpha\tilde\lambda_{\dot\alpha}$. The fourth Schouten identity (equation (91)) can be proven analogously, or by using charge conjugation and re-labelling on the third Schouten identity.

D Gluon polarisation vector

External gluon polarisations appear in the QCD Feynman rules (see Appendix B) and hence need to be well understood to calculate the S-matrix in the helicity basis. The following derivation of the gluon polarisation was introduced by Xu, Zhang and Chang[18] [77] and this section is heavily based on the review by Mangano and Parke [27]. Note that the following description uses the four-component Dirac spinors.

In four dimensions the physical Hilbert space of a massless vector is isomorphic to the physical Hilbert space of a massless spinor up to a Z_2 transformation. This is because they both lie in one-dimensional representations of the $SO(2)$ rotation group. This isomorphism is realised through a linear transformation which relates like-helicity vectors and fermions:

$$\epsilon_\mu^+(k) = A\overline{U}_+(k)\gamma_\mu V \tag{219}$$

$$\epsilon_\mu^-(k) = \left(\epsilon_\mu^+(k)\right)^* \ , \tag{220}$$

where $\epsilon_\mu^\pm(k)$ is the polarisation vector of a positive energy massless vector of momentum k, $\overline{U}_+$ is a massless spinor defined in equation (49), γ_μ the Dirac matrix, V an arbitrary Dirac spinor and A the normalisation constant. Note that different gauge choices give different values for spinor V and we can always choose a gauge such that:

$$\not{p}V(p) = 0 \ , \qquad p^2 = 0 \ , \qquad p\cdot k \neq 0 \ , \tag{221}$$

so that spinor $V(p)$ also obeys the massless Dirac equation and V and $\overline{U}_+$ are not parallel. Here p is called the reference momentum, and can be arbitrarily chosen so long as equation (221) holds. Using the bra and ket notation for spinors we see that:

$$\epsilon_\mu^+(k,p) = A\langle k^+|\gamma_\mu|p^+\rangle \tag{222}$$

$$\epsilon_\mu^-(k,p) = A^*\langle k^-|\gamma_\mu|p^-\rangle \ . \tag{223}$$

We must now normalise the polarisation vectors according to:

$$\epsilon_\mu^\pm(k,p)\cdot\epsilon_\mu^\pm(k,p) = 0 \qquad \epsilon_\mu^\pm(k,p)\cdot\epsilon_\mu^\mp(k,p) = -1 \ . \tag{224}$$

[18] This method was also independently introduced by Gunion and Kunszt [75], and by Kleiss and Stirling [76].

Method	Convergence	n_{eval}/point	Worse than MC in $d >$
Trapezoidal Rule	$1/n^{2/d}$	2^d	4
Simpson's Rule	$1/n^{4/d}$	3^d	8
Monte Carlo	$1/\sqrt{n}$	1	-

Table 14: Convergence after n evaluations in d dimensions, for two common numerical methods and for Monte Carlo. The third column shows the number of function evaluations required per point in d dimensions.

Using first charge conjugation (equation (85)) and then the Fierz Rearrangement (equation (87)) we have that:

$$\begin{aligned}\epsilon^+_\mu(k,p)(\epsilon^\mu)^-(k,p) =& |A|^2\langle k^+|\gamma_\mu|p^+\rangle\langle k^-|\gamma_\mu|p^-\rangle \\ =& |A|^2\langle k^+|\gamma_\mu|p^+\rangle\langle p^+|\gamma_\mu|k^+\rangle \\ =& 2|A|^2[kp]\langle kp\rangle \\ =& -2|A|^2\langle kp\rangle[pk] \\ =& -2|A|^2 s_{kp} = -1 \ ,\end{aligned} \tag{225}$$

where in the last line we used the spinor representation of the momentum invariant (equation (83)). Hence:

$$A = \frac{e^{i\phi(k,p)}}{\sqrt{2}\langle pk\rangle} \qquad A^* = \frac{e^{-i\phi(k,p)}}{\sqrt{2}[kp]} \ , \tag{226}$$

where we used equation (84) to redefine s_{kp} in terms of positive and negative helicity spinors respectively and $\phi(k,p)$ is some phase. If we set the phase equal to 0 we get our form for the polarisation vector:

$$\epsilon^\pm_\mu(k,p) = \pm\frac{\langle k^\pm|\gamma^\mu|p^\pm\rangle}{\sqrt{2}\langle p^\mp|k^\pm\rangle} \ . \tag{227}$$

All that remains is to prove that the polarisation is indeed orthogonal. Using the Fierz Rerrangement (equation (87)) we see that:

$$\begin{aligned}\epsilon^+_\mu(k,p)(\epsilon^\mu)^+(k,p) =& \frac{\langle k^+|\gamma_\mu|p^+\rangle\langle k^+|\gamma^\mu|p^+\rangle}{\sqrt{2}\langle pk\rangle^2} \\ =& \frac{2\langle pp\rangle[kk]}{\sqrt{2}\langle pk\rangle^2} = 0 \ ,\end{aligned} \tag{228}$$

with a similar argument holding for $\epsilon^-_\mu(k,p)(\epsilon^\mu)^-(k,p)$. Notice that equation (228) is doubly zero. Hence we need only one of these zeros for an epsilon contraction to vanish, leading to equation (96), namely:

$$\epsilon^\pm(k,p)\cdot\epsilon^\pm(k',p) = \epsilon^\pm(k,p)\cdot\epsilon^\mp(p,p') = 0 \ . \tag{229}$$

E Monte Carlo integration

To evaluate the total cross section of a $2 \to n$ process we must evaluate a $3n-4$ dimensional integral, often for $n \gg 1$ [37, 59]. This would be very slow for our usual 1-D integration methods such as Simpson's rule or the Trapezoidal rule, since the convergences of these methods both decrease with increased dimensionality (see Table 14). Conversely, the MC method of integration converges as $1/\sqrt{n}$ independently of the number of dimensions, hence why we use MC integration to evaluate cross sections. Note that because MC integration uses random numbers, we cannot rule out the possibility that the particular sequence of random numbers used leads to a numerical integral which deviates strongly from the true value of the integral. Therefore we must slightly alter our definition of convergence. We say that the sequence $\{A\}$ converges to B if an n exists for which the probability for $|A_{i>n} - B| < \epsilon$ for any $\epsilon > 0$ is greater than P, for any $P \in [0,1]$ [78].

The MC integration is based on the fact that the value of an integral is equal to the average of the integrand [60]. That is:

$$I = \int_{x_1}^{x_2} dx f(x) = (x_2 - x_1)\left\langle f(x)\right\rangle \ , \tag{230}$$

where $\langle f(x) \rangle$ is the average of $f(x)$. Therefore taking N values of x distributed randomly in the region (x_1, x_2) allows us to estimate the integral I using:

$$I \approx I_N = (x_2 - x_1) \frac{1}{N} \sum_{i=1}^{N} f(x_i) \ , \tag{231}$$

where x_i is given by:

$$x_i = (x_2 - x_1) \rho_i + x_1 \ , \tag{232}$$

and ρ_i is a uniform random number between 0 and 1. In particle physics we are often interested in integrating the function $f(u_1, \ldots, u_d) \equiv f(x)$ which depends on d variables $(u_1, \ldots, u_d)$ over the unit hypercube $[0, 1]^d$ [79]. Therefore we simplify equation (231) as:

$$I_N = \frac{1}{N} \sum_{i=1}^{N} f(x_i) \ . \tag{233}$$

To estimate the accuracy of equation (233) we must first introduce the variance $\sigma^2(f)$ of the function $f(x)$:

$$\sigma^2(f) = \int dx \left((f(x) - I)^2 \right. \ . \tag{234}$$

We can then use the Central Limit Theorem to determine the standard deviation of I_N. Doing so gives that:

$$\lim_{N \to \infty} \text{Prob} \left(\frac{\sigma(f)}{\sqrt{N}} \leq \frac{1}{N} \sum_{i=1}^{N} f(x_i) - I \leq \frac{\sigma(f)}{\sqrt{N}} \right) = \frac{1}{\sqrt{2\pi}} \int_{-1}^{1} dt e^{-t^2/2} = 0.682 \ , \tag{235}$$

and hence the standard deviation σ_{MC} of the MC integral is:

$$\sigma_{MC} = \frac{\sigma(f)}{\sqrt{N}} \ , \tag{236}$$

or equivalently that the MC integral converges as $1/\sqrt{N}$.

It is worthwhile to mention briefly that we have just described a flat distribution over phase space, i.e. each point in phase space has an equal probability of being sampled. However the integral is almost always not flat, and we are often most interested in the areas of phase space for which the integrand is strongly peaked. Therefore we use techniques such as importance sampling or multi-channel integration to sample phase space more often in the areas of interest. This has the benefit that the regions of interest converge faster than if we use a flat sampling. While these methods are very important in MC event generators, their details are unimportant in this thesis. For a review of these and other similar methods see e.g. [59, 79].

F Parton energy fractions

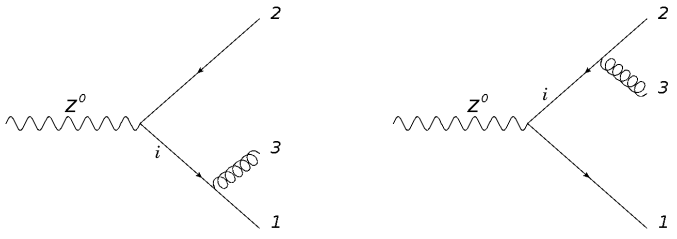

Figure 13: An example of 3-body decay. The Z^0 is considered at rest

The purpose of this appendix is to derive equation (149) starting from equation (145), and therefore show our understanding of the topic beyond just copying the literature. Before we do so, we first motivate the energy fractions x_i which we use. Consider the three body Z^0 decay shown in Figure 13. We have from momentum conservation that the momentum of the virtual quark (k_i) is:

$$k_i = k_Z - k_2 \ , \qquad k_i^2 = k_Z^2 + k_2^2 - 2 k_Z \cdot k_2 \ , \tag{237}$$

where k_Z is the Z^0 momentum and k_2 the anti-quark's momentum. This implies that the off-shell mass of this particle is:

$$m_i^2 = m_Z^2 + m_2^2 - 2(E_2 E_Z - \vec{\mathbf{k}}_Z \cdot \vec{\mathbf{k}}_2) = m_Z^2 - 2E_z E_2 \ , \tag{238}$$

where E_Z, m_Z and E_2, m_2 are the energies and masses of the Z^0 and anti-quark respectively, and we've used that the anti-quark is massless, and that the Z^0 is at rest. Noting that $E_Z = E_{cm}$, i.e. the centre of mass energy and $m_i^2 = s_{13}$ gives that:

$$s_{13} = E_{cm}^2 - 2E_{cm}E_2 \ , \tag{239}$$

or that:

$$\frac{s_{13}}{E_{cm}} = 1 - 2\frac{E_2}{E_{cm}} = 1 - x_2 \ , \tag{240}$$

Placing the sum of invariants in equation (145) on a common denominator and using equation (146) gives that:

$$\begin{aligned}
\frac{2s_{12}}{s_{13}s_{23}} + \frac{1}{s}\left(\frac{s_{13}}{s_{23}} + \frac{s_{23}}{s_{13}}\right) &= \frac{2(s)s_{12} + s_{13}^2 + s_{23}^2}{s_{13}s_{23}s} \\
&= \frac{2s_{12}(s_{12} + s_{13} + s_{23}) + s_{13}^2 + s_{23}^2}{s_{13}s_{23}s} \\
&= \frac{2s_{12}^2 + 2s_{12}s_{13} + 2s_{12}s_{23} + s_{13}^2 + s_{23}^2}{s_{13}s_{23}s} \ ,
\end{aligned} \tag{241}$$

and substituting equation (240) then expanding gives that:

$$\begin{aligned}
\frac{2s_{12}}{s_{13}s_{23}} + \frac{1}{s}\left(\frac{s_{13}}{s_{23}} + \frac{s_{23}}{s_{13}}\right) &= \frac{2s^2(1-x_3)^2 + 2(1-x_3)(1-x_2) + 2(1-x_3)(1-x_1) + s^2(1-x_2)^2 + s^2(1-x_1)^2}{s^3(1-x_2)(1-x_1)} \\
&= \frac{x_1^2 + x_2^2 + 8 - 8x_3 + 2x_3^2 - 4x_2 + 2x_3x_2 - 4x_1 + 2x_2x_3}{s(1-x_2)(1-x_1)} \\
&= \frac{x_1^2 + x_2^2 + 2\left[(x_3-2)^2 + x_2(x_3-2) + x_1(x_3-2)\right]}{s(1-x_2)(1-x_1)} \\
&= \frac{x_1^2 + x_2^2 + 2(x_3-2)\left[x_1 + x_2 + x_3 - 2\right]}{s(1-x_2)(1-x_1)} \ .
\end{aligned} \tag{242}$$

Now we the term in the square brackets and substitute the definition of x in terms energies ($x_i = E_i/E_{cm}$):

$$x_1 + x_2 + x_3 - 2 = \frac{2(E_1 + E_2 + E_3)}{E_{cm}} - 2 = \frac{2E_{cm}}{E_{cm}} - 2 = 0 \ , \tag{243}$$

and hence:

$$\frac{2s_{12}}{s_{13}s_{23}} + \frac{1}{s}\left(\frac{s_{13}}{s_{23}} + \frac{s_{23}}{s_{13}}\right) = \frac{x_1^2 + x_2^2}{s(1-x_2)(1-x_1)} \ . \tag{244}$$

We then use this result, $g_s^2 = 4\pi\alpha_s$, $C_F = 8/3$ and that $dx_1 = -ds_{23}/s$ and $dx_2 = -ds_{13}/s$ to get that:

$$g_s^2 C_F \left[\frac{2s_{12}}{s_{13}s_{23}} + \frac{1}{s}\left(\frac{s_{13}}{s_{23}} + \frac{s_{23}}{s_{13}}\right)\right] \frac{1}{16\pi^2 s} ds_{13} ds_{23} = \frac{2\alpha_s}{3\pi} \frac{x_1^2 + x_2^2}{(1-x_1)(1-x_2)} dx_1 dx_2 \ . \tag{245}$$

G Working for all-gluon squared colour matrix

In this appendix we repeat section 2.3.2 in more detail, to show evidence of a deeper understanding the topic than one can get from simply copying the literature. Recall the notation:

$$\begin{aligned}
(a_1 a_2 \dots a_n) =& \mathrm{Tr}(t^{a_{\sigma_1(1)}} t^{a_{\sigma_1(2)}} \dots t^{a_{\sigma_1(n)}}) \\
(b_1 b_2 \dots b_n) =& \mathrm{Tr}(t^{b_{\sigma_2(1)}} t^{b_{\sigma_2(2)}} \dots t^{b_{\sigma_2(n)}}) \ ,
\end{aligned} \tag{246}$$

where σ_1 and σ_2 are two different permutations of the gluons. Therefore the colour matrix C_{ij} can be re-written as:

$$C_{ij} = \sum_{a_1,\dots,a_n=1}^{N_C^2-1} (a_1 a_2 \dots a_n)(b_1 b_2 \dots b_n)^* \ . \tag{247}$$

Since σ_2 is some permutation of σ_1, and since the trace is cyclic we can re-write equation (26) as:

$$C_{ij} = \sum_{a_1,\ldots,a_n=1}^{N_C^2-1} (a_1 a_2 \ldots a_n)(b_1 b_2 \ldots b_n)^* = \sum_{a_1,\ldots,a_{n-1}=1}^{N_C^2-1} \sum_{a_n} (a_1 a_2 \ldots a_n)(a_n a_{m_{n-1}} \ldots a_{m_1}) \ , \tag{248}$$

where $\{a_m\}$ is the remaining ordered set of t matrices in the σ_2 permutation. We can then write the traces in component notation and use the Fierz identity (equation (13)) to get that:

$$\begin{aligned}
C_{ij} &= \sum_{a_1,\ldots,a_{n-1}=1}^{N_C^2-1} \sum_{a_n} (a_1 a_2 \ldots a_n)(a_n a_{m_{n-1}} \ldots a_{m_1}) \\
&= \sum_{a_1,\ldots,a_{n-1}=1}^{N_C^2-1} \sum_{a_n} (a_1)_{ij} \ldots (a_{n-1})_{kl} (a_n)_{li} (a_n)_{pq} (a_{m_{n-1}})_{qr} \ldots (b_{m_1})_{sp} \\
&= \sum_{a_1,\ldots,a_{n-1}=1}^{N_C^2-1} (a_1)_{ij} \ldots (a_{n-1})_{kl} (a_{m_{n-1}})_{qr} \ldots (a_{m_1})_{sp} \\
&\qquad \times [\delta_{lq}\delta_{ip} - \frac{1}{N_C}\delta_{li}\delta_{pq}] \\
&= \sum_{a_1,\ldots,a_{n-1}=1}^{N_C^2-1} [(a_1)_{ij} \ldots (a_{n-1})_{kl} (a_{m_{n-1}})_{lr} \ldots (a_{m_1})_{si} \\
&\qquad - \frac{1}{N_C}(a_1)_{ij} \ldots (a_{n-1})_{ki} (a_{m_{n-1}})_{qr} \ldots (a_{m_1})_{sq}] \\
&= \sum_{a_1,\ldots,a_{n-1}=1}^{N_C^2-1} [(a_1 a_2 \ldots a_{n-1} a_{m_{n-1}} \ldots a_{m_1}) \\
&\qquad - \frac{1}{N_C}(a_1 a_2 \ldots a_{n-1})(a_{m_{n-1}} \ldots a_{m_1})] \ .
\end{aligned} \tag{249}$$

The first term in the final line of equation (249) can have either of the following forms:

$$\sum_{\Lambda, a_{n-1}} (\Lambda_1 a_{n-1} a_{n-1} \Lambda_2) \ , \quad \text{or} \quad \sum_{\Lambda, a_{n-1}} (\Lambda_1 a_{n-1} \Lambda_2 a_{n-1}) \ ,$$

where Λ_i is some string of t matrices. Note that in the second expression it is likely that we have had to cyclically permute a_{n-1} to the final position, such that Λ_1 has more t matrices than Λ_2. If we have the first form, then we use equation (10) to get that[19]:

$$\begin{aligned}
\sum_{\Lambda, a_{n-1}} (\Lambda_1 a_{n-1} a_{n-1} \Lambda_2) &= \sum_{\Lambda} (\Lambda_1)_{ij} (a_{n-1})_{jk} (a_{n-1})_{kl} (\Lambda_2)_{li} \\
&= \sum_{\Lambda} \frac{N_C^2 - 1}{N_C} \delta_{jl} (\Lambda_1)_{ij} (\Lambda_2)_{li} = \sum_{\Lambda} (\Lambda_1 \Lambda_2) \ ,
\end{aligned} \tag{250}$$

and if we have the second form then we again use the Fierz equation to get that:

$$\begin{aligned}
\sum_{\Lambda, a_{n-1}} (\Lambda_1 a_{n-1} \Lambda_2 a_{n-1}) &= \sum_{\Lambda} (\Lambda_1)_{ij} (a_{n-1})_{jk} (\Lambda_2)_{kl} (a_{n-1})_{li} \\
&= \sum_{\Lambda} (\Lambda_1)_{ij} (\Lambda_2)_{kl} [\delta_{ji}\delta_{kl} - \frac{1}{N_C}\delta_{jk}\delta_{li}] \\
&= \sum_{\Lambda} (\Lambda_1)(\Lambda_2) - \frac{1}{N_C}(\Lambda_1 \Lambda_2) \ .
\end{aligned} \tag{251}$$

[19]Note that in $SU(N_C)$ we must generalise C_F from $C_F = 8/3$ to $C_F = (N_C^2 - 1)/N_c$.

We can keep doing this until we find terms proportional to:

$$(a_1 a_1) = \frac{N_C^2 - 1}{N_C}\delta_{ii} = N_C^2 - 1 \ , \tag{252}$$

which allows us to calculate the colour factors C_{ij}. Note that the leading contribution to the colour matrix comes from the diagonal, i.e. when permutations $\sigma_1 = \sigma_2$. To leading order in N_C the leading contribution to the colour factor is [27]:

$$C_{ii} = \sum_{a_1,\ldots,a_n=1}^{N_C^2-1} (a_1 a_2 \ldots a_n)(a_1 a_2 \ldots a_n)^* = N_C^{n-2}(N_C^2 - 1)[1 + \mathcal{O}(1/N_C^2)] \ . \tag{253}$$

H VinciaMHV colour matrices

In this appendix we give the explicit colour matrices used in our MHV code. These were calculated using MadGraph[20] and can be derived using the method in section 2.3.4. Recall that we can write the full amplitude in the form:

$$\sum_{\text{colours}} |M_n(q, g_1, g_2, \ldots, \bar{q})|^2 = g_s^{2n-4} A^\dagger_{\sigma_i} C_{ij} A_{\sigma_j} \ , \tag{254}$$

with σ_i and σ_j each being some permutation of the gluons. Equation (254) implies that the colour matrix C_{ij} is dependent on the order of gluon permutations. In our code we use the `std::next_permutation()` function to lexicographically permute the gluons. This means if we replace the numerical sequence $1, 2, 3, \ldots, n$ with the alphabetical sequence $a, b, c, \ldots, n$, then the set of permutations is in alphabetical order. For example, the lexicographical order of $1, 2, 3, 4$ is:

$$\begin{aligned}
&(1,2,3,4),\ (1,2,4,3),\ (1,3,2,4),\ (1,3,4,2),\ (1,4,2,3),\ (1,4,3,2),\\
&(2,1,3,4),\ (2,1,4,3),\ (2,3,1,4),\ (2,3,4,1),\ (2,4,1,3),\ (2,4,3,1),\\
&(3,1,2,4),\ (3,1,4,2),\ (3,2,1,4),\ (3,2,4,1),\ (3,4,1,2),\ (3,4,2,1),\\
&(4,1,2,3),\ (4,1,3,2),\ (4,2,1,3),\ (4,2,3,1),\ (4,3,1,2),\ (4,3,2,1) \ .
\end{aligned}$$

The colour matrix C_n for the process with a single quark anti-quark pair and $n-2$ gluons is:

- $n = 4$:

$$C_4 = \frac{1}{3}\begin{pmatrix} 64 & -8 \\ -8 & 64 \end{pmatrix} \ , \tag{255}$$

- $n = 5$:

$$C_5 = \frac{1}{9}\begin{pmatrix} 512 & -64 & -64 & 8 & 8 & 80 \\ -64 & 512 & 8 & 80 & -64 & 8 \\ -64 & 8 & 512 & -64 & 80 & 8 \\ 8 & 80 & -64 & 512 & 8 & -64 \\ 8 & -64 & 80 & 8 & 512 & -64 \\ 80 & 8 & 8 & -64 & -64 & 512 \end{pmatrix} \ , \tag{256}$$

- $n = 6$: The first row is given by:

$$\begin{aligned}
27 \times (C_6)_{1j} = (&4096,\ -512,\ -512,\ 64,\ 64,\ 640,\\
&-512,\ 64,\ 64,\ -8,\ -8,\ -80,\\
&64,\ -8,\ 640,\ -80,\ 568,\ 496,\\
&-8,\ -80,\ -80,\ 496,\ 496,\ -224) \ ,
\end{aligned} \tag{257}$$

  with all other rows given by the appropriate lexicographical permutation of the first row and relabelling. For example, $27 \times (C_6)_{13} = -512$ and relates to the gluon permutations $(1, 2, 3, 4)$ and $(1, 3, 2, 4)$. Relabelling $4 \leftrightarrow 3$ gives the permutations $(1, 4, 3, 2)$ and $(1, 4, 2, 3)$, corresponding to the element $(C_6)_{65}$, and hence $27 \times (C_6)_{65} = -512$.

[20] In fact MadGraph uses the standard QCD convention for t matrices and a different gluon permutation technique. Therefore we had to first correct the colour matrices so that they were consistent with our conventions.

- $n = 7$: The first row is given by:

$$\begin{aligned} 81 \times (C_7)_{1j} = (&32768,\ -4096,\ -4096,\ 512,\ 512,\ 5120,\ -4096,\ 512,\ 512,\ -64,\\ &-64,\ -640,\ 512,\ -64,\ 5120,\ -640,\ 4544,\ 3968,\ -64,\ -640,\\ &-640,\ 3968,\ 3968,\ -1792,\ -4096,\ 512,\ 512,\ -64,\ -64,\ -640,\\ &512,\ -64,\ -64,\ 8,\ 8,\ 80,\ -64,\ 8,\ -640,\ 80,\\ &-568,\ -496,\ 8,\ 80,\ 80,\ -496,\ -496,\ 224,\ 512,\ -64,\\ &-64,\ 8,\ 8,\ 80,\ 5120,\ -640,\ -640,\ 80,\ 80,\ 800,\\ &4544,\ -568,\ 3968,\ -496,\ 4040,\ 4112,\ -568,\ 152,\ -496,\ -424,\\ &-1072,\ -352,\ -64,\ 8,\ -640,\ 80,\ -568,\ -496,\ -640,\ 80,\\ &4040,\ -1072,\ -1072,\ 3536,\ 3536,\ -928,\ 8,\ 80,\ 80,\ -496,\\ &-496,\ 224,\ 80,\ 800,\ -496,\ 4112,\ -424,\ -352,\ -496,\ -424,\\ &224,\ -352,\ 3536,\ -928,\ 4112,\ -352,\ -352,\ -928,\ -928,\ 1088)\ , \end{aligned} \tag{258}$$

  and again all other rows are given by the appropriate lexicographical permutation of the first row and relabelling.

References

[1] Georges Aad et al. Hunt for new phenomena using large jet multiplicities and missing transverse momentum with ATLAS in 4.7 fb^{-1} of $\sqrt{s} = 7$ TeV proton-proton collisions. *JHEP*, 07:167, 2012.

[2] Lance J. Dixon. A brief introduction to modern amplitude methods. http://arxiv.org/abs/1310.5353, 2014.

[3] Gavin P. Salam. Towards Jetography. *Eur. Phys. J.*, C67:637–686, 2010.

[4] Matteo Cacciari. Phenomenological and theoretical developments in jet physics at the LHC. To appear in *IJMPA*, 2015.

[5] Michelangelo L. Mangano, Mauro Moretti, Fulvio Piccinini, Roberto Pittau, and Antonio D. Polosa. ALPGEN, a generator for hard multiparton processes in hadronic collisions. *JHEP*, 0307:001, 2003.

[6] Torbjörn Sjöstrand, Stefan Ask, Jesper R. Christiansen, Richard Corke, Nishita Desai, et al. An Introduction to PYTHIA 8.2. *Comput.Phys.Commun.*, 191:159–177, 2015.

[7] M. Bahr, S. Gieseke, M.A. Gigg, D. Grellscheid, K. Hamilton, et al. Herwig++ Physics and Manual. *Eur. Phys. J.*, C58:639–707, 2008.

[8] T. Gleisberg, Stefan. Hoeche, F. Krauss, M. Schonherr, S. Schumann, et al. Event generation with SHERPA 1.1. *JHEP*, 0902:007, 2009.

[9] Johan Alwall, Michel Herquet, Fabio Maltoni, Olivier Mattelaer, and Tim Stelzer. MadGraph 5 : Going Beyond. *JHEP*, 06:128, 2011.

[10] Glennys R. Farrar and Filippo Neri. How to Calculate 35640 O (α^5) Feynman Diagrams in Less Than an Hour. *Phys. Lett.*, B130:109–114, 1983. [Addendum: Phys. Lett.B152,443(1985)].

[11] A. Kersch and F. Scheck. Amplitude and Trace Reduction Using Weyl-van Der Waerden Spinors: Pion Pair Decay $\pi^+ \to e^+e^-e^+\nu_e$. *Nucl. Phys.*, B263:475, 1986.

[12] Kaoru Hagiwara and D. Zeppenfeld. Helicity Amplitudes for Heavy Lepton Production in e^+e^- Annihilation. *Nucl. Phys.*, B274:1–32, 1986.

[13] Stephen J. Parke and T.R. Taylor. An Amplitude for n Gluon Scattering. *Phys. Rev. Lett.*, 56:2459, 1986.

[14] Frits A. Berends and W. Giele. The Six Gluon Process as an Example of Weyl-Van Der Waerden Spinor Calculus. *Nucl. Phys.*, B294:700, 1987.

[15] Frits A. Berends, W. T. Giele, and H. Kuijf. Exact Expressions for Processes Involving a Vector Boson and Up to Five Partons. *Nucl. Phys.*, B321:39, 1989.

[16] George Georgiou and Valentin V. Khoze. Tree amplitudes in gauge theory as scalar MHV diagrams. *JHEP*, 0405:070, 2004.

[17] Freddy Cachazo, Peter Svrcek, and Edward Witten. MHV vertices and tree amplitudes in gauge theory. *JHEP*, 0409:006, 2004.

[18] Lance J. Dixon, Johannes M. Henn, Jan Plefka, and Theodor Schuster. All tree-level amplitudes in massless QCD. *JHEP*, 1101:035, 2011.

[19] Marcus T. Grisaru, H. N. Pendleton, and P. van Nieuwenhuizen. Supergravity and the S Matrix. *Phys. Rev.*, D15:996, 1977.

[20] Stephen J. Parke and T.R. Taylor. Perturbative QCD Utilizing Extended Supersymmetry. *Phys. Lett.*, B157:81, 1985.

[21] Michelangelo L. Mangano and Stephen J. Parke. Quark - Gluon Amplitudes in the Dual Expansion. *Nucl. Phys.*, B299:673, 1988.

[22] Frits A. Berends and W.T. Giele. Recursive Calculations for Processes with n Gluons. *Nucl. Phys.*, B306:759, 1988.

[23] Andrew J. Larkoski, Juan J. Lopez-Villarejo, and Peter Skands. Helicity-Dependent Showers and Matching with VINCIA. *Phys. Rev.*, D87(5):054033, 2013.

[24] Walter T. Giele, David A. Kosower, and Peter Z. Skands. A simple shower and matching algorithm. *Phys. Rev.*, D78:014026, 2008.

[25] Johan Alwall, Pavel Demin, Simon de Visscher, Rikkert Frederix, Michel Herquet, Fabio Maltoni, Tilman Plehn, David L. Rainwater, and Tim Stelzer. MadGraph/MadEvent v4: The New Web Generation. *JHEP*, 09:028, 2007.

[26] Ronald Kleiss and Hans Kuijf. Multi-gluon cross-sections and 5-jet production at hadron colliders. *Nucl. Phys.*, B312:616, 1989.

[27] Michelangelo L. Mangano and Stephen J. Parke. Multiparton amplitudes in gauge theories. *Phys. Rept.*, 200:301–367, 1991.

[28] Lance J. Dixon. Calculating scattering amplitudes efficiently. arXiv:hep-ph/9601359v2, 1996.

[29] Ruth Britto, Freddy Cachazo, Bo Feng, and Edward Witten. Direct proof of tree-level recursion relation in Yang-Mills theory. *Phys. Rev. Lett.*, 94:181602, 2005.

[30] Tanju Gleisberg and Stefan Hoeche. Comix, a new matrix element generator. *JHEP*, 12:039, 2008.

[31] D. J. Gross and Frank Wilczek. Asymptotically Free Gauge Theories. 1. *Phys. Rev.*, D8:3633–3652, 1973.

[32] D. J. Gross and Frank Wilczek. Asymptotically Free Gauge Theories. 2. *Phys. Rev.*, D9:980–993, 1974.

[33] H. David Politzer. Reliable Perturbative Results for Strong Interactions? *Phys. Rev. Lett.*, 30:1346–1349, 1973.

[34] H. David Politzer. Asymptotic Freedom: An Approach to Strong Interactions. *Phys. Rept.*, 14:129–180, 1974.

[35] Peter Skands. Introduction to QCD. arXiv:1207.2389v4, 2015.

[36] R. Keith Ellis, W. James Stirling, and B.R. Webber. QCD and collider physics. *Camb. Monogr. Part. Phys. Nucl. Phys. Cosmol.*, 8:1–435, 1996.

[37] Michael E. Peskin and Daniel V. Schroeder. *An Introduction to quantum field theory*. Westview Press, 1995.

[38] Gunther Dissertori, Ian Knowles, and Michael. Schmelling. *Quantum Chromodynamics*. Oxford Science Publications, 2003.

[39] Michelangelo L. Mangano, Stephen J. Parke, and Zhan Xu. Duality and Multi - Gluon Scattering. *Nucl. Phys.*, B298:653, 1988.

[40] Vittorio Del Duca, Alberto Frizzo, and Fabio Maltoni. Factorization of tree QCD amplitudes in the high-energy limit and in the collinear limit. *Nucl. Phys.*, B568:211–262, 2000.

[41] D. Zeppenfeld. Diagonalization of Color Factors. *Int. J. Mod. Phys.*, A3:2175–2179, 1988.

[42] P. Cvitanovic, P. G. Lauwers, and P. N. Scharbach. Gauge Invariance Structure of Quantum Chromodynamics. *Nucl. Phys.*, B186:165, 1981.

[43] David A. Kosower. Color Factorization for Fermionic Amplitudes. *Nucl. Phys.*, B315:391, 1989.

[44] Paul A. M. Dirac. The Quantum theory of electron. *Proc. Roy. Soc. Lond.*, A117:610–624, 1928.

[45] Paul A. M. Dirac. The Quantum theory of electron. 2. *Proc. Roy. Soc. Lond.*, A118:351, 1928.

[46] H. Weyl. Electron and Gravitation. 1. (In German). *Z. Phys.*, 56:330–352, 1929. [Surveys High Energ. Phys.5,261(1986)].

[47] B. L. van der Waerden. Spinoranalyse (In German). *Nachr. von Ges. Wiss. zu Gottingen Math.-Phys. KI.*, pages 100–109, 1929.

[48] K. F. Riley, M. P. Hobson, and S. J. Bence. *Mathematical Methods for Physics and Engineering, Chapter 26.* Cambridge University Press, 3rd edition, 2006.

[49] Herbi K. Dreiner, Howard E. Haber, and Stephen P. Martin. Two-component spinor techniques and Feynman rules for quantum field theory and supersymmetry. *Phys. Rept.*, 494:1–196, 2010.

[50] L. Infeld and B. L. van der Waerden. The Wave Equation of the Electron in the General Relativity Theory. *Sitzungsber. Preuss. Akad. Wiss. Berlin (Math. Phys.)*, 1933:380–401, 1933.

[51] W. L. Bade and Herbert Jehle. An introduction to spinors. *Rev. Mod. Phys.*, 25:714–728, Jul 1953.

[52] Rudolf Haag, Jan T. Lopuszanski, and Martin Sohnius. All Possible Generators of Supersymmetries of the s Matrix. *Nucl. Phys.*, B88:257, 1975.

[53] J. Wess and J. Bagger. *Supersymmetry and supergravity.* Princeton University Press, 1992.

[54] Joseph D. Lykken. Introduction to supersymmetry. arXiv:hep-th/9612114, 1996.

[55] Stephen P. Martin. A Supersymmetry primer. *Adv. Ser. Direct. High Energy Phys.*, 21:1–153, 2010.

[56] Z. Kunszt. Combined Use of the Calkul Method and N=1 Supersymmetry to Calculate QCD Six Parton Processes. *Nucl. Phys.*, B271:333, 1986.

[57] Marcus T. Grisaru and H. N. Pendleton. Some Properties of Scattering Amplitudes in Supersymmetric Theories. *Nucl. Phys.*, B124:81, 1977.

[58] Daniel Z. Freedman and Antoine Van Proeyen. *Supergravity.* Cambridge Univ. Press, Cambridge, UK, 2012.

[59] Andy Buckley et al. General-purpose event generators for LHC physics. *Phys. Rept.*, 504:145–233, 2011.

[60] Andreas Papaefstathiou. How-to: Write a parton-level Monte Carlo event generator. arXiv:1412.4677v1, 2014.

[61] Torbjörn Sjöstrand. Monte Carlo Tools. In *Proceedings, 65th Scottish Universities Summer School in Physics: LHC Physics (SUSSP65)*, pages 309–339, 2009.

[62] Michael H. Seymour and Marilyn Marx. Monte Carlo Event Generators. arXiv:1304.6677v1, 2013.

[63] Gösta Gustafson and Ulf Pettersson. Dipole Formulation of QCD Cascades. *Nucl. Phys.*, B306:746, 1988.

[64] A. Gehrmann-De Ridder, T. Gehrmann, and E. W. Nigel Glover. Antenna subtraction at NNLO. *JHEP*, 09:056, 2005.

[65] T. Kinoshita. Mass singularities of Feynman amplitudes. *J. Math. Phys.*, 3:650–677, 1962.

[66] T. D. Lee and M. Nauenberg. Degenerate Systems and Mass Singularities. *Phys. Rev.*, 133:B1549–B1562, 1964.

[67] V. N. Gribov and L. N. Lipatov. Deep inelastic e p scattering in perturbation theory. *Sov. J. Nucl. Phys.*, 15:438–450, 1972. [Yad. Fiz.15,781(1972)].

[68] Guido Altarelli and G. Parisi. Asymptotic Freedom in Parton Language. *Nucl. Phys.*, B126:298, 1977.

[69] Yuri L. Dokshitzer. Calculation of the Structure Functions for Deep Inelastic Scattering and e^+e^- Annihilation by Perturbation Theory in Quantum Chromodynamics. *Sov. Phys. JETP*, 46:641–653, 1977. [Zh. Eksp. Teor. Fiz.73,1216(1977)].

[70] K. A. Olive et al. Review of Particle Physics. *Chin. Phys.*, C38:090001, 2014.

[71] Lance J. Dixon, E. W. Nigel Glover, and Valentin V. Khoze. MHV rules for Higgs plus multi-gluon amplitudes. *JHEP*, 12:015, 2004.

[72] S. D. Badger, E. W. Nigel Glover, and Valentin V. Khoze. MHV rules for Higgs plus multi-parton amplitudes. *JHEP*, 03:023, 2005.

[73] Edward Witten. Perturbative gauge theory as a string theory in twistor space. *Commun. Math. Phys.*, 252:189–258, 2004.

[74] Matteo Bertolini. Introduction to Supersymmetry. `http://people.sissa.it/~bertmat/susycourse.pdf`, 2015.

[75] J. F. Gunion and Z. Kunszt. Improved Analytic Techniques for Tree Graph Calculations and the $ggq\bar{q}l\bar{l}$ Subprocess. *Phys. Lett.*, B161:333, 1985.

[76] R. Kleiss and W. James Stirling. Spinor Techniques for Calculating $p\bar{p} \to W^{\pm}/Z^0$ + Jets. *Nucl. Phys.*, B262:235–262, 1985.

[77] Zhan Xu, Da-Hua Zhang, and Lee Chang. Helicity Amplitudes for Multiple Bremsstrahlung in Massless Nonabelian Gauge Theories. *Nucl. Phys.*, B291:392, 1987.

[78] F. James. Monte Carlo Theory and Practice. *Rept. Prog. Phys.*, 43:1145, 1980.

[79] Stefan Weinzierl. Introduction to Monte Carlo methods. arXiv:hep-ph/0006269v1, 2000.